RFF REPORT

Measurement and Monitoring of the World's Forests

A Review and Summary of Remote Sensing Technical Capability, 2009–2015

Matthew Fagan and Ruth DeFries

DECEMBER 2009

RESOURCES FOR THE FUTURE

Preface

This report is part of a series of studies carried out under an initiative at Resources for the Future (RFF) to consider the economic, technical, and institutional issues associated with the goal of improving global forest measurement and monitoring. Companion studies under this initiative include an RFF discussion paper documenting uncertainties and discrepancies in existing forest measurement (Waggoner 2009) and another RFF report providing perspectives on "how good is good enough" in improving measurement and monitoring (Macauley and coauthors forthcoming). The financial support of the Alfred P. Sloan Foundation is gratefully acknowledged for all work under this initiative.

Acknowledgements

Special contributions were made by Molly Macauley, Paul Waggoner, Roger Sedjo, Michael Obersteiner, Craig Dobson, Josef Kellndorfer, and Miriam Marlier. Steffen Fritz, Ralph Dubayah, Steven Sesnie, and Bonnie Tice also helped.

Table of Contents

Measurement and Monitoring of the World's Forests: A Review and Summary of Remote Sensing Technical Capability, 2009–2015

Matthew Fagan and Ruth DeFries *

Executive Summary

Forests are ecosystems of fundamental importance to humanity, yet we know little about the global status of forests. We can make more current and informative maps of Mars than of the Amazon basin or the Russian boreal forest. This gap in our knowledge arises from several sources, including a historical shortage of tools to observe the entire globe; the lack of consistent global initiatives on forests; balkanized, inconsistent recordkeeping; and the absence of a concerted and systematic effort to inventory and monitor the world's forests.

To understand the planetary carbon budget, it is imperative to generate accurate and reliable estimates of global forest cover and the amount of biomass and carbon harbored by the planet's forests. Yet widespread uncertainties in forest measurements have hampered efforts to obtain this basic scientific data. Indeed, the most significant weaknesses in estimates of the planetary carbon budget derive from uncertainties about terrestrial ecosystems. Satellite-based estimates of forest cover and biomass have begun to fill this need.

To measure forests worldwide, satellite imagery is a practical necessity. Aerial observations are expensive at present and only cover small areas at a time. Ground measurements are also expensive and are logistically challenging and spatially restricted. Neither aerial nor ground observations are well suited to continuous measurement of the entire global forest. Satellite mapping is necessary to detect deforestation and regrowth in remote tropical forests and to track the northern expansion of boreal forests in a warming world. The greatest strengths of satellite-based measurements are their unparalleled, unbiased measurements, their monthly to daily frequency, and—above all—their synoptic nature. Satellites provide a general view of the whole Earth that is not possible with any other forest measurement method.

Scope

We evaluate current and near-term (2009–2015) technologies for measuring and monitoring global forests. We focus primarily on remote sensing (defined in this report as the analysis of satellite and aerial imagery), because this technology meets the steep logistical challenge of measuring the world's forests in an accurate, repeatable, and inexpensive manner. We emphasize the observations needed to provide accurate, basic measures of forest attributes for use by forest scientists, decisionmakers, and the public. We also illustrate how the resulting data would address

* Matthew Fagan (mef2153@columbia.edu) is a graduate student in the Department of Ecology, Evolution, and Environmental Biology at Columbia University. Ruth DeFries (rd2402@columbia.edu) is the Denning Professor of Sustainable Development in the Department of Ecology, Evolution, and Environmental Biology at Columbia University.

some of the most compelling questions that persist about our forests. Remote sensing can ultimately help to answer these important questions:

- Where are forests being lost and gained?
- How are biodiversity and regional climates responding to forest loss and regrowth?
- How do forests affect the global carbon budget?
- How can forest management be improved by carbon markets and satellite technology?
- How will forests respond to climate change?

In this report, we evaluate the technical capacity of satellite imagery to measure and monitor global forests. In particular, we examine satellite observations of forest area, volume, biomass, and carbon. These measurements are fundamental to our understanding of the status and trends of forests around the globe and to our grasp of the role that forests play in modulating global climate. We evaluate current capacity and predict future capacity from expected satellite launches and technological developments between 2009 and 2015. Our findings are summarized in the table on page vi.

Current and Emerging Satellite Technologies

Satellite sensors are either passive or active. Passive sensors receive reflected optical and thermal radiation from Earth's surface. Although they are capable of obtaining very high-resolution images and distinguishing among types of land cover (such as vegetation, bare soil, and snow), they cannot penetrate cloud cover. Active sensors are less challenged by cloud cover because these sensors emit radiation and measure the reflections from Earth's surface. Active sensors can provide a three-dimensional picture of the ground, although they cannot reliably render landscapes with sharp changes in elevation, such as mountainous regions.

In general, satellite technology involves a combination of pixel resolution and image size, with an increase in one dimension requiring a reduction in the other dimension. Coarse-resolution satellites can generate images of very large areas, but the pixel resolution may be 1,000 meters (m). Conversely, some sensors can render extremely high-resolution pictures—with pixel sizes less than half a meter—but only over limited areas. Moderate-resolution satellites, such as those with a pixel size of 30 m and an image width of 185 kilometers (km), are often seen as a good compromise for land mapping. The Landsat system, sponsored by the United States, is the oldest and most popular moderate-resolution sensor, but because of technical failures in the operating satellites, Landsat imagery coverage is not currently global. Alternative sensors exist, but the planned launches of the Landsat Data Continuity Mission (LDCM) and the European Sentinel-2 series of remote sensing satellites are important for continued global land mapping.

The recent availability of free imagery from Landsat and the China–Brazil Earth Resources Satellite (CBERS) missions has revolutionized global forest mapping and will continue to do so into the future. Even with free or low-cost imagery, however, cost remains a critical parameter for worldwide mapping. For example, the required processing capability is large because the volume of imagery is enormous.

Satellite groups or constellations improve coverage by enabling more frequent, cloud-free observations of any given point on Earth. Several of these constellations are currently in orbit, and

more are planned. Geostationary satellites, stationed at some 22,000 miles above Earth (most Earth-observing satellites are only a few hundred miles above Earth) can provide rapid and repeated scans of a very large area. The pixel size obtained at a geostationary altitude is only about 2.5 km; by 2014, however, the resolution is expected to improve to approximately 1 km pixel size, making it possible to monitor global vegetation at coarse-resolution in real time. High-resolution (0.3–10 m pixel) sensors will continue to increase in number; these sensors do not acquire continuous, cloud-free, worldwide coverage for forest mapping, but they are ideal for validating estimates from moderate-resolution sensors.

Active sensors (synthetic aperture radar, known as SAR; and light detection and ranging laser, known as LIDAR) are currently a small proportion of the satellite fleet, but will dramatically increase in number and complexity in the next few years, making new types of analysis possible. The first LIDAR satellite—the Ice, Cloud, and land Elevation Satellite (ICESat)—will be followed by two others that can address issues in forest management. These other satellites are ICESat-II and the U.S. Deformation, Ecosystem Structure and Dynamics of Ice satellite (DESDynI). Two new SAR satellites that are likely to launch between 2009 and 2015 will revolutionize mapping of forest biomass. DESDynI will be the first combined SAR–LIDAR mission, and it will integrate the relative strengths of SAR and LIDAR to create unparalleled measurements of ecosystem structure and forest height. The European Space Agency's planned BIOMASS satellite is a long-wavelength SAR, specifically designed to penetrate forests and measure forest biomass in real time.

Although new satellite technology can revolutionize scientific monitoring and measurement of Earth, it is not fail-safe. Satellites and satellite launches can, and do, fail. As a result, global forest measurements need to be accurate and repeated over long time periods. And, at the end of their operating lifetimes, usually after five to ten years or so, the satellites and sensors need to be replaced to enable continued measurement and observation over time.

Remote Sensing and Global Forest Measurement

For any worldwide forest monitoring effort to succeed, there must be consensus on forest definitions, past reference maps (so that change can be detected), and selected forest metrics. We have chosen the Forest Identity (Kauppi et al. 2006) as an organizing principle for the central metrics of this report. The Forest Identity relates four forest attributes (area, volume [density of growing stock], biomass, and sequestered carbon) that provide a useful starting point for global forest monitoring.

Current maps of forest area have medium to high accuracy.[1] Monitoring volume, biomass, and carbon on a regional to global scale is possible with current technology but accuracy is lower (see table on page vi). Similarly, we can develop past reference maps for forest area (maps of what an area once looked like), but past reference maps for volume, biomass, or carbon will require innovative reprocessing of old imagery. For forest area, "accuracy" is roughly defined as the percentage of pixels in the remote sensing imagery that correctly identify land-cover type. For forest volume, biomass, and carbon, accuracy refers to the match between predictions from remote imagery and observed ground measurements.

[1] In this report, the overall accuracy of satellite imagery analysis is designated by five standard adjectives: very high accuracy (>90 percent), high accuracy (>80 percent), acceptable accuracy (>70 percent), low accuracy (50–70 percent), and poor accuracy (<50 percent). Where alternative qualifiers (for example, "mixed") are used, we provide the actual accuracy (say, 67 percent).

Designing a satellite-based, worldwide forest monitoring system requires choices in budgeting, processing logistics, sampling frameworks, and the collection of validation (or "ground-truth") data from forest inventories and high-resolution imagery. Collection of ground-truth data is typically necessary as a means of determining the accuracy of remote sensing. These data are particularly essential when attempting to estimate forest volume, biomass, and carbon using remote sensing technology. Archiving and standardizing global ground-truth data for forests would be a significant contribution to global forest science. Ground data, aerial imagery, and high-resolution satellite imagery are expensive and require coordination in a sampling hierarchy for efficiency.

In current coarse-resolution world forest maps, forest area is measured with medium accuracy as two classes (forest/nonforest) or categorized with low accuracy into homogenous forest types based on leaf persistence (for example, evergreen forest). Recent improvements in classification techniques and the combination of distinct types of satellite imagery (called imagery fusion) have allowed moderate-resolution mapping of forest types with high accuracy (80–90 percent). Currently, complete forest clearing can be detected with the highest accuracy.

With current technology, it remains difficult to distinguish primary forests from tree plantations and older secondary forests in remote sensing images. It is also challenging to detect forest degradation in which a forest is partially cleared by human activity. Significant progress on these problems has been made in certain geographic regions, but accurate global forest maps with multiple classes remain elusive. In the years between 2009 and 2015, we can expect to see numerous improvements that promise to address many of these challenges. Some of the anticipated advances include:

- hyperspectral satellites that produce imagery with great sensitivity across the electromagnetic spectrum,
- improved revisit times from optical and SAR satellite constellations,
- improved algorithms for analyzing large amounts of remote imagery, and
- additional high-resolution and active imagery available for fusions.

Active and passive satellite imagery is sensitive to forest structure (both vertical and horizontal), and forest structure can be used to estimate forest volume, biomass, and aboveground carbon. Both SAR and LIDAR are directly sensitive to forest volume. SAR images tend to "saturate" (or fail to penetrate) in dense forests but they can cover large areas. Conversely, LIDAR data do not saturate but can only measure small areas. In open forests, stereo and high-resolution imagery can also measure forest height and canopy structure and have the potential to aid LIDAR and SAR measurements of forest volume and biomass.

Dense forests represent a challenge to satellite estimation of forest volume and biomass. Scientists seek to overcome this challenge by several means. Three approaches have shown medium to high accuracy when used in dense forests:

- long-wavelength SAR;
- measurements of forest canopy height using LIDAR or interferometric SAR (InSAR) sensors; and
- fusions of active and passive imagery.

Future satellite launches of LIDAR, long wavelength SAR, and InSAR sensors will significantly improve estimates of biomass, forest volume, and carbon in the near term and may provide information crucial to the development of a global, ground-level elevation model. If such a model were available, scientists could create accurate, worldwide maps of forest height and, in turn, generate global reference maps that estimate historical forest biomass as far back as the mid-1990s.

Summary and Conclusions

It is possible to improve global measurements of forest area, structure, biomass, and carbon using remote sensing technologies that are currently available or expected to be in use between 2009 and 2015 (see table on page vi). We are capable of generating highly accurate measurements of forest area now; technical developments over the next six years will increase the frequency of moderate-resolution forest imagery and improve our ability to analyze the data generated. These developments will facilitate discrimination between forest types and the detection of temporal changes. Refining the accuracy of coarse-resolution maps and developing an accurate moderate-resolution, global forest map over the next several years could improve forest area measurements. Such an effort would improve the quality of world forest maps tenfold; we could create moderate-resolution world forest maps going back to 1975, as we have already done for the United States and other countries. Historical maps would serve as baselines from which to measure and monitor changes in forest area.

Today, forest volume, biomass, and carbon stocks can only be estimated conservatively and the accuracy is extremely variable (see table on page vi) depending on the study and methods used—although recent imagery fusions show promise. Integration with high-quality forest inventory and LIDAR data is essential for improving biomass estimates from satellites. Worldwide collection of forest inventory data is necessary to achieve acceptably accurate global estimates of forest volume, biomass, and carbon from current satellite imagery. Future SAR and LIDAR satellite launches, such as DESDynI, BIOMASS, and SAR constellations, are expected to achieve good to high accuracy in mapping forest volume and biomass. However, it will be necessary to validate these estimates with extensive ground-truth data and supplement them with historical reference maps of biomass. A coordinated global effort is needed to achieve these objectives.

For decades, the only institutional effort to generate global forest measurements was the inventory assembled by the Food and Agriculture Organization of the United Nations (FAO). Despite the best efforts of the FAO, these estimates are widely recognized as inaccurate. Nations self-report their forest inventories and differ in how they define forests as well as give technical means, funding, and priority to the measurement. To fill gaps in data or reconcile conflicting data, the FAO often must depend on untested assumptions, the chance of data aggregation errors, and changes in the definition of what constitutes a forest. If we are to understand forest ecosystems—and if we hope to understand the planetary carbon budget and the role that forests play in modulating climate—we must improve our ability to measure and monitor forest volume, biomass, carbon, and trends. Remote sensing has a strong track record in global forest measurement and planned sensor launches offer even greater potential. A technical approach that integrates satellite and ground-truth data—and an institutional means to implement it—will enable accurate, global monitoring of the world's forests for the first time in history.

Expected Improvements in Accuracy in Remote Sensing of Global Forest Identity

Identity	Sensors	Current (2009) capability	Limitations	Expected (2009–2015) capability	Limitations
Area	**Optical and radar, moderate resolution**	>80% accuracy for forest/nonforest maps at moderate resolution (~30–50 m pixels).	Lack of detailed global forest types. Current coarse-resolution maps have more detail, but ~65% accuracy.[a]	>80% accuracy for global maps of nonforest and several forest types, at moderate resolution (30 m).	Availability of free, moderate-resolution imagery depends on a few key satellites (e.g. LDCM).
	Optical, high resolution	>90% accuracy for forest/nonforest maps.[b]	Many images are needed to map large areas:[c] images are difficult to standardize for analysis.	A global set of high-resolution images will be gathered by 2015.	Difficulties in standardization are likely to persist, limiting use for global mapping.
Volume	**Optical, high resolution**	40–90% accuracy for forest volume estimates.	See above. Accuracy is low in closed forests with tree canopy overlap.	See above. Regional equations correcting for canopy overlap may be developed.	See above.
	SAR (Radar)	50–95% accuracy; >80% is common for forest volume.	Limited to low-biomass forests; higher biomass decreases accuracy.	>80% accuracy in dense, high biomass forests.[d]	Accurate volume estimates require the launch of a few key satellites.[e]
	InSAR (Radar-derived height)	30–80% accuracy for forest volume estimates (from forest height).	Lack of ground elevation data prevents global forest height/volume estimation.	The amount/diversity of InSAR data will increase.[d] Processing innovations may create ground elevation maps.	A global ground elevation map may be difficult to develop.
	LIDAR (Laser-derived height)	45–97% accuracy; >80% accuracy is common for forest volume.	LIDAR sampling is spatially limited, data intensive, and expensive.	Global sampling of forest and ground height will come from new satellite sensors.[f]	Satellite sensors will be spatially limited; global LIDAR coverage requires expensive aerial platforms.
Biomass	Same sensors and accuracy as volume; estimated through correlation with ground-truth points.[g]				
Carbon	Same as biomass; estimated through a standard conversion from biomass, with minor inaccuracy (+/-8% max).				

Notes: [a] Forest types are general (e.g., deciduous forest) in global coarse-resolution maps (>200 m pixels). Their forest/nonforest accuracy is 70–80%.

[b] Currently, forest-type mapping accuracy for high-resolution imagery is similar to that of moderate-resolution imagery.

[c] A very large number of expensive images are needed to create a global map (see Table 5). Global image coverage does not currently exist.

[d] Advances in satellite technology and image processing will allow fusing of InSAR and SAR for synergy in volume/biomass estimation.

[e] These include DESDynI and BIOMASS. Innovations in processing SAR imagery from multiple satellites may also improve volume estimates.

[f] Global LIDAR sampling of forest volume will allow synergy with forest type maps for regional forest volume estimation.

[g] Accurate ground-truth points from forest inventory data are critical to any effort to measure forests using remote sensing (see Section 5.1.5).

Chapter 1. Forests, Their Measurement, and the Need for Global Remote Sensing

Sometimes, if you stand on the bottom rail of a bridge and lean over to watch the river slipping slowly away beneath you, you will suddenly know everything there is to be known.

-Winnie the Pooh

1.1 Current Needs for Forest Monitoring

Forest ecosystems are fundamentally important to humanity. They moderate the climate, protect streams and soil, generate oxygen, supply wood and other products, provide beauty and recreation, and house a treasure-trove of biodiversity. We depend on forests for their ecosystem services—and have done so since the dawn of civilization. It is surprising, then, that we know so little about the global status of forests. We can make more current and informative maps of Mars than of the Amazon basin or the Russian boreal forest. There are several reasons for the gaps in our knowledge:

- a dearth (until relatively recently) of tools to observe the world on a global scale,
- a historical lack of interest in forests by the political and economic communities (with the exception of timber companies),
- poor and inconsistent records of global forest cover, and
- an absence of a concerted effort to systematically inventory and monitor the world's forests.

Maturing observation technologies and intense public interest in protecting and managing forests make this the time to explore and better understand the world's forests.

In this report, we evaluate current and upcoming (2009–2015) technologies for measuring and monitoring global forests. We focus primarily on remote sensing (which we define as the analysis of satellite and aerial images) because this technology meets the steep logistical challenge of measuring the world's forests in an accurate, repeatable, and inexpensive manner. Remote sensing extends existing ground data to expand our understanding of forests beyond geographically localized areas. Remote sensing is a rapidly developing field driven by technological advancements in data gathering and processing and has already yielded many important discoveries in recent decades about the changing Earth.

Many critical questions about the world's forests remain understudied by forest scientists. We focus on the observations needed to provide accurate, basic measures of forest attributes to inform forest scientists, decisionmakers, and the public. We also illustrate how the resulting data would address compelling questions that persist about our forests.

Which countries are gaining and losing forests, and why?

We begin with this simple question because it is often at the heart of public understanding of the status of the world's forests. For instance, loss of rainforest in tropical regions is often in the

news. Yet at present, national statistics track only net changes in forest cover and hide forest loss in countries undergoing reforestation and forest regrowth (Grainger 2008). In addition, country-measured statistics on forest attributes have often been inconsistent and unreliable. As a result, long-term changes are difficult to track (Waggoner 2009). It is clear that an increase in forest cover after a long period of deforestation occurred in the United States and Europe in recent centuries (Rudel et al. 2005). More recent forest transitions in temperate and tropical countries are disputed because of uncertain forest statistics (Grainger 2008; Rudel et al. 2005). Improved and continued global forest monitoring and careful analysis of archival remote sensing imagery would allow more accurate forest measures.

How are forest loss, forest regrowth, and the replacement of forests by tree plantations affecting forest biodiversity?

Remote sensing measurements of forest area indicate a decline in tropical forest area from at least the 1980s onward, and forest regrowth has compensated for only some of the forest loss (Mayaux et al. 2005; DeFries et al. 2002; Hansen et al. 2008b). Characterizing the response of tropical biodiversity to deforestation and regrowth has been difficult because we lack extensive data on the movement of forest species across fragmented landscapes and on the conservation value of human-modified habitats (Chazdon et al. 2009; Gardner et al. 2008). Even the area of tropical forest regrowth today is debated (Grainger 2008; Asner et al. in press) because of difficulties in distinguishing regrowth and tree plantations (Sanchez-Azofeifa et al. 2009). In other types of forests, evidence suggests that species-rich mature (old-growth) temperate forests are in decline, but there is limited global measurement of the rate of this decline or of logging disturbance in mature forests (FAO 2006; GOFC-GOLD 2008). Improved and systematically collected, well-calibrated observations about forests will enhance our ability to monitor and understand these changes. New remote sensing analyses of human-modified landscapes could set conservation priorities and improve predictions of species persistence in modified landscapes.

How will changes in forest cover affect climate patterns, and how will forests respond to climate change?

The idea that deforestation decreases rainfall is an old one (Marsh 1878), but it was difficult to scientifically test the idea until the advent of climate circulation models and regional forest maps (e.g., Malhi et al. 2009; Ramos da Silva et al. 2008). In Brazil, models predict that deforestation of approximately 40 percent of the Amazon rainforest would result in a large decline in rainfall throughout the basin and have notable consequences for agriculture in the eastern portion (Ramos da Silva et al. 2008). In Canada, increases in boreal forest cover may actually increase regional warming (Bala et al. 2007). Evaluating the effects of different patterns of deforestation on precipitation requires detailed, updated forest maps in areas that often have high cloud cover and rapid land-use change.

Forests will be a key indicator of change as climate change advances. Forests will continue to undergo changes in phenology (the timing of leaf-out and leaf-fall), productivity, and flammability (Goetz et al. 2005; Phillips et al. 2009). Coupled climate–carbon models predict a marked increase in respiration in tropical forests with warming and drying, which may set in place a positive feedback (Tian et al. 1998; Field et al. 2007). In the case of boreal and temperate forests, climate change is expected to drive significant range shifts and forest expansion in high latitudes (Loehle 2000; MacDonald et al. 2008). Coordinated monitoring of forests would create a valuable record of

the effect of climate change on natural systems and provide a warning indicator of sudden shifts, such as changes in leaf water content before forest fires (Chuvieco 2008).

How do forests contribute to the global carbon budget and the "missing sink," and how can forest carbon be measured and valued to mitigate climate change?

Terrestrial ecosystems absorb carbon dioxide through vegetation growth and emit carbon dioxide through metabolism and decay (respiration) and land-cover change (e.g., deforestation). The amount of carbon stored in vegetation (its carbon stock) is roughly equivalent to the amount stored in the atmosphere, and about 87 percent of the carbon in aboveground vegetation is stored in forests (Houghton 2007; Le Toan et al. 2008). Strong evidence suggests that the terrestrial ecosystem has functioned as a carbon sink for the last 25 years, taking up almost a third of anthropogenic emissions (Canadell et al. 2007). However, the exact size and cause of this "missing sink" is not well known because the uncertainty in carbon sink and emissions estimates is very high (Canadell et al. 2007; Le Toan et al. 2008). Although evidence suggests a large carbon sink in the regrowing forests in the Northern Hemisphere, sinks in the tropics may also be important (Fan et al. 1998; House et al. 2003). Recent evidence suggests that this terrestrial "braking" on accelerating human fossil-fuel emissions may be decreasing (Canadell et al. 2007), but without sound estimates of its original size, it is difficult to project what impact losing the missing sink will have on global climate change (Le Toan et al. 2008).

A range of 7 percent to 30 percent appears to characterize the role of forest destruction in anthropogenic emissions (Canadell et al. 2007; IPCC 2007). There is intense interest in quantifying forest carbon for an international trading framework on reduced emissions (Herold and Johns 2007; Olander et al. 2008; Gibbs et al. 2007). Extrapolating from ground-based plots underestimates spatial variation in forest carbon (Houghton et al. 2001; Houghton 2005), and ground data must be supplemented by accurate, real-time maps of forest area and biomass (Waggoner 2009; Gibbs et al. 2007).

What is the impact of forest cover on streamflows and erosion protection?

Although it is commonly accepted that forests play a significant role in protecting watersheds, there is relatively little evidence relating forest cover to flooding (Laurance 2007). Forest mapping and monitoring is critical to relating land-use change to ongoing measurements of water quantity and quality. Active areas of research include the effective width and continuity of riparian buffers and the best configuration of regional forest cover to minimize soil erosion (Allan 2004). To improve our understanding of hydrology, erosion, and forests, we need to obtain more detailed measures of forest attributes and monitor forests in a systematic way to detect changes.

How can rapid fire-detection and other forest observations by satellite improve forest management and certification?

Satellite technology is capable of revolutionizing the management of forest areas. Real-time fire-detection systems could help combat wildfire and illegal clearing in remote forests, and high-resolution imagery could improve monitoring and verification of forest management for sustainable harvest and carbon sequestration (Davies et al. 2009; Souza and Roberts 2005a).

1.2 A Brief History of Global Forest Measurement and Remote Sensing

Terrestrial ecosystems are the single greatest source of uncertainty in the global carbon budget (IPCC 2007). The total area of the global forest, its trend in recent years, the amount of biomass and carbon locked up in our forests—all these estimates, which would seem basic scientific knowledge, are poorly known (Grainger 2008; Houghton 2005).

There is strong evidence that forests once covered many modern agricultural and arid landscapes, but regular monitoring of global forest area did not begin until the twentieth century (Williams 2008). The Food and Agriculture Organization of the United Nations (FAO) started reporting information about global forests in 1948, publishing an inventory every five years until 1963, when the effort was halted because of poor tropical forest data (Grainger 2008). The FAO published two assessments of global forest resources in the 1970s (Mayaux et al. 2005), then resumed regular reporting in 1981. The organization published Forest Resource Assessments (FRA) for 1980, 1990, 2000, and 2005 (Grainger 2008). FAO reports have been widely criticized for inaccuracy (for example, see Waggoner 2009); errors in estimating forest area are attributed to changes in definitions of forests, revisions of estimates based on conflicting data, unreliable national inventory estimates, and data aggregation errors (Grainger 2008; Houghton 2005). Historical FAO estimates of forest area are demonstrably assumption-dependent and do not exist for some countries (Grainger 2008; Houghton 2005). As Waggoner (2009) points out, it is unclear from FAO statistics whether global forest area is declining or growing.

Remote sensing of forests began in 1972 with the launch of Landsat, the first in a series of Earth observations satellites in the Landsat program (DeFries 2008). The first continental scale maps of land cover were produced by Tucker et al. (1985) and Townshend et al. (1987) from 4 kilometer (km) resolution imagery from the Advanced Very High Resolution Radiometer (AVHRR) satellite, followed by the first global land-cover map from DeFries and Townshend (1994) at 1 degree resolution using AVHRR imagery. Loveland et al. (1999) produced a 1.1 km resolution global land-cover map from AVHRR satellite imagery, followed by several global land-cover maps at 0.5–1 km resolution (reviewed in Mayaux et al. 2005 and Achard et al. 2007). The highest-resolution global land-cover map to date was produced in 2007 using data from Europe's Medium Resolution Imaging Spectrometer (MERIS) on the Environmental Satellite (Envisat) spacecraft (Bicheron et al. 2008). That map has a resolution of 300 meters (m).

In addition to these global mapping efforts, numerous satellite imagery studies have monitored global forest area, especially in tropical areas (e.g., DeFries et al. 2002; Hansen et al. 2008b; Achard et al. 2007; Mayaux et al. 2005). All satellite-based estimates have supported the FAO's assertion that net tropical forest area has been declining for the last three decades (Mayaux et al. 2005; DeFries et al. 2002; Hansen et al. 2008b). For the 2000 FRA reports, the FAO sampled 10 percent of the global forest using satellite imagery, but these data were insufficient for national estimation in many countries (Tucker and Townshend 2000). For the 2010 FRA, the satellite observation effort has been expanded globally to sample forest cover at latitudinal grid intersections (Mayaux et al. 2005). Because tropical deforestation is spatially concentrated near roads and agricultural frontiers, this analysis will only capture national deforestation trends in larger countries (Achard et al. 2007; Tucker and Townshend 2000).

1.3 Diversity of Forest Types

The boreal, temperate, and tropical forests are estimated to contain about half of the terrestrial carbon with the majority of forest carbon stored in forest soils. The amount of carbon stored in forest soils varies by region because of temperature (see Table 1; Malhi et al. 1999). In boreal forests, aboveground forest carbon is the tip of an iceberg of soil carbon; low soil temperatures and forest shade slow decay and the release of soil carbon. The open boreal forest, which is composed of conifers and a few species of deciduous trees, stretches across the northern high latitudes (Malhi et al. 1999). Clouds, long northern winters, and short growing seasons make some types of satellite observation of higher latitudes difficult (Kasischke and French 1997).

Table 1. Comparison of Estimated Area and Carbon Stocks of Forests at Different Latitudes

Latitude (forest type)	Area (million hectares)	Carbon density: vegetation (tons/hectare)	Carbon density: soils (tons/hectare)	Carbon stock: vegetation (gigatons)	Carbon Stock: soils (gigatons)
High (boreal forest)	1,372	65	343	88	471
Middle (temperate forest)	1,038	57	96	59	100
Low (tropical forest)	1,755	121	123	212	216
Sum total	4,165			359	787

Source: Dixon et al. 1994.

The temperate forests, with shorter winters, encompass deciduous forests, conifer-dominated forests, and forests of broadleaf evergreens in drier areas (Malhi et al. 1999). Widespread historical clearing of temperate forests emitted significant amounts of carbon dioxide into the air from biomass burning and disturbance to carbon-rich forest soils (Houghton 2007). The term "secondary forest" describes forests that are regrowing after a disturbance, such as logging or fire. Much of the recent carbon uptake in northern latitudes is believed to reside in secondary forests, which are growing larger and storing soil carbon (Houghton 2005; Fan et al. 1998). Satellite observations have difficulty detecting small changes in tree height and diameter in growing forests (Houghton 2005).

Highly biodiverse tropical forests cover a large band around Earth's rainy equator and can be classified by elevation (montane forests), tolerance (flooded forests, mangroves), and the length of the dry season, which can be nonexistent (evergreen tropical rain forest) or several months long (deciduous tropical dry forest). The most common forest type, tropical rain forest, is characterized by tall trees (>30 m), dense canopies, and very high biodiversity (Malhi et al. 1999). Tropical forests have been rapidly cleared in recent decades and about half of their carbon is stored in their living mass, which is emitted when they are cleared (Malhi et al. 1999; DeFries et al. 2002). Tropical forests evaporate (or transpire) immense amounts of water from their leaves. An estimated 50 percent of the rain in the Amazon basin is from transpiration (Salati and Vose 1984). The intense, daily cloudiness of tropical forests blocks the view of many types of satellites and decreases the frequency of clear, cloud-free images (Asner 2001; Olander et al. 2008).

1.4 For Global Forest Measurement, Why Use Satellite Imagery?

To measure forests globally, satellite imagery is a practical necessity. Both aerial and ground observations are expensive at present and only cover small areas at a time; ground measurements are simply impossible over such a large land area (Houghton 2005; Patenaude et al. 2005). Detecting rapid changes in the area of remote tropical forests (both deforestation and regrowth) requires satellite mapping (Achard et al. 2007), as will detecting the northern expansion of boreal forests in a warming world (MacDonald et al. 2008). The greatest strengths of satellite-based measurements are their unparalleled, unbiased measurements, their monthly to daily frequency, and—above all—their synoptic nature. Satellites provide a general view of the whole Earth that is unavailable to any other forest measurement method. For example, satellite imagery is well suited for detecting country-level deforestation in a REDD (reducing emissions from deforestation and forest degradation) agreement (Olander et al. 2008), but also detects forest invasions of rangeland, for example, or forest regrowth after the abandonment of farmland (Houghton 2005).

Satellites can measure forest quantities, like canopy chemistry or daily leaf phenology, that are arduous or impossible to collect with ground crews (Ustin et al. 2004; DeFries 2008). Although hand-collected forest data are often more accurate than satellite measurements at the point and time the data are obtained, satellites collect data across broad areas, sampling the full range of variation in forest metrics and capturing broad trends and dynamic change in the world's forests (Houghton 2005). As such, satellite data allow for integration across ground measurements, extending them to the global forest. Put simply, satellite imagery measures forests on continental scales, detects changes in forests that we do not expect or could not measure, and detects them in real time.

1.5 Scope and Purpose

In this report, we evaluate the current and future technical capacity of satellite imagery to measure and monitor global forests. Other researchers have provided extensive reviews of current capacity (Andersson et al. 2009; Sanchez-Azofeifa et al. 2009; Herold et al. 2008; Olander et al. 2008; Achard et al. 2007; DeFries et al. 2007; Patenaude et al. 2006; Mayaux et al. 2005; Rosenqvist et al. 2003), and we summarize their findings here. We also predict future capacity from expected satellite launches and technological developments during 2009–2015. This time window effectively captures in-development satellite technology (although satellites rarely launch on time) and allows an in-depth look at how well we will be able to measure the world's forests in the coming years.

The widespread uncertainties in current forest measurement make improvements in global forest monitoring a scientific imperative. This report focuses on observations of forest area, biomass, and carbon, addressing the capacity of satellite imagery to answer questions posed above (Section 1.1). There are many characteristics of forests that are not well estimated globally and are worth monitoring (Chuvieco 2008; Myneni et al. 2007; Gardner et al. 2007; Phillips et al. 2009), including several that are important for answering individual questions above (e.g., fragmentation and forest biodiversity). Forest area, biomass, and carbon are basic forest measurements that are fundamental to answering scientific questions about forests (Kauppi et al. 2006). As such, they represent a critical first step in global forest measurement.

Chapter 2. Remote Sensing and Forest Measurement: An Overview

This chapter is intended as a brief introduction to remote sensing and an overview of current and emerging sensor technologies—those already familiar with the topic should begin with section 2.4. Remote sensing is generally defined as observing and analyzing a distant target using information from the electromagnetic spectrum (Jensen 2007). Remote sensing for forest measurement is mainly conducted from airborne and satellite missions (Jensen 2007; CEOS 2009; Patenaude et al. 2005; Olander et al. 2008). We use remote sensing in this restricted sense as observations obtained from aircraft and satellites. In remote sensing terminology, the hardware that obtains the observations is referred to as an instrument, or a sensor, and is mounted on a plane or satellite. Remote sensing produces images of Earth's surface for analysis and interpretation. Analysis may range from qualitative observations from trained image interpreters to quantitative measurements from complicated computer algorithms. By analyzing multiple images of the same location, remote sensing detects land-cover change (modifications in the biophysical cover of Earth) over time.

2.1 Comparing Satellite and Airborne Remote Sensing

Satellite- and airborne-mounted sensors differ dramatically in their altitude, image coverage, costs, and spatial resolution. Spatial resolution is defined as the Earth area represented in one pixel of a remote sensing image (see Figure 1 for a comparison of different resolution sensors). Airborne sensors function at a much lower altitude than satellite sensors and as a result have a much smaller image coverage, or swath, than satellite-mounted sensors. For example, aerially mounted sensors have a swath of 5–11 km, whereas the coverage of satellite-mounted sensors is 15–3,000 km (Appendix). Airborne sensors are also limited by fuel cost and range, crew logistics, weather, and the need for national permission to fly and take images. Satellites orbit repeatedly around the entire globe and their sensors image regardless of weather. Because of provisions in the 1967 U.N. Outer Space Treaty (UNOOSA 2009), it is not necessary to obtain permission before taking satellite images of any country. By contrast, overflight permissions are required for aerial sensors. As there are no expenses for crew and fuel, satellites have much lower operational costs and can image much larger areas for a fraction of the price of airborne missions (Patenaude et al. 2005; see Table 2 for a cost comparison).

Airborne missions do have some advantages over satellite missions. Airborne missions are much cheaper to launch, because the sensor is the main expense in developing the mission. Satellite missions, by contrast, cost hundreds of millions of dollars to construct and launch into orbit, and unsuccessful launches do occur (Table 2). In addition, airborne missions often provide higher-quality data than satellite missions. Because a sensor mounted on a plane is closer to the Earth, the identical sensor will have higher resolution than if it were mounted on a satellite. Airborne missions are also more flexible in their flight path and instrumentation than satellites. Satellites must follow a fixed orbital path (see Figure 2a), but planes can time their missions to avoid cloud cover. Updating instruments—say, to use new technology—is also easier for airborne missions than on orbiting satellites. As a result, planes often carry newer sensor technology than satellites do. Interest has been growing in unmanned aerial systems (UAS) for active sensors (see next section);

unmanned systems have longer flight duration per mission and can fly at night but are more costly to purchase and operate than equivalent satellite imagery (Swanson et al. 2009).

Figure 1. An Image Taken with Different Spatial-Resolution Sensors

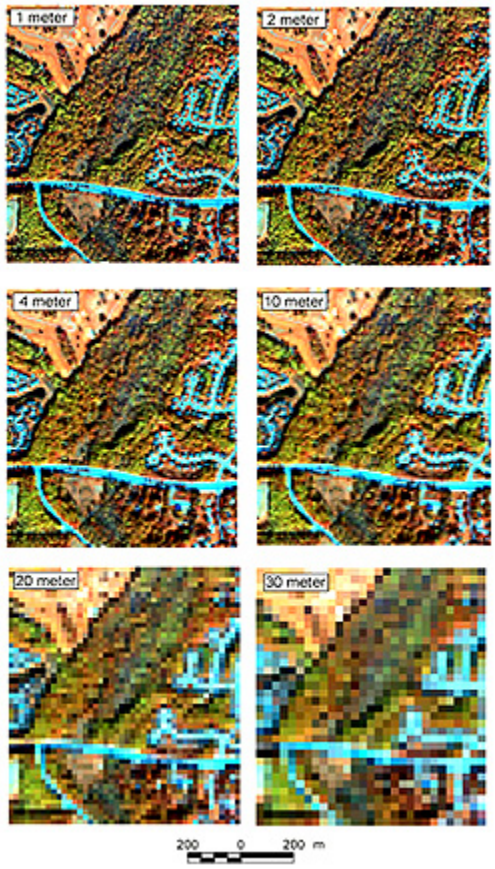

Source: Short 2009.

In summary, airborne missions are relatively expensive to conduct and do not cover a broad area but are flexible and can provide high quality data (Olander et al. 2008; Andersson et al. 2009). Satellites can monitor a broad area less expensively and thus are viewed as the best way to measure global forests remotely (Olander et al. 2008; Andersson et al. 2009; DeFries 2008; Sanchez-Azofeifa et al. 2009). With approximately four billion hectares of forest area, any global effort to measure the world's forests will have to rely heavily on satellite-based remote sensing, with airborne data used as a supplement in areas where satellite data are lacking in quality, coverage, or accuracy.

Table 2. Cost Comparison of Airborne, Ground, and Satellite Data for Forest Inventory over the United Kingdom

	Monitoring from remote sensing	Forest area (square kilometers, km^2)	Approximate Costs[a]				
			Ground survey[b]	Optical[c]	Radar		LIDAR (light detection and ranging laser)
				Satellite	*Airborne*	*Satellite or Shuttle* [c]	*Airborne*
				~£0.10/km^2	~£250/km^2	~£0.10/km^2	~£300/km^2
Alberta Ground Cover Characterization (AGCC) loss from Article 3.3 D activities	Total UK forest area plus afforestation and reforestation (AR) since 1990	28,000	~£3,500,000	Less than ~£3,000	~£7,000,000	Less than ~£3,000	~£8,400,000
AGCC gains from Article 3.3 AR activities (forest growth only)	All UK forest area planted after December 1989	4,500	~£307,000	Less than ~£1,000	~£615,000	Less than ~£1,000	~£738,000
AGCC gains from Article 3.4 FM activities (forest growth only)[d]	All UK forest area planted after 1940[e]	19,245	~£1,822,000	Less than ~£2,000	~£3,644,000	Less than ~£2,000	~£4,373,000

Notes: Data for 2002. AGCC (aboveground carbon content); D (deforestation); AR (afforestation and reforestation); FM (forest management).

a Costs, rounded to the £1,000 , provide guidance only and are for image acquisition without processing. Costs are for acquiring one dataset only (i.e., for forest to non-forest land cover change detection, at least two datasets are required).
b Medium resolution (15-50 m).
c Data collection only, no processing. Estimates based on costs for generating the Country Side Survey 2000, http://www.cs2000.org.uk/ (Steve Smith, 2004, personal communication).
d Only if FM elected by the UK.
e Based on the assumption that all forests above 50 years of age have reached maturity and do not contribute significantly to the carbon sink, i.e., trees planted in 1970 contribute "significantly" as a sink for 30 years after 1990.

Source: Patenaude et al. 2005.

Figure 2a. Pointable Satellites Can Image Many Targets Off Their Orbit by Tilting Their Sensor

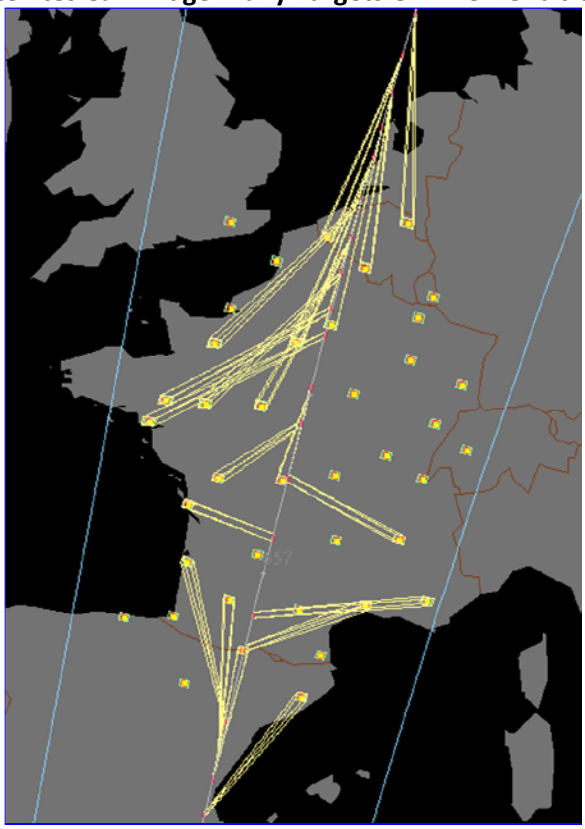

Note: The Pleiades satellite (20 km swath) is shown here.

Figure 2b. Satellite Constellation over Earth

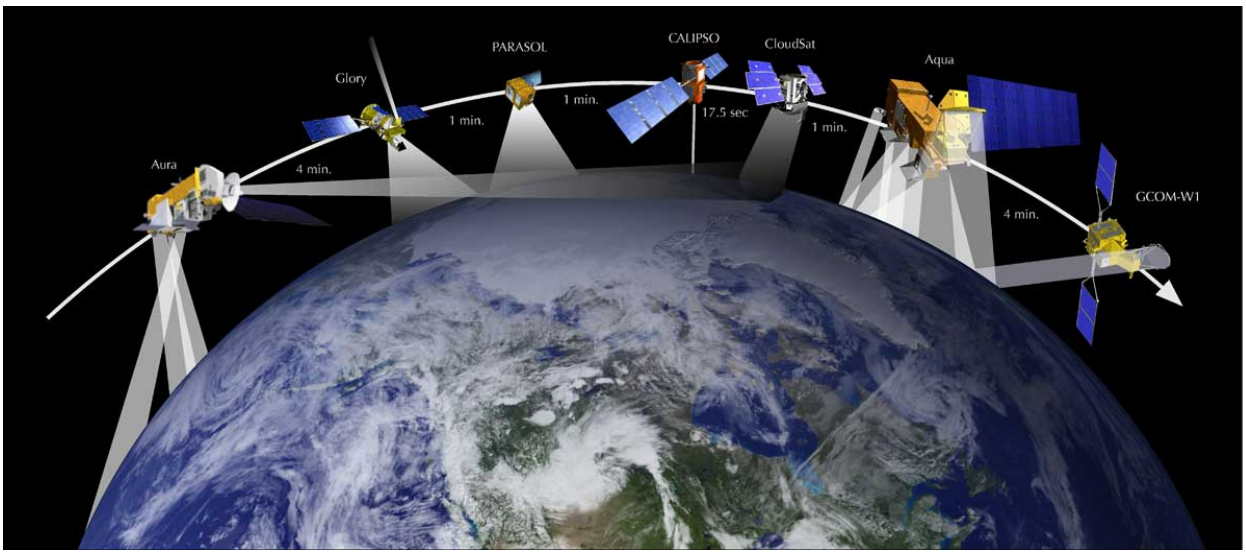

Source: Image courtesy of NASA. Credit: Ed Hanka.

2.2 Passive and Active Remote Sensing: An Overview

Remote sensing instruments come in two main varieties: passive and active. Passive sensors, like cameras, receive reflected and emitted electromagnetic energy from the Earth, and include optical and thermal sensors (Jensen 2007; see Figure 3). Active sensors aim electromagnetic radiation, such as laser light or microwaves, toward Earth and read the reflected radiation, operating much like a laser range finder or sonar (Jensen 2007, see Figure 4).

Figure 3. Comparison of Spectrums of Vegetation, Bare Soil, Snow, and Water

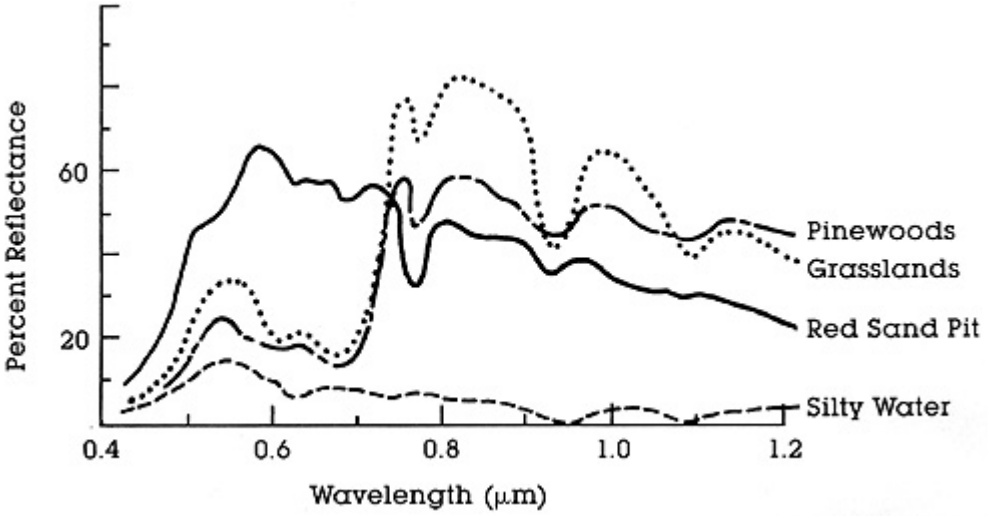

Note: Note the strong increase in reflectance of near-infrared radiation by the pines and grasses, which is diagnostic of vegetation.
Source: Short 2009.

Figure 4. Polarization of SAR Waves (HV example)

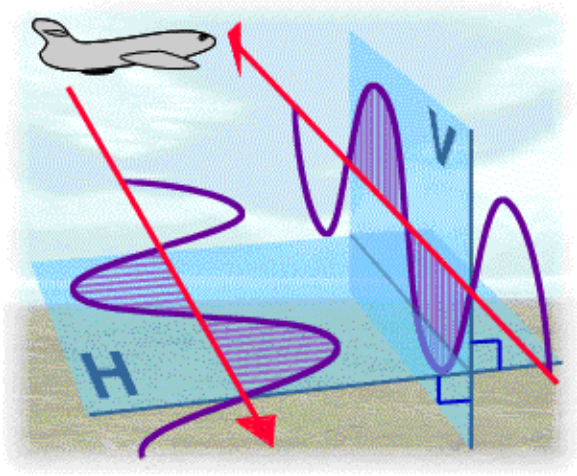

Source: Natural Resources Canada 2005.

2.2.1 Passive Remote Sensors: Considerations and Limitations

Passive sensors can capture a wide range of the electromagnetic spectrum that comes from Earth, from reflected visible light (0.4–0.7 micrometers, abbreviated as μm) to reflected near-infrared radiation (0.7–1.3 μm), reflected short-wave infrared (1.3–3 μm), and emitted thermal infrared (3–14 μm). The electromagnetic radiation that sensors receive has already interacted with the Earth's surface (primarily through chemical absorption and physical scattering), so it contains information about chemical and physical properties of the surface (Figure 3; Jensen 2007). For example, passive sensors can distinguish vegetation, bare soil, snow, and water quite easily, all based on their relative reflection across the electromagnetic spectrum (see Figure 3 for a partial comparison). As a result, passive sensors excel at detecting changes in land cover (Hansen et al. 2008b; Cohen and Goward 2004; Asner et al. 2005), vegetation phenology (Myneni et al. 2007; Soudani et al. 2008), and differences in ecosystem type (Patenaude et al. 2005).

Current passive sensors are not uniformly sensitive to all regions of the spectrum; they receive most strongly in certain bands of the spectrum, which may be narrow (e.g., 0.415–0.42 μm) or broad (e.g., 0.4–0.7 μm). For example, a broadband sensor that received all visible light (0.4–0.7 μm) equally would image the Earth in black and white. By contrast, the Landsat multispectral sensor has six bands of intermediate width that are spread from the visible (blue, green, red) through near- and thermal-infrared wavelengths (see Figure 5 for a comparison of the bands of different satellites). Hyperspectral sensors, a relatively new technology, have very high spectral resolution and measure hundreds of narrow bands that are quite sensitive to chemical absorption signatures (Figure 5).

Figure 5. Bandwidth of Multispectral versus Hyperspectral Satellites

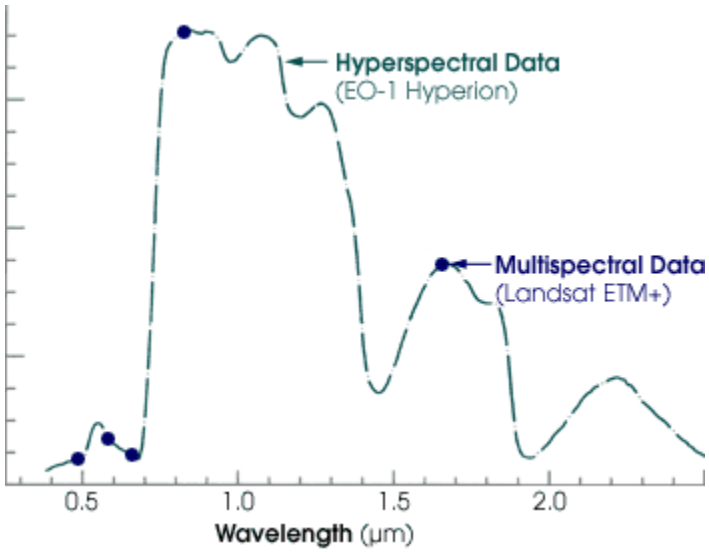

Note: The multispectral bands indicated here are only shown as center points, but they are actually quite wide. Hyperspectral sensors have tens to hundreds of narrow bands and are able to produce a continuous spectrum.
Source: NASA 2009b. Graph by Robert Simmon.

Passive optical sensors vary dramatically in their spatial resolution as well as their spectral resolution. These sensors are classed as high resolution (images with pixels 0.4–10 m in width), moderate resolution (10–200 m), or coarse resolution (>200 m) (Figure 1, Appendix). Because of technological tradeoffs that are unlikely to change in the near future, the spatial resolution of passive sensors is inversely related to the dimension of the swath they can capture (Andersson et al. 2009; Rosenqvist et al. 2003; CEOS 2009; see Figure 6. At one extreme are the commercial high-resolution satellites like GeoEye-1, which has a maximum resolution of 0.41 m and an image width of 15.2 km. At the other extreme are the coarse-resolution sensors like AVHRR, which has a resolution of 1.1 km and an image width of 3000 km. Some geostationary satellites can image the entire Earth disc at 1 km resolution. (Geostationary satellites orbit at a high altitude above the equator and are synchronized with Earth's rotation, allowing them to operate as if fixed over one point on Earth.) Moderate-resolution sensors split the difference between the two extremes. Landsat 5, for example, has a resolution of 30 m and an image width of 185 km. Observing the entire Earth using a high-resolution sensor is like using a telescope to observe the entire landscape below a promontory—detail is high, but it takes a long time to see everything. In the same analogy, using coarse resolution sensors to observe Earth is like viewing a landscape through binoculars.

Figure 6. Spatial Resolution, Cost, and Swath for Current Optical Satellite Sensors

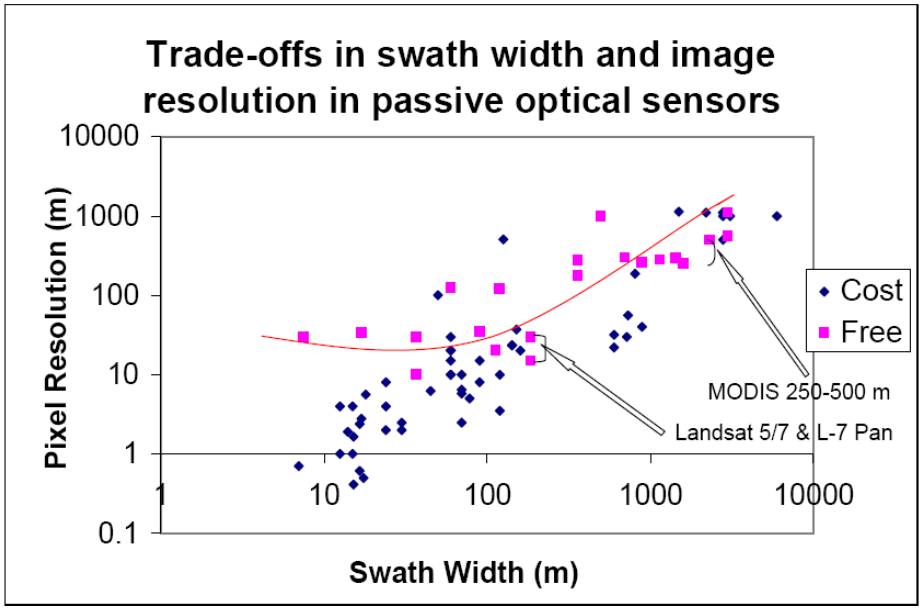

Notes: All data is from the Appendix. Due to changing prices, cost is simply noted as free or not free ("cost"). Both axes are logarithmic for display purposes. The red line highlights good performance among free sensors. Higher resolution sensors face steep tradeoffs in smaller image swath.

For satellites, this tradeoff in spatial resolution and image size also extends, with exceptions, to the time it takes for a satellite to image the same location on Earth (the return time). Polar-orbiting satellites have an orbit that crosses both the Earth's poles, allowing the spacecraft to image Earth in successive north-oriented strips as the planet turns underneath the craft's orbit (Figure 7a). By orbiting at different speeds and angles, satellites generally space their observations to match the width of their imaging window (Figure 7b). Coarse-resolution satellites, therefore, can image the

entire Earth quickly and revisit the same location every few days. More moderate-resolution satellites can take 10 to 20 days to revisit a location (see Appendix).

Figure 7a. Example of a Fixed Polar Orbit—Landsat satellite

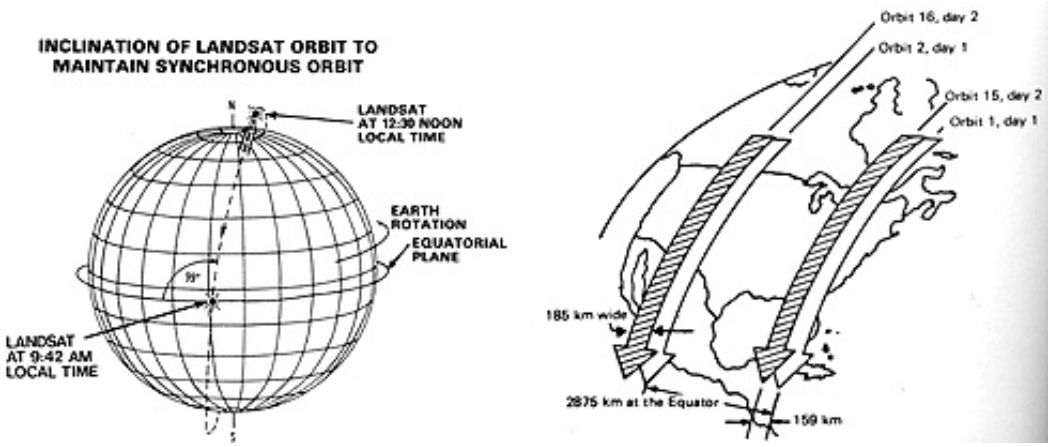

Source: Short 2009.

Figure 7b. Satellite Orbits are Spaced to Fit the Image Swath

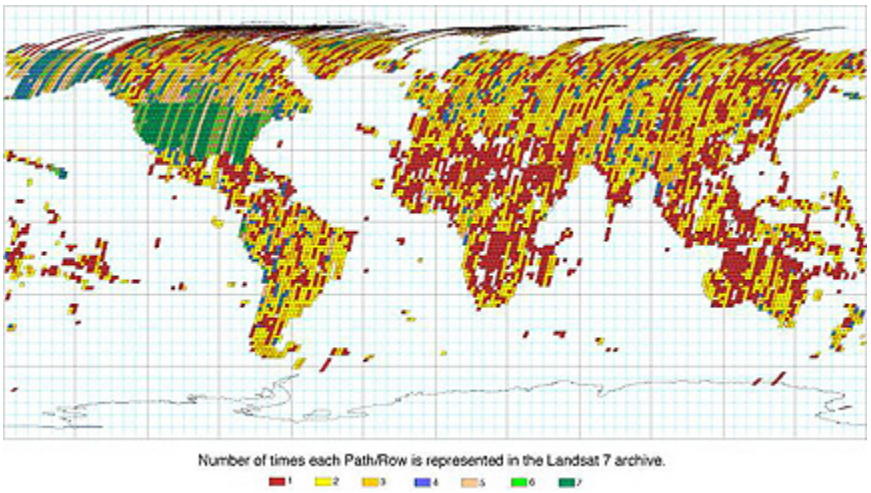

Source: Short 2009.

The exceptions to the image size–return time tradeoff include unusual orbits, pointable satellites, and satellite constellations. Some satellites have unusual orbits that allow frequent revisits of certain locations; for example, geostationary satellites observe the same location in real time. Pointable satellites can image the same spot from several orbits away by turning on their sides (Figure 2a). Satellite constellations are groups of satellites that, when entrained in the same orbit, fly over a location with great frequency (Figure 2b).

Return time is very important to passive sensors, because clouds interfere with the reflection of radiation. The only way for passive, satellite-mounted sensors to acquire a cloud-free image is to return frequently enough to capture all of the landscape without clouds. This is especially true in tropical areas, which are covered by clouds for most of the year (Asner 2001; Olander et al. 2008).

2.2.2 Active Remote Sensors: Considerations and Limitations

Active sensors emit electromagnetic radiation toward Earth, typically microwaves (known as synthetic aperture radar, or SAR) or lasers (light detection and ranging, known as LIDAR), and then receive the reflection of their emitted energy. Unlike passive sensors, active sensors are able to penetrate clouds (although LIDAR is cloud-sensitive) and image during both day and night (before daily convective cloud building). Active sensors thus have a major advantage in tropical areas (Rosenqvist et al. 2003; Olander et al. 2008). In general, active sensors explicitly measure the three-dimensional shape and texture of ecosystems but have difficulty with topography. In addition, images from active sensors are typically more challenging to analyze than images from optical images (Kasischke et al. 1997). Orbiting active sensors are increasing in number and complexity, and most experts expect that analysis of SAR images, in particular, will become easier and more common in the coming decade (Rosenqvist et al. 2003; CEOS 2009).

Synthetic Aperture Radar (SAR)

SAR systems emit microwaves and measure the strength of signal return, also known as backscatter. The strength of the SAR backscatter depends on how it interacts with the surface vegetation and the topography of the landscape. In forested areas, most of the SAR signal reflects off water-containing biomass (Kasischke et al. 1997) before reaching the ground. Unlike two-dimensional passive sensors, in which the reflection from a bare mountain appears the same as the reflection from a flat desert, the emitted energy of active sensors responds to the three-dimensional shape of landforms and ecosystems (Rosenqvist et al. 2003; Figure 8). In mountainous areas, SAR signal reflection is dominated by interactions with topography, and the vegetation signal is harder to analyze due to black shadows and areas of strong, false returns from topography (Jensen 2007; Rosenqvist et al. 2003; Figure 8).

Several adjacent bands of SAR microwave radiation are in use, and large variation exists in center wavelength between the X-band (~3 centimeters, or cm), C-band (~5.6 cm), L-band (~25 cm), P-band (~65 cm), and VHF (1–15 m) microwave radars (Kasischke et al. 1997; Patenaude et al. 2005). These differences in wavelength affect how the SAR radiation interacts with soil moisture and the water content of vegetation. Shorter wavelengths (e.g., C and X band) tend to be more strongly reflected by smaller structures like twigs and thin branches at the top of a forest canopy, so the majority of the shorter wavelength backscatter does not penetrate very far into a forest. Longer wavelengths (e.g., L-, P-, and VHF-band) tend to be more strongly reflected by larger structures like trunks. The strength of SAR backscatter from vegetated areas is often correlated with the amount of woody biomass in that area (Dobson et al. 1995b; Kasischke et al. 1997). However, SAR bands X through P all tend to achieve maximum signal return (saturate) at increasing levels of biomass (Figure 9). The C and X bands saturate at lower thresholds of woody biomass because most of the shorter-wavelength SAR radiation is reflected from the top of dense canopies.

Advanced SAR sensors can emit and receive radiation with defined polarizations. Although natural microwaves undulate in all directions as they propagate, it is possible for SAR systems to emit and receive microwaves that only propagate in vertical or horizontal angles (Figure 4). This increases the ability of SAR sensors to measure the roughness and structure, or texture, of the land surface (SAR texture is more strictly defined as the variability in backscatter return over a defined area). For example, open fields may reflect more horizontally polarized microwaves than an irregular forest canopy (Jensen 2007). Newer SAR sensors can have very high spatial resolution (e.g., 1 m), but it is often necessary to degrade resolution to remove random "speckle" errors by averaging across four or more pixels. Practically, this means that SAR resolution will always be between three and four times lower than specified (Rosenqvist et al. 2003).

Figure 8. Difference between Passive (top) and Active (bottom) Sensor Sensitivity to Topography on a Mountain Island

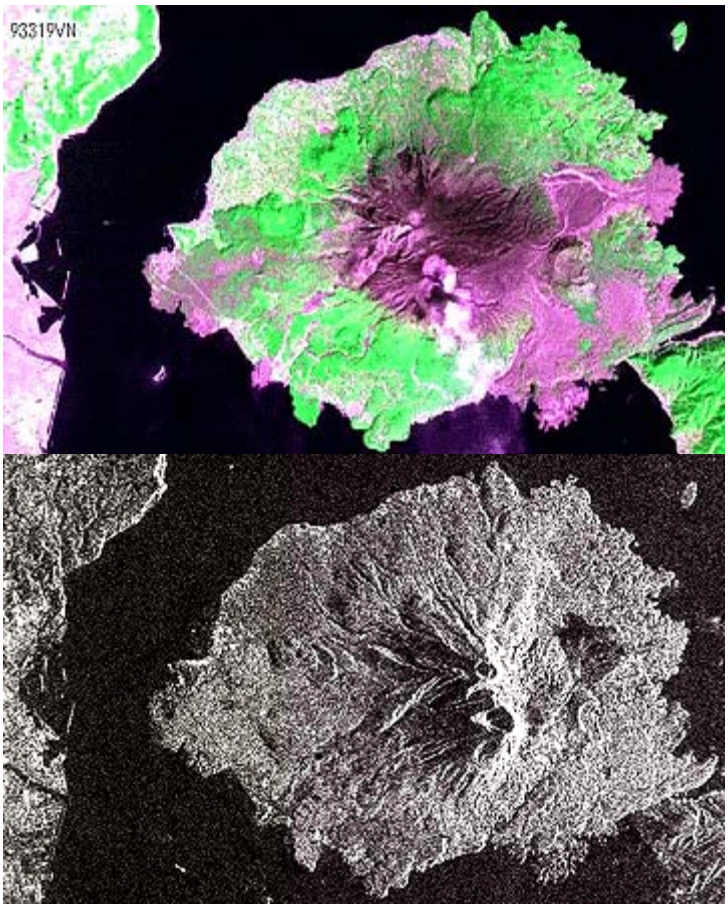

Note: Note the shadows and response to topography in the black-and-white SAR image.
Source: Short 2009.

Figure 9. Saturation of SAR at High Forest Biomass

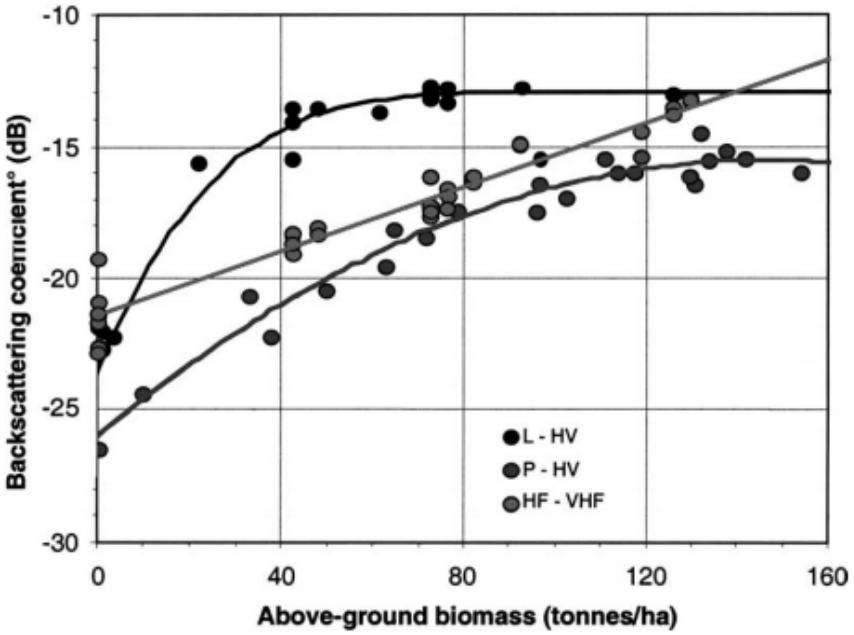

Note: This graph shows the saturation of SAR backscatter from the L-band (dark line, top), P-band (gray, bottom), and VHF-band (light gray, middle) over a forest in Landes, France. In this study, L- and P-band sensitivity to increasing biomass is limited after 100 Mg/ha; other studies have achieved higher sensitivity by combining polarizations.
Source: Le Toan et al. 2004.

It is possible to obtain exact measurements of distance to Earth by using two or more SAR sensors that receive signals from the same target. This is known as interferometry, and it operates on the same principles that an owl uses to determine sound direction and distance. With two separated SAR sensors, the backscatter signal does not arrive at the exact same time or strength at each sensor. Differences between the paired SAR signals can be used to determine the angle and distance of the target relative to the sensor (Balzter 2001). There are two types of interferometry: repeat-pass interferometry, by which two sensors image the target at different times and angles; and spatial interferometry, by which two sensors separated by a baseline distance image the target at the same time. Interferometric SAR (InSAR) data can be gathered from two images on different days (e.g., from satellites flying in a known orbit or formation) or from a sensor specifically built to contain two SAR sensors.

Using SAR interferometry, passive stereo imaging, or LIDAR (discussed below), it is possible to produce a three-dimensional map of Earth 's surface, called a digital elevation model (DEM), that is accurate to less than a meter of error. The first global DEM was produced in 2000 by the Shuttle Radar Topography Mission (SRTM), in which a C- and X-band InSAR sensor was mounted on the space shuttle (Jensen 2007). This DEM is degraded for military reasons from 30 to 90 m pixels outside the United States, and in forests with moderate or higher biomass, it confuses tree-canopy height for the ground (Bourgine and Baghdadi 2005; Kellndorfer et al. 2004).

Correcting SAR images with accurate, ground-level DEMs greatly improves backscatter interpretation and allows direct forest height measurement using interferometry (Ticehurst et al. 2004; Kellndorfer et al. 2004). The development of a global, ground-level DEM for forested regions would enable a significant advance in the ability of SAR to measure forests (Kellndorfer et al. 2004; Bourgine and Baghdadi 2005).

Light Detection and Ranging (LIDAR)

LIDAR systems emit coherent light and measure the timing of signal return from the Earth's surface. They are essentially laser altimeters, or range finders, that measure the distance to targets with great precision by timing how long an emitted laser takes to reflect off the ground target (Dubayah et al. 2000). The targets that LIDAR samples are small areas called footprints, and the lasers reflect from foliage and woody biomass as well as from the ground surface. Current LIDAR systems differ from SAR systems in that they sample footprints at discontinuous intervals, rather than receive wave reflections from entire landscapes (Figure 10). Interpolation between LIDAR sampling footprints is necessary to generate vegetation canopy maps or DEMs (Lefsky et al. 2002b; Figure 11a). The resolution of this technology depends on the sampling density of LIDAR footprints.

Figure 10. Potential LIDAR sampling footprints for the U.S. Deformation, Ecosystem Structure, and Dynamics of Ice Satellite (DESDynI) mission

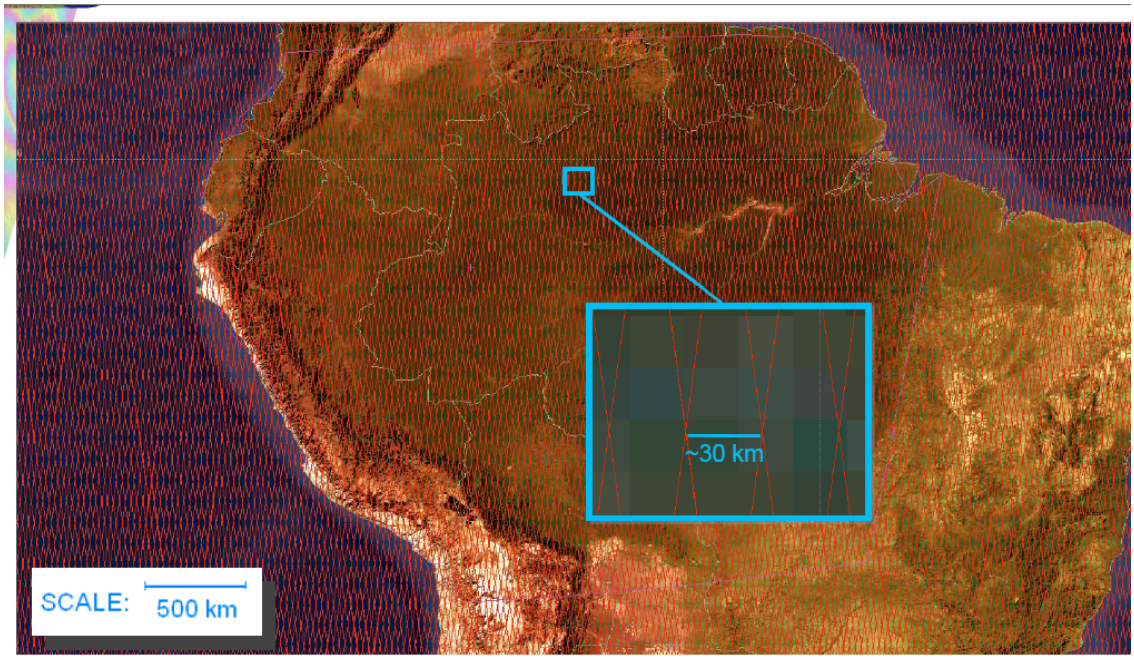

Note: Example footprints are dots indicated on the inset. Footprints not to 30 km scale. LIDAR footprints will be taken just along the red lines.
Source: Oberto et al. 2008. Courtesy of NASA.

LIDAR systems differ in their footprint size, firing frequency, and the information recorded from the laser pulse. There are currently two main types of LIDAR systems: small footprint, discrete-posting systems; and large footprint, waveform-recording systems (Lefsky et al. 2002b). A third

experimental type, flash LIDAR, scans large areas and receives returns in a similar fashion to SAR (Swanson et al. 2009). Because this type is experimental, we will not discuss it further in this report.

Small-footprint LIDARs sample small areas (submeter width) at high density (multiple footprints per meter, Figure 11a). They record single or multiple return times, or posts, from the returned laser pulse (e.g., first return, last return, and/or the peak laser returns, Figure 11a). A large number of small-footprint LIDAR measurements allow creation of very realistic maps of bare areas and the tops of vegetated canopies (Lefsky et al. 2002b; Figure 11b). Small-footprint LIDAR pulses are able to penetrate to the ground through dense vegetated canopies only if they are spaced very closely (Clark et al. 2004b). The large number of closely spaced footprints required to image a forest canopy currently limits small-footprint LIDAR to aerial surveying of small swaths (e.g., 5 km; Swanson et al. 2009; Dubayah et al. 2000).

Figure 11a and b. Returns from Small-Footprint LIDAR

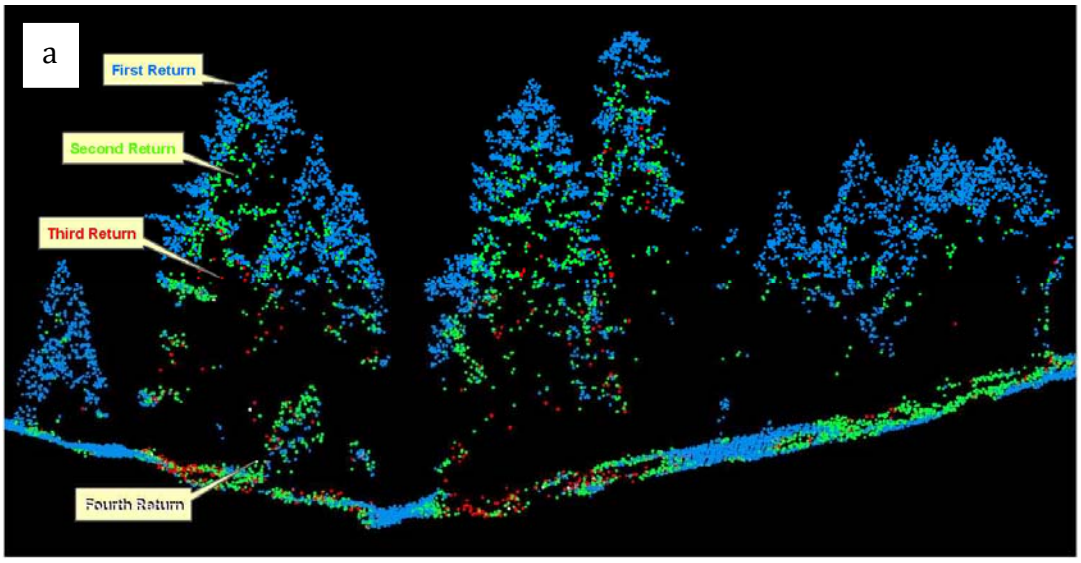

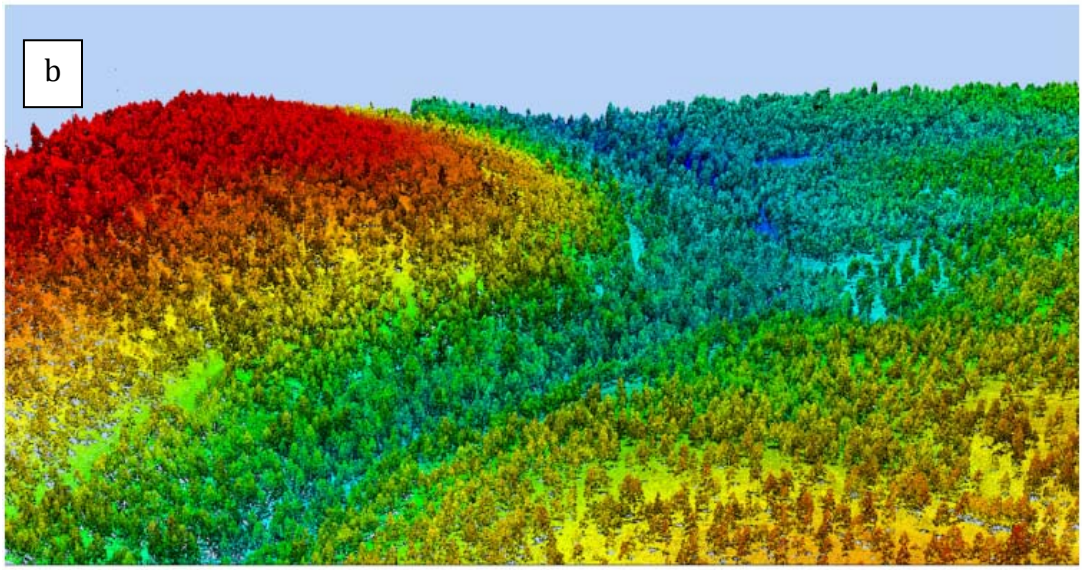

The first graphic (a) shows discrete returns from a small-footprint LIDAR image, with each footprint along a transect ordered and represented as a dot. The second image (b) is an oblique view of all of the discrete point LIDAR returns; elevation is indicated by color.
Source: Images courtesy of ImageTree Corp.

Figure 11c. Example Waveform from a Large-Footprint LIDAR

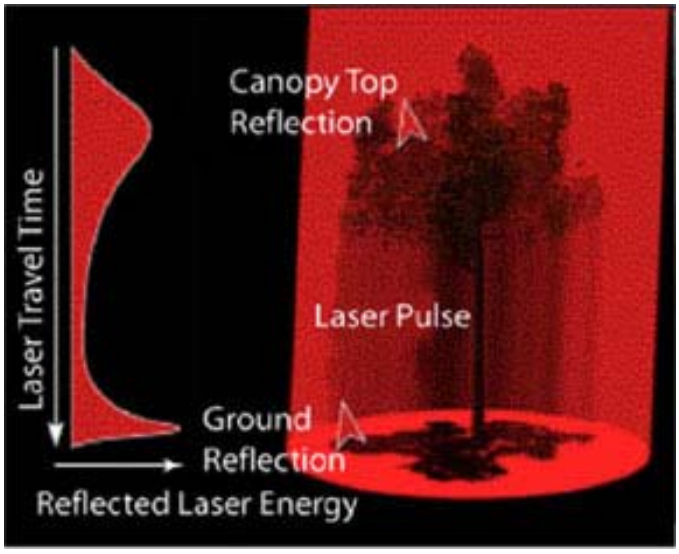

Note: The graph on the left-hand side of Figure 11c indicates the actual waveform data collected by the sensor, and the image is illustrative of the interactions taking place.
Source: Courtesy of the Jet Propulsion Laboratory, NASA.

It is possible to record more information from each laser pulse, and large-footprint LIDARs use laser pulses large enough to penetrate individual tree canopies (e.g., 10–30 meters in diameter, Figure 11c). From each footprint, the first laser return indicates the top of the vegetated canopy, the last laser return indicates the ground elevation (Lefsky et al. 2002b), and the amount of returned energy per time indicates the height and area of the reflecting surfaces. By displaying the

distribution of signal returns by return time, LIDAR systems create a waveform image of the vegetation structure and topography at the sampling point (Figure 11c). LIDAR waveforms are used to create highly accurate, three-dimensional models of actual forest structure; forest height, aboveground biomass, and other quantities can be estimated from large-footprint LIDAR (Lefsky et al. 2002b; Dubayah et al. 2000).

The utility of LIDAR for forest mapping is only limited by the width and density of footprints. At wide intervals, significant interpolation is necessary to estimate forest height or underlying topography. Accuracy is lower in heterogeneous areas (Hudak et al. 2002). While small-footprint, aerial LIDAR typically samples a small area very intensively, large-footprint, aerial LIDAR may sample 25 m footprints spaced at 50 m intervals. LIDAR missions must balance footprint width, number, and spacing to measure large areas accurately. Aerial LIDAR systems are commonly used in both scientific and commercial forest measurement; these primarily are small-footprint sensors, which despite their limited image swath have impressive detail over imaged forests (Figure 11b).

Because of the distance of satellites from the Earth and the amount of area the satellite are designed to cover, satellite-based LIDAR missions are large footprint and widely spaced between orbital swaths (e.g., 50 m footprints spaced at 1–3 km intervals) (Oberto et al. 2008; NASA 2009a; Figure 10). There is currently only one satellite-mounted LIDAR sensor, ICESat GLAS (the Geoscience Laser Altimeter System, carried on the Ice, Cloud and Land Elevation Satellite), and although its large footprint (~65 m) was not explicitly designed for forest measurement, the mission is being used to estimate forest biomass and improve DEMs (NASA 2009a; Nelson et al. 2009). Follow-on missions to this LIDAR mission are being planned, but the missions are likely to have short lifetimes of only three to five years because the lasers burn out after a set number of uses (NASA 2009a).

2.3 Putting It All Together: Remote Sensing Fusion

Remote sensing for forest measurement uses measured quantities (e.g., canopy greenness and radar backscatter) to estimate other quantities of interest (leaf water content, forest biomass). Incorporating more than one source of remote sensing data, known as image fusion, typically improves estimates of forest properties. These estimates can also be improved by including information from geographically referenced datasets organized using geographic information systems (GIS; Figure 12a). For lack of a better term, we define the integration of remote sensing and GIS data as "GIS fusion." GIS fusion is standard practice in remote sensing. Image fusion has only recently increased in prevalence. Both practices greatly increase the power and utility of remotely sensed data.

Figure 12a. Example of GIS—Remote Sensing Fusion

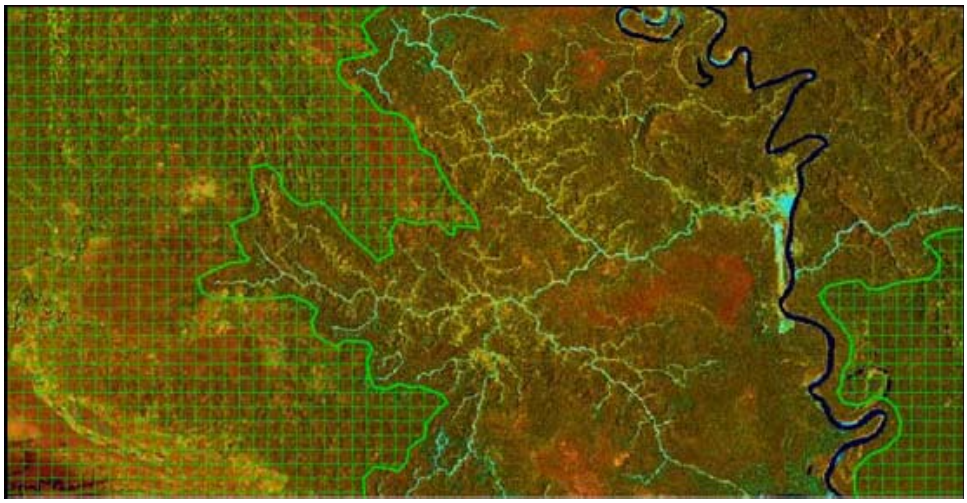

Note: Undisturbed forests (green grid) can be mapped by overlaying GIS data on road networks (blue) onto a satellite-derived forest map.
Source: GOFC-GOLD 2008.

Figure 12b. Example of Image Fusion

Note: In this case, a lower-resolution color Satellite Pour L'Observation de la Terre (SPOT) image is being fused with a higher-resolution SPOT panchromatic image, in a type of coarse-fine image fusion known as pan-sharpening. Notice the boat wakes that appear only in the higher-resolution panchromatic and fused images.
Source: Short 2009.

2.3.1 Image Fusion

Satellite imagery from two or more sensors can be combined to create a single image (or dataset) with higher resolution and/or utility (Treuhaft et al. 2003; Walker et al. 2007; Roy et al. 2008; Dalponte et al. 2008; Saatchi et al. 2007). All types of images can be fused. Fusion refers to the creation of new maps by combining data from overlapping images (Figure 12b). The two most common types of fusions are active–passive and coarse–fine, but the potential for image fusion is limited only by available data.

Passive and active sensors measure very different quantities about Earth's surface and differ in uses. Because a passive sensor measures reflectance from surfaces with different physical and chemical properties, the sensor measures light absorption by green, photosynthesizing leaves. The degree of light absorption by photosynthezing leaves is a proxy for estimating forest productivity (the rate of biomass production). An active sensor can estimate secondary forest biomass by measuring the three-dimensional structure of forests. Because productivity is positively correlated with biomass in low-biomass forests (Keeling and Phillips 2007), fusing a passive image with an active SAR image yields better estimates of productivity and biomass than either image by itself.

For passive sensors, current limits on data storage and the capability of sensors mean that no one sensor can simultaneously maximize pixel resolution, spectral resolution (number of bands), and area of coverage (Andersson et al. 2009; Jensen 2007). Thus, it is difficult to cover large areas with high-resolution imagery without having to "mosaic" (or combine) thousands of diverse images taken at different times (Andersson et al. 2009; Figure 13). Each image must be corrected for differences in solar illumination and atmospheric haze, and such correction is often difficult. One way to improve the resolution of wide-swath sensors is to fuse high-resolution imagery with coarse resolution imagery. In pan-sharpening fusion, the high-resolution imagery is used to increase black-and-white (panchromatic) detail in the coarser color image (Figure 12b; Qian et al. 2007). In training fusion, high-resolution images are used to correct the estimates of the coarser resolution imagery in an iterative process. Both of these methods can dramatically improve the resolution and utility of coarser-resolution imagery (Qian et al. 2007; e.g., Hansen et al. 2003).

2.3.2 GIS Fusion

Fusing GIS data with remote images is routine (e.g., Jensen 2007). Use of GIS allows organization and display of datasets with exactly known geographic locations (geo-referenced data). These locations can be ground derived (e.g., city building datasets) or taken directly from remotely sensed imagery (e.g., road, land cover, or DEM datasets). Integrating GIS data with remote sensing imagery makes new analyses possible (e.g., roads and logging; Asner et al. 2006) and can improve estimates from remote sensing data (e.g., climate and biomass; Baccini et al. 2004). Geo-referenced data are used regularly to quantify and improve the accuracy of remote sensing analyses and predictions in a process known as ground-truthing. Ground-truth data are high accuracy data used to evaluate, or validate, the accuracy of maps derived from satellite imagery. These data are a crucial component of remote sensing (see Section 3.1.3). The increasing integration of GIS and remote sensing has facilitated display and communication of satellite imagery between scientists and for the public, as witnessed by the explosive growth in mapping in society and the widespread use of Google Earth, Microsoft's Bing Maps, and other products.

Figure 13. Mosaic of Moderate-Resolution Landsat 7 Images

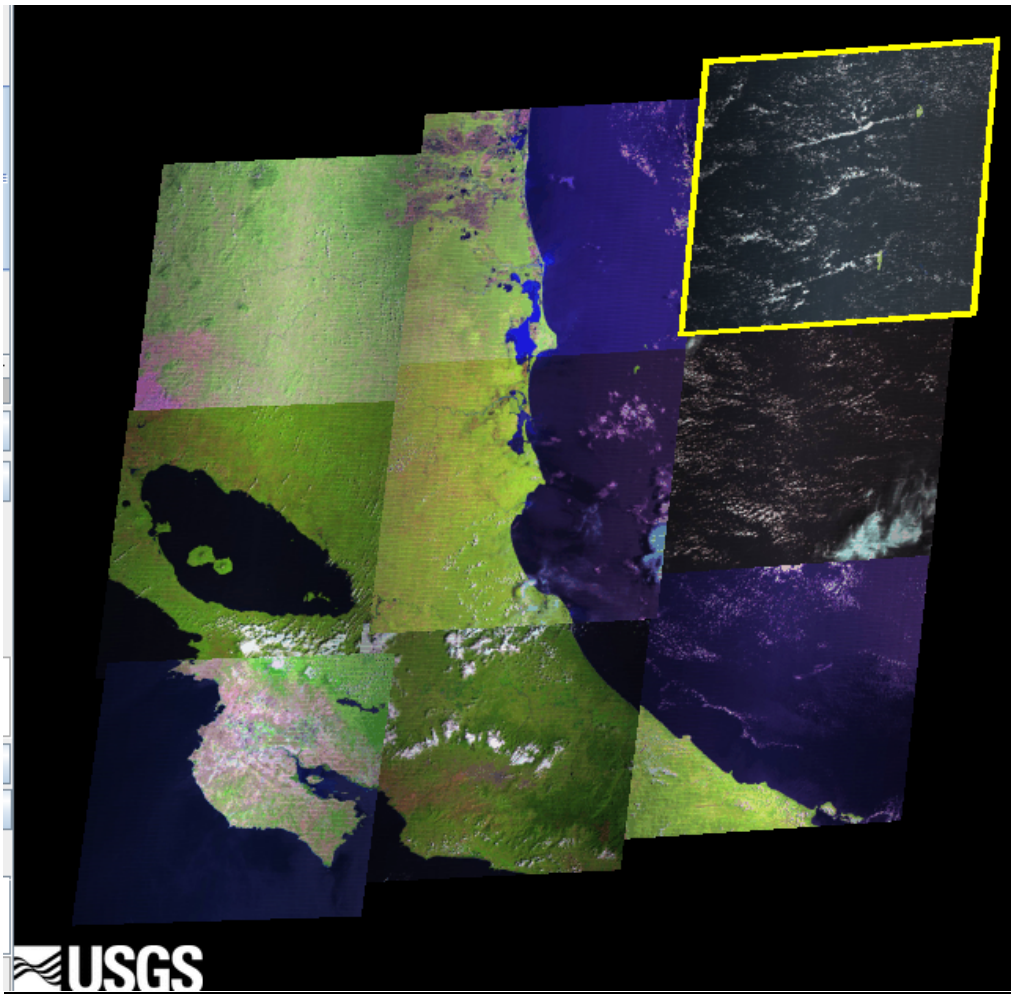

Source: Image courtesy of U.S. Geological Survey Global Visualization Viewer (GLOVIS).

2.4 An Overview of Current and Near-Term Earth-Observing Technology

There are many Earth-observing satellites (EOS) currently in orbit, both active and passive, including approximately 110 nonmilitary satellites (UCS 2009). There are about 75 distinct sensor types focused on observing the Earth's surface with coarse or higher (<1.5 km) spatial resolution, and these are the subject of this section.

Between 2009 and 2015, we expect approximately 87 additional surface-focused EOS to be launched, many of them bearing new types of sensors. The majority of EOS are not commercially owned, but many national agencies sell their imagery at commercially competitive prices. The Appendix summarizes the characteristics of current and expected EOS. We divide the sensors into five categories: high-resolution passive sensors (<6 m), moderate-resolution passive sensors (6–150 m), coarse-resolution optical sensors (>150 m), active sensors, and future (2009–2015) satellite sensors. We discuss other miscellaneous EOS and notable airborne sensors only briefly. When an individual sensor spans categories depending on its mode or band, we place it in the more

dominant category for that sensor. We gathered all of the data and specifications on satellites from the sources noted in the Appendix and publicly available websites.

2.4.1 Current Sensor Technology

Multispectral passive satellites make up the vast majority of EOS and have been increasing in spatial resolution, spectral resolution, and return frequency in recent years. Spatial resolution has increased in moderate-resolution satellites, but the advent of high-spatial resolution, pointable commercial satellites has changed the cost and availability of high-resolution imagery. These increases in spatial resolution have often come at the cost of image swath (see Figure 6), but technology is improving overall, as illustrated by the wide swath but moderate resolution of the Disaster Monitoring Constellation (DMC). There are a few hyperspectral satellites currently in operation (e.g., the U.S. Moderate Resolution Imaging Spectroradiometer (MODIS), the Hyperion instrument on the U.S. Earth Observing Mission-1, and the Compact High Resolution Imaging Spectrometer (CHRIS) on the European Space Agency's Project for On-Board Autonomy (PROBA) spacecraft), but in general most satellites measure between one and 12 bands (Appendix). Several notable coarse-resolution satellite constellations have been in operation for decades, including AVHRR and GOES, the U.S.-launched Geostationary Operational Environmental Satellites. The recent launching of more moderate- to high-resolution constellations, such as MODIS, the DMC series, and the RapidEye series, is dramatically changing return times for forest measurement (Appendix). Whereas Landsat produces images once every 16 days, and cloud-free images in some areas only occur once a year (Olander et al. 2008; Asner 2001), the DMC series has daily imaging capability (see the Appendix).

Recent and upcoming SAR sensor launches will increase the number of active sensors in orbit. Modern SAR satellites have higher and more flexible spatial resolution, greater image swath flexibility, and more polarization modes than previous satellites (see the Appendix). Japan's Advanced Land Observing Satellite (ALOS), which includes an L-band sensor with four polarization modes, has been used for global forest cover mapping since its launch in 2007 (Olander et al. 2008). There is only one functioning land-observing LIDAR satellite. The biggest barrier to widespread usage of active sensors remains the technical difficulty of processing SAR data, but the cost of SAR data, although equal to some optical sensors, is also a barrier to global mapping (Patenaude et al. 2005).

From the standpoint of global forest measurement, the most significant recent advance in remote sensing analysis is economic, not technological. As of early 2009, the U.S. Landsat archive (1972–2009) became freely available, enabling global and temporal analysis on moderate-resolution imagery (Olander et al. 2008). The regional China-Brazil Earth Resources Satellite (CBERS) archive (1999–2009) of imagery is also now free in most developing countries (GOFC-GOLD 2008; Powell et al. 2007). Currently, these two free imagery series offer the highest resolution coverage per dollar, and they have a good temporal record (Figure 6). In conjunction with other free MODIS and AVHRR data, it is now possible to survey global forests daily with coarse-resolution images and create moderate-resolution forest maps with monthly to annual frequency. The Landsat Data Continuity Mission, or LDCM (and the upcoming Landsat 7 imagery mosaics, see below), will continue this free data policy and make it possible to develop a long-term, global record of land use and land cover (Loveland et al. 2008).

Coarse-Resolution Passive Sensors

Coarse-resolution passive sensors have a pixel size of 200–1,500 m, receive radiation in the optical through thermal range, and have image swaths ranging from 360 km to the full Earth disk (Figure 6, Appendix). It would take between 14 and 40 AVHRR or 25–80 MODIS images to cover the 13.4 billion hectare (ha) global land area (estimates are inexact for coarse-resolution images that include land and water; Table 3). Because coarse-resolution is useful for monitoring weather and climate, many coarse-resolution sensors are parts of large constellations. For example, the AVHRR sensor constellation included 12 satellites between 1978 and 2009, including several satellites operating simultaneously (Jensen 2007). Although many coarse-resolution sensors only have a few visible or near-infrared bands at resolutions too coarse to detect most land-cover change, the very high repeat times make these sensors ideal for monitoring phenology, fire, and other ephemeral events. The advent of "moderate" coarse sensors (e.g., MODIS, MERIS, 250–300 m) has improved global land-cover mapping (Herold et al. 2008). A recently launched hyperspectral coarse-resolution sensor mounted on the Indian Microsatellite (Interactive Multisensor Snow and Ice Mapping System Hyper-Spectral Imager, IMS HySI) has potential for land-cover mapping as well (Appendix).

Coarse-resolution sensors are mounted on both polar-orbiting satellites and geostationary satellites. Although geostationary satellites image the entire Earth disk in real time, current sensors are ultracoarse (>1.5 km) in resolution and only the GOES series is described here as an example in the Appendix. There are several long-term, similar geostationary satellites series supported by the United States (GOES), Europe (Meteostat), Russia (Elektro), and China (FY–3 and –4).

Table 3. Costs of Imagery for Wall-to-Wall Sampling of the Global Land Area

Satellite sensor	Sensor type (pixel size)	Number of images required	Price per km^2 (in US$, 2009)	Estimated total cost
MODIS	Coarse-resolution (250–1,000 m)	25-80	Free	$0
Landsat 7 ETM	Moderate-resolution (28.5 m)	3921	Free, formerly $0.02 in 2008	$0, formerly $2,683,700
GeoEye-1	High-resolution (1.65 m)	580,787	$25 (for a basic image of Europe)	$3,354,625,000
ALOS Phased Array type L-band SAR **(PALSAR)**	Coarsest-resolution mode (100 m)	1096	$0.0017	$230,075

Note: Created from Appendix 1 for selected sensors; the number of required images is an estimate based on the 134,184,000 km^2 global land area (see text). Prices change; these estimates are for 2009. ALOS PALSAR would likely be degraded to 400 m resolution for accuracy.

Moderate-Resolution Passive Sensors

Moderate-resolution (10–200 m pixel) passive sensors can receive optical through thermal radiation and have image swaths ranging from 60–890 km (Figure 6, Appendix). It would take approximately 3,921 Landsat images to cover the global land area Table 3. There are currently five major moderate-resolution satellite series: Landsat, the Satellite Pour L'Observation de la Terre

(SPOT), CBERS, the Indian Remote Sensing (IRS) satellites, and the DMC series (Achard et al. 2007; Powell et al. 2007). In addition, China, Argentina, Thailand, and Russia all support individual moderate-resolution satellites, but it is unclear whether China's data are available to the public. Additionally, there are several experimental moderate resolution satellites, most notably the hyperspectral Hyperion and CHRIS sensors, and these have shown promise for hyperspectral imaging as a means of distinguishing land covers (Ustin et al. 2004).

The Landsat series (satellites 1–7, 1972–present; Jensen 2007) is the workhorse for global land-cover analysis. Unfortunately, Landsat 5 is only transmitting data in regions with ground stations, and Landsat 7 had a scan-line failure in 2003 that caused black stripes to appear in the sides of its images. The United States Geologic Survey (USGS) is working to mosaic Landsat 7 images to correct the scan-line problem, but the next Landsat is not due to be launched until 2012 (Loveland et al. 2008). A continual record of global land cover requires filling the 2003–2012 Landsat data gap. There are several possible approaches. The Advanced Spaceborne Thermal Emission and Reflection Radiometer (ASTER, launched in 1999) is a moderate-cost satellite that has near-global coverage (Jensen 2007). SPOT (1–5, 1986–present; Jensen 2007) is a satellite series with global coverage but data are relatively expensive to purchase (Figure 6). The CBERS series (three satellites, 1999–present; Jensen 2007) is a growing constellation of satellites with free imagery, but the imagery is focused over Brazil, China, and most recently, Africa. The IRS series (seven satellites, 1988–present; Jensen 2007) is a large, long-running constellation with global image coverage available at some cost. Finally, the DMC series is a constellation of satellites from different countries in the same orbit; images from daily overflights are providing an important commercial backup to Landsat (GOFC-GOLD 2008).

High-Resolution Passive Sensors

High-resolution (0.3–10 m pixel) passive sensors receive optical through near-infrared radiation and have image swaths ranging from 11 to 70 km (Figure 6, Appendix). There have been a number of commercial and national launches since the first high-resolution satellite, IKONOS, launched in 1999, and these additions to the fleet of EOS have led to the formation of commercial high-resolution constellations. These constellations include high-resolution instruments operated by several U.S. companies, including GeoEye and DigitalGlobe. One of the challenges of using high-resolution imagery for global forest mapping is that approximately 580,787 GeoEye-1 images are required to cover the global land area (Table 3). Most of the high-resolution satellites have five bands; four narrow bands in the visible and near-infrared, and one higher-resolution panchromatic band that can have sub-meter resolution (for national security requirements, pan resolution is actually degraded to 0.5 m on U.S. commercial satellites). There have been several recent launches of solely panchromatic sensors with primary applications in defense and mapping. Most high-resolution sensors are pointable, decreasing their effective return time from, for example, 26 days to three days. This results in spotty global coverage, particularly for forests, as the coverage is often concentrated in densely populated and less cloudy areas. The recent development of cheap microsatellites that can be launched as a constellation (e.g., RapidEye) or as an on-demand sensor (e.g., the U.K.'s microsatellite, TopSat) could dramatically increase the global coverage and return time of high-resolution sensors (Kramer and Cracknell 2008).

Active Sensors

Active sensors (SAR and LIDAR) currently make up a small proportion of land-observing satellites; there are approximately nine SAR sensors and one LIDAR sensor in orbit (Appendix). Active sensors have resolutions ranging from 1–1,000 m and image swaths ranging from 10–500 km; it would take approximately 1,096 ALOS images to cover the global land area. In the last decade, SAR satellite technology has improved to four polarity options and variable resolution (with smaller swaths at higher resolutions) in different imaging modes. Until 2006, all publicly available SAR satellites carried C-band sensors (Jensen 2007) except for the L-band Japanese Earth Resources Satellite (JERS-1) mission that ran from 1992–1997, the short-lived Seasat (L-band) and Almaz (S-band) missions, and the brief SRTM and Shuttle Imaging Radar (SIR) -A, SIR-B, and SIR-C/X shuttle missions. The Canadian RADARSAT series has been gathering C-band SAR imagery since 1995, and the Envisat ASAR has been gathering C-band as well since 2002. The most recent satellite launches, ALOS (L-Band), TerraSAR-X, X-band), and Constellation of Small Satellites for Mediterranean Basin Observation (COSMO-SkyMed, X-band), have increased the diversity of SAR bands in orbit. ALOS provides global coverage, TerraSAR-X is the first satellite in an interferometric constellation, and COSMO-SkyMed is a microsatellite SAR constellation with a variety of modes. When evaluating the spatial resolution of SAR satellites, given in the Appendix, it is important to remember that their effective resolution after speckle averaging will be three to four times more coarse, approximately 50–100 m.

The first ground-measuring LIDAR altimeter, ICESat, was launched in 2004 and a follow-on is planned. While the swaths ICESat measures do not cover the entire land surface, the instrument has provided useful information for modeling ice, elevation, and forest structure (NASA 2009a).

2.4.2 Expected Sensor Technology, 2009–2015

Future satellite launches will fill current data gaps, provide follow-on missions, populate constellations, and provide new functionality. The diversity of countries with satellites in orbit will increase with new satellites from Spain, Turkey, Taiwan, the United Arab Emirates (UAE), Sweden, Ukraine, Malaysia, and Nigeria. The majority of launches will come from China, the United States, countries in the European Union, Argentina, and India, with notable smaller contributions from Brazil, Russia, Canada, and Japan (Appendix).

Among follow-on missions, the LDCM, CBERS-3, and the ultrahigh-resolution GeoEye-2 merit mention for their advanced technology. Both national and commercial high-resolution optical missions will continue to increase in number as microsatellite technology lowers the costs of production (CEOS 2009; Olander et al. 2008; Kramer 2008). Several new SAR constellations are planned (TerraSAR, Sentinel 1, RADARSAT, ALOS, and Satélite Argentino de Observación Con Microondas, or SAOCOM-1 series). The Sentinel-2 series, a moderate-resolution optical constellation, is also planned. There will be several new moderate-resolution hyperspectral sensors (Environmental Mapping and Analysis Program, or EnMap; Hyperspectral Infrared Imager, HyspIRI; Technology Experimental Satellite Hyperspectral, TES-HYS; Satélite de Aplicaciones Científicas F (SAC-F), and Prisma). Most notably, of the 87 or so land-observing missions planned between 2009 and late 2015, 25 will mount SAR sensors, two will mount LIDAR, and one will mount both—a dramatic increase in the number and diversity of functioning active sensors.

Overall, it is likely that spatial resolution, return times, and SAR capabilities will improve over the 2009–2015 period, with significant new hyperspectral, InSAR, and LIDAR functionality. Despite the unpredictable nature of government data policies and imagery prices, as well as uncertainties relating to launch schedules and success, the next six years will likely bring a significant expansion in the capacity of remote sensing to monitor the Earth's surface.

Expected Coarse-Resolution Passive Sensors

Approximately 27 coarse-resolution sensors are planned for launch between 2009 and 2015, but it is unclear if data will be publicly available from nine sensors to be launched by China. Most launches will continue constellations (e.g., GOES, Fengyun 3[FY-3]), with the AVHRR sensor continuing on Meteorological Operational Satellite A (MetOp-A) and MetOp-B. The United States plans to launch a new satellite series, the National Polar-orbiting Operational Environmental Satellite System (NPOESS), as a replacement to the MODIS and AVHRR satellites, but NPOESS has lower maximum resolution than MODIS and may be more suitable as an AVHRR follow-up (Townshend and Justice 2002). Two sensors that may be more suitable successors to MODIS are the Global Change Observation Mission C1 (GCOM-C1, with 11 bands at 250 m resolution) and the Sentinel-3 series (with 21 bands at 300 m resolution). Most experts agree that it will be difficult to match the combination of resolution, revisit time, and free imagery that MODIS currently offers for global land-cover analysis.

In addition to GCOM-C1 and the Sentinel-3 series, there will be a few technical improvements in coarse-resolution sensors. Gisat will mount a coarse sensor, a moderate sensor, and a coarse-resolution hyperspectral sensor. SAC-D will be a coarse-resolution thermal infrared sensor to measure the temperature and energy release of fires. Most significantly, real-time monitoring of vegetation and productivity will become possible after 2014, with the launch of visible and near-infrared (VNIR) geostationary sensors with a resolution of 1 km. These sensors, starting with GOES-R, offer a significant improvement over current technology.

Expected Moderate-Resolution Passive Sensors

At least fifteen satellites bearing moderate-resolution sensors are planned for launch. These are Nigeria-Sat-2, Amazonia-1, RASAT, SAC-F, ARGO, CBERS-3, CBERS-4, Kanopus-V, Resourcesat-2, Resourcesat-3, LDCM (Landsat 8), Gisat, HyspIRI, Sentinel-2A, and Sentinal-2B. The multispectral ARGO, LDCM, Resourcesat-2, Gisat, and Sentinel-2 sensors are expected to collect global data. Several hyperspectral moderate-resolution sensors are under development. Of the six planned hyperspectral sensors (EnMap, HyspIRI, TES-HYS, Gisat, Prisma, and SAC-F), only HyspIRI has a swath size suited to frequent global coverage. If launching agencies support global data collection, this increasing diversity will safeguard global coverage against the loss of a single satellite. Resolution in the SPOT series has improved to the point where SPOT-5 and SPOT-6 are considered wide-swath, high-resolution sensors. The LDCM will have nine bands and maintain continuity in a critical imagery series, India's Resourcesat-3 will have 23 m resolution and an extra-wide swath of 700 km, and the Sentinel-2 series will be an advance in sensor technology, with high-resolution (10 m) capability, 13 bands, a wide swath (240 km), and three dedicated bands for atmospheric correction. If the LDCM fails to launch or operate properly, an interruption in free access to global imagery is likely.

Expected High-Resolution Passive Sensors

Although it is difficult to anticipate commercial launches, the next several years will see an increase in the number of "standard" (four-band VNIR, resolution 1–10 m) high-resolution sensors (Appendix). Several countries have taken advantage of the lower cost of microsatellites to create high-resolution sensors with technical assistance from aerospace companies (e.g., DubaiSat (UAE) and Malaysia's RazakSat). Microsatellite technology has led to the high-resolution RapidEye constellation of six satellites. The constellation will be completed by the addition of the satellite ARGO in mid-2009. With high revisit times and a larger swath than many high-resolution satellites (78 km), RapidEye has the potential to develop global coverage quickly (RapidEye 2009).

Some improvements in high-resolution sensor capabilities and lower data costs are expected. WorldView-2 will have substantial spectral and spatial resolution with eight bands in the VNIR and 1.8 m resolution. The Vegetation and Environment Monitoring New Micro-satellite (VENμS) will also offer high spectral and spatial resolution, with 12 bands in the VNIR with a resolution of 5.3 m. Pleiades-1 and Pleiades-2 are extremely pointable (+/- 50°) and will add flexible, high-resolution capacity to the SPOT series. SPOT-6 will also continue the SPOT series, with a wide swath (60 km) and higher resolution (8 m, 2 m pan). GeoEye-2 will have the highest spatial resolution (0.25 m) in the 2009–2015 interval. Prisma will integrate a 2.5 m resolution pan camera with hyperspectral imagery, and the Sentinel 2 series (discussed above) will have high-resolution imagery (10 m) in the VNIR with a very wide swath. Finally, CBERS-3 and CBERS-4 will combine high-resolution imagery with a moderate-resolution imager and a coarse-resolution thermal imager.

Expected Active Sensors

SAR and LIDAR sensors will make up a third of new launches from 2009–2015, with an increase in the diversity of SAR bands (C, X, S, L, and possibly P), functions (InSAR and dual InSAR/LIDAR), and number of SAR constellations. The TerraSAR-X (X band) constellation will fly in interferometric formation to produce a high-resolution digital elevation model for commercial purposes. The resolution will be 1 m before speckle averaging. The COSMO–SkyMED constellation (X-band) will be integrated with the planned SAOCOM-1 constellation (L-band) for twice-daily overflights in two bands. The RADARSAT Constellation (C-band) will continue the long-running RADARSAT series of imagery and decrease revisit time (eoPortal 2009). The Sentinel-1 constellation (C-band) will have an interferometric mode and variable swath width. Finally, the launch of ALOS-2 will create a high quality, L-band constellation.

There are several advances in active sensor technology planned for launch, including a variable C/X-band sensor (Disaster Management SAR, or DMSAR), interferometric sensors (InSAR, several satellites), a LIDAR follow-on mission (GLAS), a high-resolution S-band sensor (Huanjing IC [HJ-1C]), a LIDAR-InSAR integrated L-band sensor (U.S. Deformation, Ecosystem Structure and Dynamics of Ice satellite, or DESDynI), and potentially a P-band interferometric sensor (BIOMASS). Of these, DESDynI, GLAS, and BIOMASS merit special mention for their potential to inform forest measurement and monitoring. DESDynI would be the first integrated InSAR-LIDAR mission, and it would combine the relative strengths of InSAR and LIDAR to create unparalleled measurement of ecosystem structure and forest height. GLAS would continue global LIDAR measurement, thus increasing the accuracy of global DEM estimates. BIOMASS is currently a sensor concept under

consideration for launch in late 2015 or early 2016 and would consist of a P-band, interferometric SAR specifically designed to measure forest biomass in real time.

2.4.3 A Cautionary Note on Planning and Satellite Technology

Although planned launches are good indicators of future possibilities for Earth observation, successful satellite launch and operation are never guaranteed. Satellite launches are usually delayed by budgetary and construction exigencies. Satellites regularly fail to launch (examples include the launch failures of Landsat 6, IKONOS-1, and the Orbital Carbon Observatory, in 1993, 1999, and 2009, respectively). Once in orbit and functioning, satellites have expected operating life spans and often outlive these, but their actual operating lifespan is a matter of chance. An instrument on Landsat 7 had a major problem four years after launch, while instruments on Landsat 5 are still functioning 24 years after launch (Powell et al. 2007; Loveland et al. 2008). Satellite-borne sensors can degrade and shift in quality over time, as well, and their image products require regular calibration and validation. Processing and distributing the data generated by the sensors are as important as having the satellite in space; many data are difficult to obtain or process or are not made widely available. As a result, long-term, global forest monitoring plans cannot rely on single satellites to carry out the bulk of data collection.

Chapter 3. Technical Considerations in Global Forest Monitoring

The use of remote sensing to provide accurate, long-term global forest measurements requires several technical and logistic choices. Agreement is required about what actually constitutes a forest and which forest quantities to measure. The selection of satellite imagery and image analysis methods must be guided by the forest measurements of interest and by basic principles of scientific inquiry, such as accuracy, repeatability, and longevity. To detect changes, it is necessary to create reference forest maps. A consistent survey method must be selected that balances analysis time, coverage, and accuracy. Finally, the logistics of image processing, cost, and ground-truthing must be considered (Sanchez-Azofeifa et al. 2009; Achard et al. 2007; Gibbs et al. 2007; Olander et al. 2008).

3.1 Measuring Forests Globally

Any global effort to monitor the world's forests must begin with common definitions and common measurements. Defining a forest is not as simple a task as it might seem, given the wide variation in forest ecosystems from country to country and the dynamic nature of forest regrowth after human disturbance. For example, at what tree density should an open ecosystem of short trees and grass be classified as a forest? Is a clear-cut deforestation? Is an abandoned tree plantation a forest?

To measure forests effectively, we must be able to compare ground measurements taken by foresters and forest ecologists to those taken by remote sensing measurements. To do this, we must be clear about which forest characteristics we are interested in measuring.

3.1.1 Defining Forests

The exact definition of forest versus nonforest has important consequences for the monitoring of deforestation and forest degradation as well as political efforts to reduce carbon emissions. Currently, only the FAO uses a single global standard definition of forest. In 2005, the FAO defined a forest as a minimum cover of 10 percent, height of 5 m, and area of 0.5 m (FAO 2006). Under the Kyoto Protocol, participating countries define forests within their borders by selecting one value of minimum area, tree height, and canopy cover from the following range: area of 0.05–1 ha, minimum tree height of 2–5 m at maturity, and minimum crown cover of 10–30 percent (UNFCCC 2001).[2]

Deforestation is defined by the United Nations Framework Convention on Climate Change (UNFCCC) as a semi-permanent conversion of forested land to other uses. This definition assumes that regrowth will not occur quickly and excludes temporary declines in canopy cover due to logging (UNFCCC 2001). Remote sensing has difficulty distinguishing areas of deforestation from intact forest when the intact forest definition includes a very low canopy cover threshold (e.g., 10 percent). The opposite is true for forest degradation, which is defined as a decrease in forest canopy cover without deforestation; lower canopy cover thresholds increase the likelihood of detecting degradation (e.g., a decrease from 90 percent to 10 percent cover).

The lack of a global standard definition for forest cover makes it difficult to create forest maps that can be readily used by all countries, but the FAO standard may be a useful starting point.

[2] An updated list of forest definitions by country can be found at http://cdm.unfccc.int/DNA/index.html.

Ideally, global forest monitoring efforts will create maps, such as a set of processed data known as the "vegetation continuous fields product" from MODIS (Hansen et al. 2003), that interested countries can resample to fit their forest definitions,

3.1.2 Forest Measurement and the Forest Identity

Historically, forest measurement has been ground based, as described in Chapter 1. Foresters and forest ecologists have measured several forest quantities including these:

- biodiversity—species richness and evenness in an area;
- canopy qualities—openness, leaf area index (LAI), leaf water content, and phenology;
- structural variables—tree density, basal area, tree height, and tree diameter at breast height (DBH);
- forest-floor qualities—litterfall, soil carbon content, and seedling density; and
- ecophysiological characteristics—transpiration rate, tree respiration, water stress, and nitrogen flux.

An organizing principle, the Forest Identity (Kauppi et al. 2006), is a central theme in the remainder of this report. The Identity relates four forest attributes (area, volume [density of growing stock], biomass [the mass of living material], and sequestered carbon) and is summarized in detail by Waggoner (2009). The Forest Identity attributes are related: forest area (ha) can be converted into volume (cubic meters, or m^3) using stem density (m^3/ha); volume (m^3) can be converted to biomass (kilograms, or kg) using wood density (kg/m^3); and biomass (kg) can be converted to carbon (kg C) using carbon density (kg C/kg). As discussed earlier, any successful global forest-monitoring project will have to integrate remote sensing and ground data. The simplicity of the Forest Identity makes it straightforward to convert between ground measurements and remote sensing (Table 4; Kauppi et al. 2006). The components of the Forest Identity tie together four scientifically and economically important forest characteristics and provide a useful starting point for global forest monitoring.

3.1.3 Comparing Forest Inventory and Remote Sensing Measurement

The same forest quantities (e.g., biomass) are estimated differently by ground forest inventory and by remote sensing (Table 4). Forest inventory typically measures tree abundance, diameter, crown width, species, and height (Song 2007; Chave et al. 2005). Although it is possible to measure all the quantities of the Forest Identity directly through destructive harvesting, foresters generally use allometric equations to estimate volume, biomass, and carbon from tree diameter, species-specific wood density, and/or height, and then extrapolate to the entire forest (Chave et al. 2005; Gibbs et al. 2007, see Table 4). Allometric equations have been developed for tropical forests (Chave et al. 2004) and higher-latitude forests (Ter-Mikaelian and Korzukhin 1997) through exhaustive measurement and selective harvesting and weighing of trees. Some allometric equations estimate total forest biomass directly from tree diameter, but given large species-to-species variation in wood density, these equations can be markedly inaccurate (Baker et al. 2004; Chave et al. 2005). There is significant variation between the biomass estimates of different allometric equations, and this variation can be a significant source of error in stand biomass estimates (Baker et al. 2004; Chave et al. 2005). Scaling up from stand-level estimates of biomass to regional

estimates often has low accuracy due to local variability in forest cover and density (Houghton et al. 2001; Houghton 2005).

In remote sensing, satellite measurements of forest area and structure are used to estimate volume, biomass, or carbon (Table 4). These estimates can be supplemented by other measures of forest leaf area, productivity, and flammability and incorporated into a forest model that can yield improved estimates (van der Werf et al. 2006; Table 4). Satellite-derived forest metrics are taken across an entire region, making extrapolation unnecessary. Two important considerations pertaining to remote sensing measurements of forests are the importance of correlation and the necessity of accurate ground data for overall accuracy.

Table 4. How Forest Inventory and Remote Sensing Estimate the Forest Identity

Forest identity	Forest inventory	Remote sensing
Area	Measured locally, at one time, in one to a few forest types.	Measured regionally and repeatedly, distinguishing forest types and ages (Optical, SAR).
Volume	Estimated using diameter at breast height, tree height.	Estimated from measures of forest height/structure (SAR, LIDAR).
Biomass	Estimated from volume and wood density measurements. Extrapolated regionally.	Estimated from area and forest structure. Estimates are improved by measures of forest flammability, productivity, leaf area, phenology, and gas flux.
Carbon	Estimated from biomass and carbon density measurements. Extrapolated regionally.	Same as biomass. Estimates are site specific, across entire regions.

Remote sensing measures reflected spectra; forest area and the horizontal and vertical structure of forests can be measured directly from these reflected spectra. Fieldwork or higher resolution imagery can be used to generate ground-truth data to assess the accuracy of these forest area and structure measurements (Jensen 2007). Remote sensing enables estimates of the other metrics in the Forest Identity (volume, biomass, and carbon) by:

- obtaining forest inventory measurements,
- correlating spectra with those measurements, and
- extrapolating from these correlations to the rest of the forest.

For example, existing field measurements of biomass are required to create forest-wide predictions of biomass from satellite imagery; another independent set of field measurements is required to assess the accuracy of these predictions.

Field estimates of volume, biomass, and carbon are derived from allometric equations. These equations can be inaccurate or biased (e.g., by not including species-specific wood density; Baker et al. 2004). Remote sensing can only be as accurate as its ground-truth data. It is possible for remote sensing to accurately predict biased estimates of biomass from standard allometric equations that,

for example, do not incorporate species-specific differences in wood density. Thus, it is difficult to assess the reported accuracy of remote sensing predictions of forest volume, biomass, and carbon. Because estimating the true value of targets is quite difficult, and only the correlations between remote sensing and ground-based estimates are reported in the literature, we have chosen to report the published accuracy of remote sensing estimates. Their accuracy is summarized here as either correlation coefficients or the percentage of variance explained by regression equations. Further refinements in ground-based measurement of forest biomass will lead to more accurate, unbiased estimates of true values from both forest inventory and remote sensing.

3.2 Criteria for a Global Forest Monitoring Program

Several principles guide consideration in designing a forest monitoring program that aims to measure the world's forests on a regular basis. One principle is accuracy, discussed more fully below. Any data generated by a forest monitoring program will have political and scientific consequences and should meet or exceed standards of accuracy for remote sensing. Another principle is repeatability, requiring consistency with earlier scientific efforts (e.g., forest definitions), transparency with scientific methodology, and public availability of source data (e.g., imagery). The data and conclusions from a forest monitoring effort will be most useful to scientists, politicians, and foresters if the data are verifiable, extendable, and relevant. A third principle is longevity; reliable, long-term data on forests are rare and the creation of a remote sensing-based, global record of forest change would be a significant scientific accomplishment (Grainger 2009). This last guiding principle has significant consequences for program design.

Satellite failure is unpredictable, so designing a forest monitoring program that depends on the successful launch or operation of a single satellite is risky. The best strategy for long-term continuous monitoring is to use a standard spatial and spectral resolution collected by several different satellite series launched continuously over decades. For example, the 30 m resolution, six-band Landsat sensor data format has been collected for a few decades, and it can be approximated by several satellite series (e.g., SPOT, Advanced Visible and Near Infrared Radiometer [Avnir], and IRS) (Powell et al. 2007). The 1.1 km resolution, multi-band AVHRR sensor data format is also supported over the long term and can be approximated by a number of satellite constellations, including SPOT, the geostationary constellations, and the Chinese FY series (see the Appendix). The SAR C-band has been taken at 30 m resolution by several different satellites over the last two decades, and C-band sensors are planned for new launches (Appendix). All these data formats would be good candidates for long-term data series on forest characteristics, and if necessary, they could be fused with other data to increase their utility (e.g., Hansen et al. 2008a).

These data formats currently have the advantage of being freely available, which facilitates program financial longevity and increases transparency. Although several commercial satellite series (SPOT, GeoEye) also have long-term, high-quality imagery archives, the rights to release these images to the public are limited. The role of these data in a global monitoring program requires funding and a means of allowing the data to be shared to maximize their usefulness.

3.3 Developing and Evaluating Reference Forest Maps

To detect change in forest characteristics of interest, baseline reference measurements are required. Biomass estimates derived from remote sensing are rare for many regions and accurate

historical reference maps of forest structure or biomass currently do not exist (Olander et al. 2008; Gibbs et al. 2007; and, e.g., Baccini et al. 2008). By contrast, it is possible to develop moderate-resolution reference maps of forest area dating to 1972 (Olander et al. 2008). For more detail on this topic, see Chapter 4.

3.3.1 Accuracy in Forest Mapping

Accuracy considerations are paramount in detecting changes in the world's forests (Grainger 2008; Gibbs et al. 2007). There can be errors of omission (not detecting or locally underestimating forest quantities) and commission (false-positive detections or local overestimates of forest quantities). We report here the greater of the two types of error when assessing prediction accuracy. For forest area, accuracy is defined as the percentage of pixels in the remote sensing imagery that is correctly identified with respect to land-cover type, so the lowest overall accuracy (mean omission or commission error across land-cover classes) is used where possible. For forest volume, biomass, and carbon, we report the match between predictions from remote imagery and observed ground measurements (i.e., the percentage of variance in ground-truth data explained by regression equations). In general, remote sensing estimates of forest area have high accuracy,[3] while estimates of forest structure and biomass are less accurate (DeFries et al. 2007; Olander et al. 2007; Rosenqvist et al. 2003).

3.3.2 Reference Maps for Carbon

Approximately 50 percent of vegetation biomass is carbon, but great uncertainty exists in estimates of global biomass stocks (see Section 4.4). The guidelines issued by the Intergovernmental Panel on Climate Change (IPCC) describe three acceptable tiers of forest measurement. Each tier is increasingly accurate and precise but also more complex and expensive in the monitoring requirements (GOFC-GOLD 2008; see Table 5 for an overview). Conservative principles of estimation can provide useful estimates of forest area and biomass for policymakers (Achard et al. 2007; Grassi et al. 2008; GOFC-GOLD 2008). Conservative principles dictate that, "a tier lower than required could be used–or a carbon pool could be ignored–if it can be demonstrated that the overall estimate of reduced emissions are [sic] likely to be underestimated" (GOFC-GOLD 2008, 12). Where large levels of uncertainty exist in biomass estimates, discounting the estimated forest carbon would be an appropriate conservative response. For example, if estimates of forest carbon vary between 60 and 90 tons per ha, 60 could be used as a default regional value (Tier 1) or could be further discounted to 40 tons per ha to account for uncertainty.

3.3.3 Forest Inventory and Reference Maps

Because forest inventory data can currently estimate local biomass more accurately than remotely sensed data, reference maps for forest biomass and other quantities could be developed from ground data by interpolating between measurement plots (Gibbs et al. 2007). This approach

[3] In this report, the overall accuracy of satellite imagery analysis is designated by five standard adjectives: very high accuracy (>90 percent), high accuracy (>80 percent), acceptable accuracy (>70 percent), low accuracy (50–70 percent), and poor accuracy (<50 percent). Where alternative qualifiers (e.g., "mixed") are used, we provide the actual accuracy is provided (e.g., 67 percent).

has many advantages where forest inventory data exist, and it can be readily integrated with satellite data on forest area (Gibbs et al. 2007).

Table 5. IPCC Tier Description for Country-Level Carbon Reporting

Tiers for emissions factors: Change in C Stocks
1. IPCC default factors.
2. Country-specific data for key factors.
3. Detailed national inventory of key C stocks, repeated measurements of key stocks through time or modeling.

Note: Tier 3 is the most detailed.
Source: GOFC-GOLD 2008.

Figure 14. Example Forest Type Map That Could Be Used for Stratification of Forest Inventory Plots

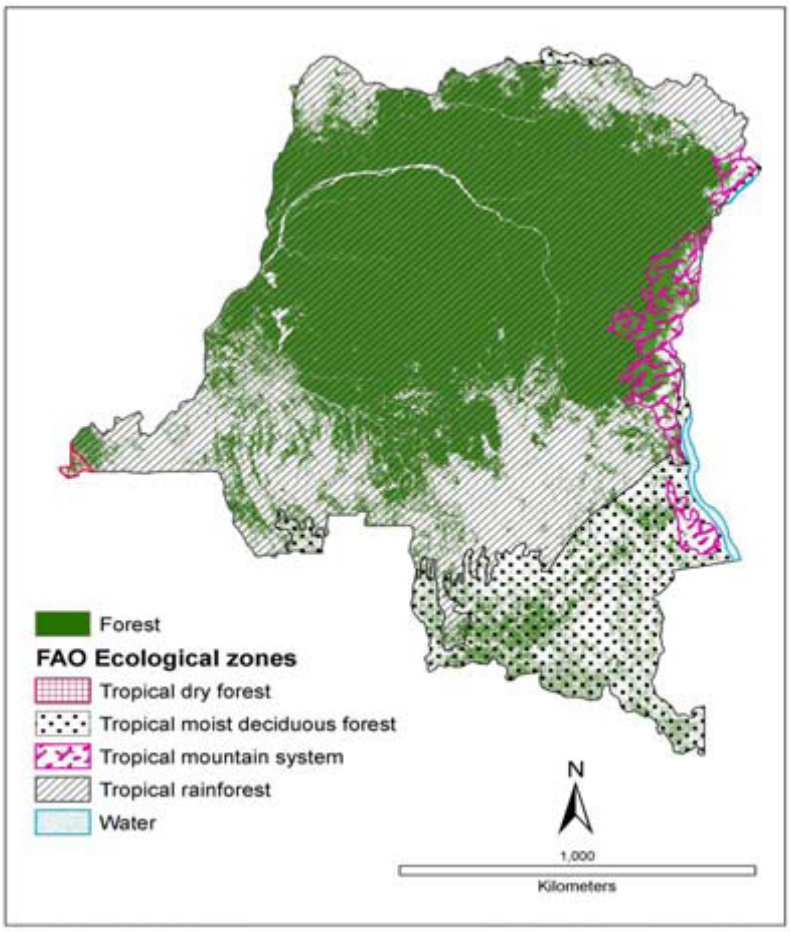

Source: GOFC-GOLD 2008.

Strict plot-to-plot interpolation across large areas is inaccurate as it ignores spatial variation in forest types and ages (Houghton et al. 2001; Gibbs et al. 2007). Stratifying forest inventories across a range of forest types and ages, and then interpolating only within the measured forest types and ages increases the accuracy of forest inventory reference maps (Gibbs et al. 2007; see Figure 14). The stratification approach, although more accurate, requires regional maps of forest type and forest age from remote sensing analyses. Remote sensing provides estimates of forest area quite well; however, distinguishing (or classifying) different forest types and ages has had variable accuracy. Image fusions and new image analysis methods may increase the accuracy of forest classifications. These methods are discussed further in Section 4.1.

3.4 Survey Methods for Determining Forest Area and Type

Three distinct strategies can be employed in using remote sensing to measure forests globally: grid sampling, change-stratified random sampling, and wall-to-wall sampling (Olander et al. 2008; Achard et al. 2007; DeFries et al. 2007). In grid sampling, moderate-resolution image "samples" are analyzed at regular spacing across a large area (see Figure 15). Examples include the FAO's 2010 FRA, which will sample the globe at one-degree intervals. The advantage of grid sampling is that it gives representative estimates of land cover over large areas with relatively little image processing. The main disadvantage is that the approach may undersample deforested areas because such areas are not randomly distributed and are likely to be concentrated in just a few areas (Achard et al. 2007). Area-stratified sampling is random sampling that is stratified by forest type, forest characteristics, or land-cover change. In change-stratified sampling, moderate-resolution sampling is heaviest in areas that coarse-resolution imagery has indicated are changing rapidly. An example is the NASA Land Cover and Land Use Change program at South Dakota State University. The program uses frequent MODIS imagery to detect change and then stratifies Landsat samples to make accurate estimates of land-cover change (Hansen et al. 2008b; see Figure 16a). MODIS cannot be used directly to estimate land-cover change since most change occurs at subpixel scales (Achard et al. 2007; Sanchez-Azofeifa et al. 2009). The advantages of change-stratified random sampling are that it maximizes change detection for a given set of imaging processing resources and yields unbiased measurements of forest change. This approach is less suited for sampling characteristics of standing forests.

The third approach, wall-to-wall sampling, completely maps a region with imagery. Examples include Brazil's PRODES program (see Figure 16b) and India's biennial forest survey as well ongoing efforts in the United States (National Land Cover Database), Europe (CORINE), Canada, New Zealand, Australia, and South Africa (DeFries et al. 2007; Herold et al. 2007). Wall-to-wall sampling is ideal for detecting land-cover change and shifts in deforestation (often referred to as leakage) between countries, but the method is logistically challenging in the need to acquire, process, and analyze the number of images required to cover the global land area.

Figure 15. Grid Sampling with Moderate-Resolution Images

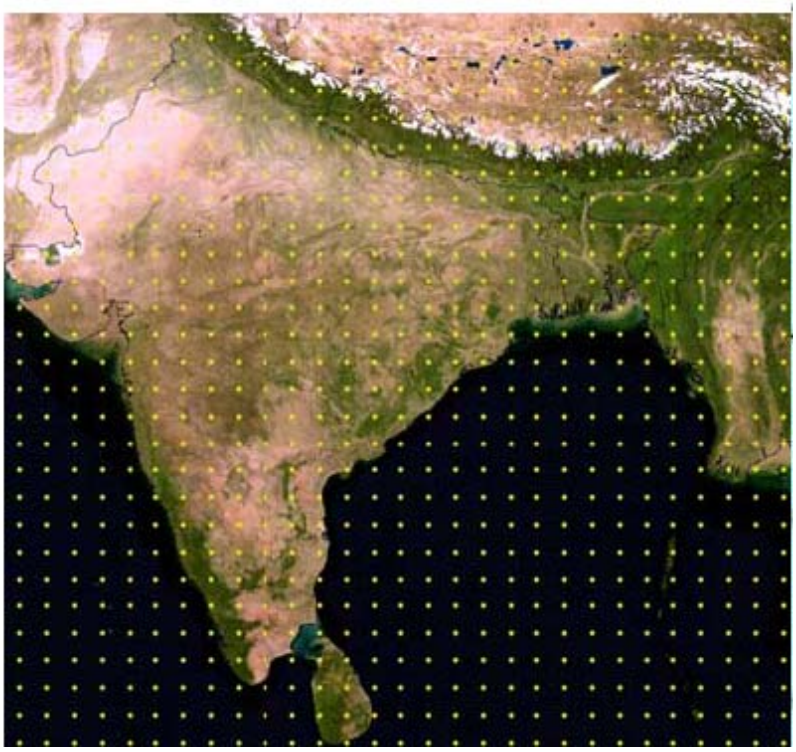

Note: Each dot is the center of a single IRS image.
Source: GOFC-GOLD 2008.

Figure 16a. Example of Resolution-Stratified Sampling

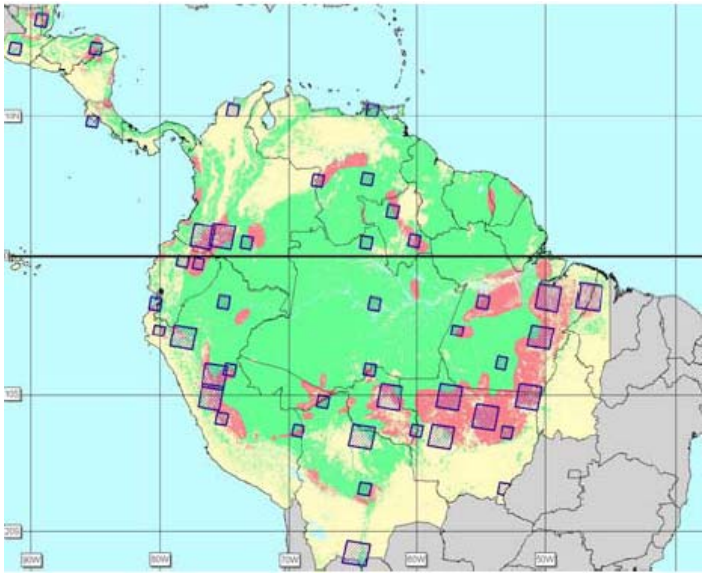

Note: Moderate-resolution samples are concentrated in areas of change (red) determined from coarser-resolution imagery.
Source: GOFC-GOLD 2008.

Figure 16b. Example of Wall-to-Wall Sampling with Moderate-Resolution Imagery in Brazil

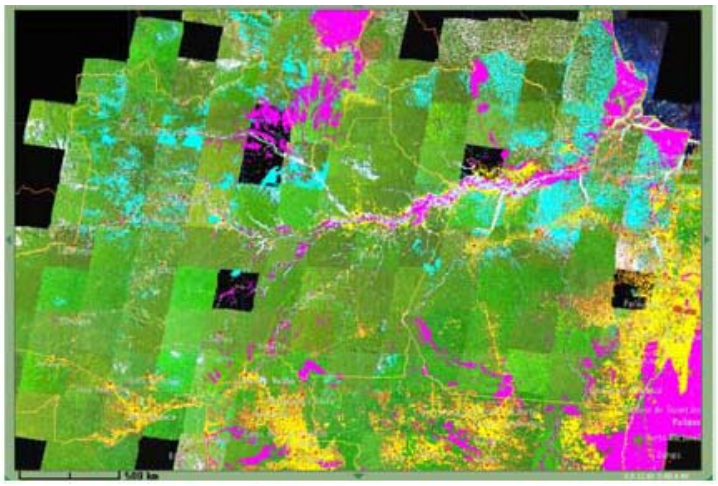

Note: Notice the difference in illumination and cloud cover between moderate-resolution images.
Source: GOFC-GOLD 2008.

3.5 Price and Logistics

The large quantities of imagery associated with global forest measurement will necessitate budgetary choices, automated processing chains, and deliberation on selection of re-sampling intervals (Achard et al. 2007; DeFries et al. 2007; GOFC-GOLD 2008; Olander et al. 2008; Rosenqvist et al. 2003). Table 3 summarizes the costs of imagery required to do wall-to-wall sampling of global forests at different resolutions. High-resolution imagery would be very expensive at current prices, as discussed in-depth in Section 4.2.2 for LIDAR. Automated analysis of imagery is quick and standardizes results, but the large number of images required to cover the world's forests at moderate resolution will require large processing resources for automated classification (Andersson et al. 2009; DeFries et al. 2007; Mayaux et al. 2005). Although modern computers are capable of processing this amount of imagery, either significant investment or computing partnerships are required (GOFC-GOLD 2008). The re-sampling interval can be affected by the amount of time required to process each year's imagery; the Brazilian National Institute for Space Research (INPE), for example, prioritizes high-change areas for early processing to ensure timely revisits (Achard et al. 2007).

Decisions on how often to sample the world's forests should take into account processing times and the availability of cloud-free passive imagery (GOFC-GOLD 2008). Cloud-free, global Landsat mosaics contain imagery every three to five years but cloud-free MODIS mosaics can be created seasonally due to their high return time (e.g., Morton et al. 2005). Clouds persist in some areas even in ostensibly cloud-free images, necessitating fusion with SAR imagery to penetrate clouds in certain tropical areas (Olander et al. 2008; Lindquist et al. 2008; Rosenqvist et al. 2008). The ALOS forest mapper program, notably, will produce global, cloud-free forest cover maps annually from 2007 onward (J. Kellndorfer, pers. comm.). With processing and cloud delays, a global forest monitoring effort may be capable of producing annual or biannual forest maps at coarse-resolution; without the use of SAR, moderate-resolution, cloud-free maps may take several years to produce.

It is expensive to integrate remote sensing estimates with forest inventory data, LIDAR data, and high-resolution imagery, yet selective ground-truthing is absolutely critical to evaluate accuracy (Gibbs et al. 2007; GOFC-GOLD 2008; Olander et al. 2008; Rosenqvist et al. 2003). High-resolution imagery collections, including Google Earth, can be used as substitutes for ground-truthing land-cover estimates (e.g., Gibbs et al. 2007; Read et al. 2003; Helmer et al. 2009; Bicheron et al. 2008), but ground data are required for biomass and carbon estimates (Gibbs et al. 2007).

In contrast to locally accurate analyses, for which conclusions are geographically restricted, global remote sensing analyses sacrifice local accuracy for greater global accuracy. A global, dispersed network of ground-truth data is necessary to quantify this accuracy (e.g., Bicheron et al. 2008). Large amounts of ground-truth data already exist in some regions, and foresters and forest ecologists continue to collect more in many organized forest-sampling programs (Herold 2009). Collecting and coordinating ground-truth data for global forest measurement would be a useful scientific undertaking (Herold et al. 2008).

Chapter 4. An Overview of Remote Sensing Capabilities for Forest Measurement: Current and Near-Term Technologies

In the preceding chapters, we noted several key limitations of remote sensing: (a) tradeoffs in swath and resolution in current sensor technology (Section 3.2), (b) the small number of active sensors currently in orbit (Section 2.4.1), (c) the relevance of inexpensive imagery for frequent global coverage (Section 3.5), (d) the wisdom of redundancy in satellite selection (Section 2.4.3), and (e) the need for ground-truthing to validate the accuracy of conclusions from remote imagery (Section 3.5). In light of these limitations, we next consider the capability of remote sensing to measure the global forest—specifically, global forest area, forest structure, and other forest properties in Table 4.

4.1 Forest Area: Current Measurement Methods

Global forest area is often measured as two classes (forest/nonforest) or binned (that is, categorized) into homogenous forest types that do not distinguish tree plantations or disturbed forests (Hansen et al. 2008b; Bicheron et al. 2008). Forests are quite distinct from most nonforest types of land cover, so forest/nonforest area can be measured with optical and SAR sensors with a high degree of accuracy (from 80 > 90 percent). Distinguishing more than two land-cover classes, such as forests of different ages or composition, can still result in high accuracy, but classification accuracy usually decreases with an increasing number of forest classes (Foody 2002) or when a larger area is examined (Olander et al. 2008). As a result, remote sensing is ideally suited to detect forest removal (deforestation or clear-cutting) but less well suited to detect forest thinning or forest replacement by industrial tree plantations (DeFries et al. 2007; Sanchez-Azofeifa et al. 2009). Challenges remain in distinguishing primary forests from tree plantations and older secondary forests (Kimes et al. 1999; Sanchez-Azofeifa et al. 2009; Song et al. 2007; Thenkabail et al. 2004), and in detecting forest degradation, which is a reduction in forest canopy cover or biomass that does not result in complete forest clearing (DeFries et al. 2007). We explore these topics further below.

4.1.1 Sensor Types and Measuring Forest Area

Each sensor type has different strengths and weaknesses for measuring forest area. Coarse-resolution sensors have the greatest capability for global coverage and high return times (Achard et al. 2007; Rosenqvist et al. 2003), but their pixel size causes them to miss the majority of deforestation events (Olander et al. 2008; DeFries et al. 2002; Sanchez-Azofeifa et al. 2009; Morton et al. 2005). High-resolution sensors enable measurement of tree crown area and fine delineation of forest composition and disturbance, but their small swaths limit their utility for repeated, cloud-free global measurement (Andersson et al. 2009). By balancing a large swath size with spatial resolution that is able to detect the majority of land-use change, moderate passive sensors are considered the best compromise for regional land-cover monitoring (Achard et al. 2007; Olander et al. 2008; Andersson et al. 2009). Finally, hyperspectral and polarized SAR sensors have improved the ability to distinguish among forest types and map forest cover (DeFries 2008; Thenkabail et al. 2004; Hoekman and Quinones 2000). Analyzing their imagery can be technically difficult, however (Kasischke et al. 1997; Ustin et al. 2004). Future refinements in image fusion techniques and new satellite technology can be expected to improve measurements of forest area and type.

4.1.2 Forest Area versus Measuring Change in Forest Area

Measuring forest area is distinct from measuring changes in forest area, for both practical and quantitative reasons. Practically, increases in forest area often result from land-cover types that are quite spectrally distinct from the original forest and would not be classified as forest area. In temperate and tropical areas, woody encroachment into grasslands creates spectrally and structurally distinct forests in unexpected areas, and forest regrowth on abandoned farms creates distinct secondary forests (Houghton 2005). Deforestation results in the conversion of forests to a variety of agricultural land covers, including spectrally similar tree plantations. Tropical forest regrowth is very rapid, making ten- to twenty-year-old forests difficult to distinguish from primary forest on a satellite image (see Section 4.1.5).

From a quantitative standpoint, measuring change in forest area is distinct from classifying two land-cover maps. To illustrate why, consider the most basic land-cover change method, post-classification; quantifying the changes between two classified land-cover maps. In this method, high classification accuracy is critical because quantifying land-cover change by comparing two land-cover maps multiplies their respective errors (Lu et al. 2004). A multitude of other methods of quantifying land-cover change over time are reviewed at length by Lu et al. (2004). There are several general methods for global land-cover analysis. Image differencing subtracts two images and then classifies the areas that have experienced changes in spectral characteristics (e.g., greenness). Combined analysis fuses both images in the same dataset and then classifies the combined dataset, labeling the changes. Hybrid analysis identifies which pixels have changed between dates and classifies only the changed areas (Lu et al. 2004).

In the discussion of measuring forest area below, we focus primarily on the accuracy of classified land-cover maps because distinguishing land-cover types is a necessary first step in accurately classifying changes in forest area.

4.1.3 Coarse Passive Sensors and Forest Area

There have been numerous global and regional efforts to map forests using coarse-resolution sensors, and others have ably reviewed them (see Table 4 in Herold et al. 2008; Table 1 in Mayaux et al. 2005; and Table 2 in Achard et al. 2007). Efforts to create global land-cover maps have used four satellites: AVHRR, MODIS, SPOT Vegetation, and Envisat/MERIS. Two main types of products have resulted from these mapping programs: land-cover classifications and tree-cover continuous fields (AVHRR and MODIS only). All these products have historically been freely available for download, increasing their use in global land-cover analysis.

The tree-cover continuous fields maps are a part of an effort to produce continuous, subpixel estimates of vegetation traits from AVHRR and MODIS data (Hansen et al. 2003). These efforts use higher-resolution Landsat and IKONOS data to train an algorithm that calculates percent tree cover for each coarse-resolution pixel. This coarse-fine fusion method yields estimates of forest cover that can be adapted for any forest definition and is capable of coarse distinctions of forest cover based on leaf type and density (Hansen et al. 2003).

Land-cover classifications assign one land-cover class per pixel and have been ongoing since 1992 (AVHRR), 2000 (MODIS, SPOT Vegetation, and 2005 (MODIS, SPOT Vegetation, and Envisat/MERIS) (Herold et al. 2008). Currently the Envisat/MERIS 300 m resolution GLOBCOVER

product is the highest resolution global land-cover map. Maps of tropical forests have also been produced at 250 m resolution from MODIS (Bicheron et al. 2008; Hansen et al. 2008b). Even just as static snapshots, these global maps have been important in climate and carbon modeling (DeFries 2008; Achard et al. 2007).

These coarse-resolution mapping efforts have several limitations. The number of land-cover classes differs between mapping efforts and land-cover classifications are often difficult to assign in disturbed, heterogeneous, or transitional ecosystems (Herold et al. 2008; Mayaux et al. 2006). Simple, coarse-resolution forest/nonforest classifications have between acceptable and high accuracy (Latifovic and Olthof 2004; Hansen et al. 2003). Coarse-resolution classifications with multiple land-cover categories have had poor to low accuracy in representing actual land cover (e.g., GLOBCOVER has 67 percent accuracy) (Bicheron et al. 2008; Latifovic and Olthof 2004; Mayaux et al. 2006). These land-cover classifications (e.g., Ground Land Cover 2000, or GLC 2000; GLOBCOVER) do not always agree with each other (Giri et al. 2005). Figure 17 indicates two different land-cover maps, the GLC 2000 and MODIS continuous fields, which disagree markedly in Central America. The scientific effort Geowiki.org is trying to use volunteer input and high-resolution imagery to revise conflicts between global land-cover maps and improve their classification accuracy (IIASA 2009).

The capacity of coarse-resolution sensors to detect forest clearing and forest fires in almost real time is particularly important to slowing deforestation in the tropics, where it is difficult to monitor remote forests. We examine this later in the chapter (Section 4.4.2). The frequent return time of MODIS permits phenology-based mapping of tropical deforestation with 89 percent accuracy, for example Morton et al. (2005). With one-day image processing, INPE uses MODIS imagery in a real-time deforestation prevention program called Detection and Monitoring of Selective Logging Activities, or DETEX, to prevent large-scale, illegal clearing in the Brazilian Amazon (DeFries 2008; Herold 2009). Coarse-resolution imagery can only detect complete clearing and only detects a low percentage of actual deforestation that is greater than10–20 ha in size (Sanchez-Azofeifa et al. 2009; Achard et al. 2007). In Costa Rica, for example, only 10 percent of deforestation was detected (Sanchez-Azofeifa et al. 2009). Coarse-resolution imagery is best used, therefore, as a detection or sampling tool to target higher-resolution sensors (i.e., the stratified sampling program mentioned in Section 3.4) (DeFries et al. 2007).

The availability of frequent, free 250–300 m resolution imagery has improved deforestation detection and land-cover mapping because the imagery matches the scale (6.25–9 ha) of large-scale forest clearings for farming and ranching and the approach can detect changes of around 10–20 ha in size (Figure 18, Achard et al. 2007). The NPOESS satellite series is intended to replace the MODIS and AVHRR satellites, but NPOESS will have 400 m to 1 km resolution (Townshend and Justice 2002), limiting it to detect only extremely large clearings between 16 ha to 100 ha in size. The Japanese GCOM-C1 (with 11 bands at 250 m resolution) and the European Sentinel-3 series (with 21 bands at 300 m resolution) may be better suited to continue the MODIS and Envisat/MERIS record (Appendix). It will be difficult to equal the combination of resolution, revisit time, and free imagery that the MODIS Terra and Aqua constellation currently offers to global land-cover analysis.

Figure 17: Coarse-Resolution Classification Disagreements

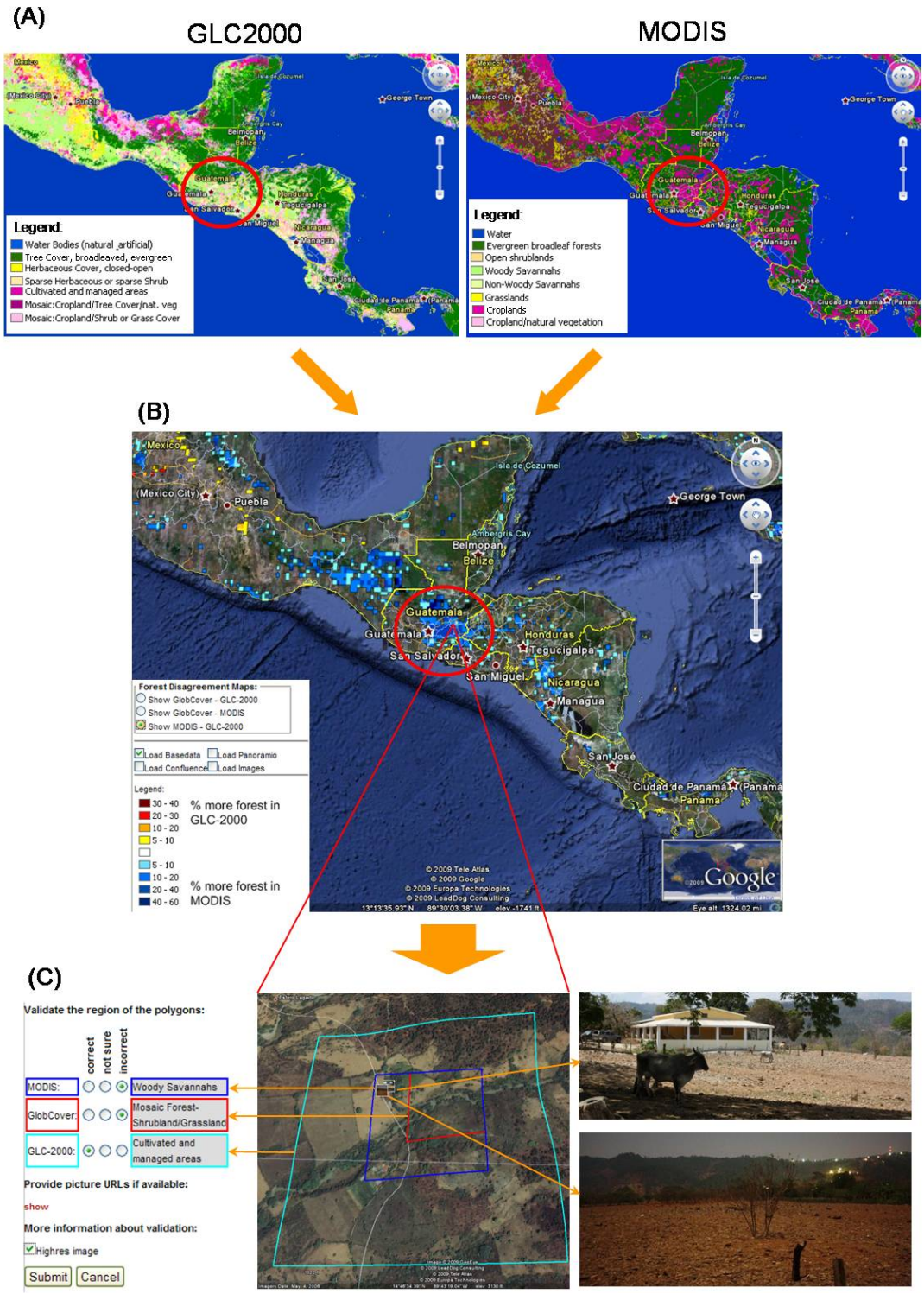

Notes: Forest cover from Mexico to Panama classified by GLC 2000 and by MODIS (A) and the disagreement between them (B). The red circle identifies a hot spot of disagreement in Guatemala and El Salvador. The Web tool allows one to validate these disagreements using high-resolution satellite imagery and GeoTagged Pictures (for example, Panoramio) (C).
Source: Created using GeoWiki, 2009.

The frequent revisit time of coarse-resolution sensors allows for near-daily monitoring of phenology, important for land-cover classification and detection of future climate change as described in Chapter One (Morton et al. 2005; Goetz et al. 2005). Repeated passes that capture seasonal leaf dynamics can improve detection of seasonal tropical forests (e.g., Morton et al. 2005) and coarse-resolution imagery will remain useful for forest measurement well into the future. Given the usefulness of the vegetation continuous fields and the potential for automated subpixel detections of deforestation (e.g., DETER), coarse-fine imagery fusions are an excellent method to increase the resolution of coarse-resolution imagery (e.g., Hansen et al. 2003). Next-generation geostationary satellites (GOES-R, FY-4) are expected to improve to 1 km resolution in the VNIR sometime around 2014. This change would enable real-time monitoring of large-scale deforestation, fires, and phenology and could provide dramatically improved inputs to carbon and climate models (Chuvieco 2008; DeFries 2008).

4.1.4 Moderate Passive Sensors and Forest Area

Moderate passive sensors have resolution on a scale appropriate for forest management (Figure 18). The sensors are able to capture forest changes at the scale of one hectare in local analyses and two to five hectares in regional analyses (Olander et al. 2008; Achard et al. 2007). Forest/nonforest cover can be distinguished by moderate sensors with greater than 90 percent accuracy in local areas. Over larger areas accuracy declines to between 85 and 90 percent (Olander et al. 2008). Several forest mapping efforts use moderate-resolution images; these include subnational and national wall-to-wall mapping (Achard et al. 2007; Herold et al. 2008) and global sampling efforts (Mayaux et al. 2005). Herold (2009) reviews national mapping efforts extensively.

Global wall-to-wall collections of moderate-resolution imagery could be constructed at considerable expense from IRS, SPOT, or DCM data, but the Landsat global mosaics are the only free, publicly available global imagery (Achard et al. 2007). As of 2009, "cloud-free," global Landsat mosaics for 1975, 1990, 2000, and 2005 have been created and efforts are under way to create an error-free Landsat 7 mosaic for 2010 (Lindquist et al. 2008; Hansen et al. 2008a). The Landsat mosaics contain date metadata for each component image to allow for correct interpretation—for example when calculating local deforestation rates. These global Landsat mosaics have been suggested by several authors as excellent sources for forest area reference maps for REDD (Gibbs et al. 2007; Olander et al. 2008; Achard et al. 2007).

Although the global Landsat mosaics offer opportunities for mapping global forests, numerous challenges arise in analyzing them for forest area. Because of obstructions in coverage in cloudy areas, most nonconstellation moderate sensors (i.e., all except the IRS and DCM series) have de facto return times of a year or more in tropical areas (Asner 2001; Olander et al. 2008). This limit can seriously compromise efforts to map seasonal forests, especially in tropical areas, because of the difficulty in distinguishing leafless forests during dry seasons when most imagery is acquired (Sanchez-Azofeifa et al. 2009; Asner 2001). To develop the global Landsat mosaics, scientists were forced to knit together images taken over several years (e.g., 1986–1991 for the 1990 mosaic). Even then, unacceptable levels of cloud cover persisted in about 25–30 percent of the Landsat mosaic images in Ecuador (Olander et al. 2008) and 16 percent of mosaic images in the Congo Basin (Lindquist et al. 2008). Aside from the detection of seasonal forests, automated classification of

Landsat mosaics requires correction for the variety of sun illumination angles (known as radiometric correction) and the creation of global or regional algorithms to classify different land covers (Lu et al. 2004; Schroeder et al. 2006; Bicheron et al. 2008). Landsat classification algorithms developed in one region are unlikely to be accurate in another region even if the regions are similar (e.g., Foody et al. 2003).

Figure 18. Resolution of Sensors Relative to Ecological Measurements

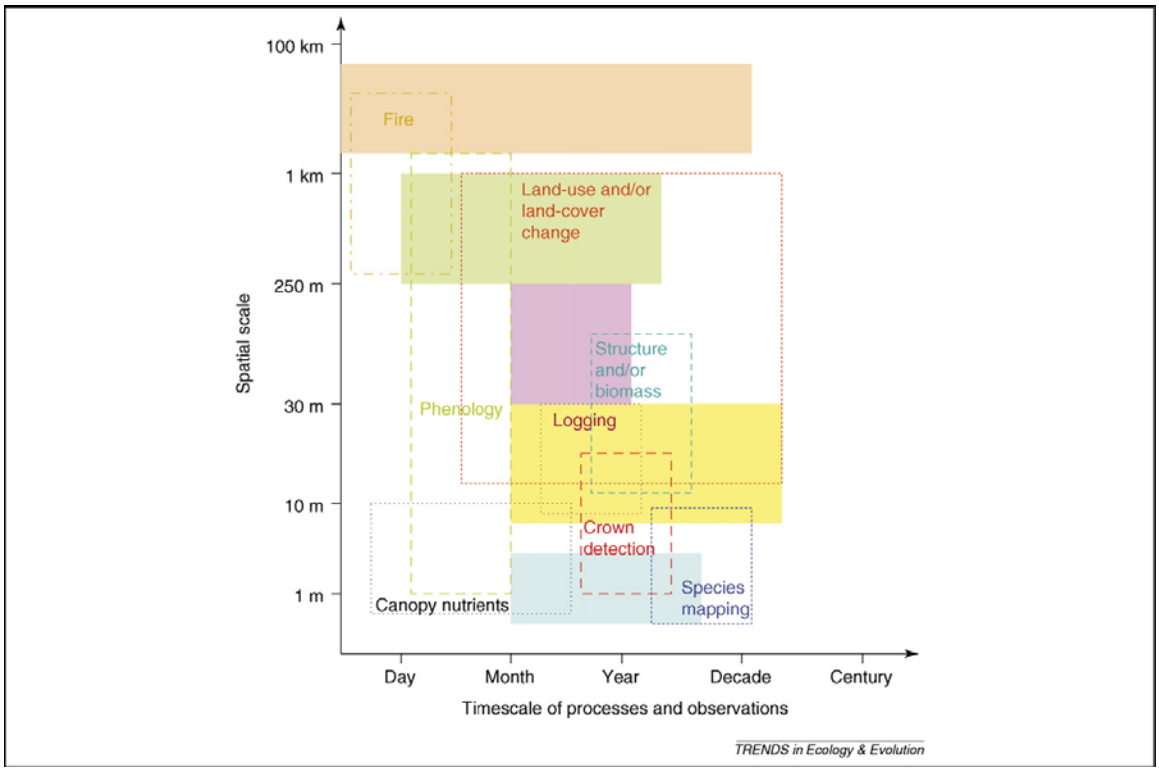

Notes: The dotted boxes indicate the temporal and spatial scale of ecological processes and human disturbances. The solid colored boxes show the spatial scale and temporal record length of selected satellite and airborne sensors (GOES—beige; MODIS—green; LIDAR/Radar—pink-purple; Landsat/Earth Observing One [EO-1]—yellow; IKONOS/Quickbird/Airborne—light blue).
Source: Chambers et al. 2007.

Regional wall-to-wall mapping efforts, global sampling efforts, and one global, moderate-resolution land-cover map (GeoCover LC; Cunningham et al. 2002) indicate that these challenges could be overcome. The current moderate-resolution GeoCover LC map has mixed global accuracy (72 percent) and very broad forest classes (Cunningham et al. 2002). An accurate, detailed 30 m resolution forest map would be a significant, tenfold improvement in global land-cover mapping (Bicheron et al. 2008). Re-processing the global 30 m Landsat archive (1983–present) to create a season-appropriate, cloud-free, and radiometrically corrected imagery time-series is feasible with current technology, although the project would be computationally intensive. Algorithms have been developed recently to eliminate clouds and cloud shadows as well as to improve the Landsat mosaics by fusing together, or compositing, time-series of Landsat and MODIS images (Lindquist et al. 2008; Roy et al. 2008; Hansen et al. 2008a). In addition, automated radiometric correction, which

is often difficult in all-forest images, has been demonstrated on a series of Landsat images (Schroeder et al. 2006; Xian et al. 2009).

4.1.5 Moderate-Resolution Imagery and Land-Cover Classification

The literature on land-cover classification with moderate-resolution imagery is extensive (partially reviewed in Sanchez-Azofeifa et al. 2009; Patenaude et al. 2005; Olander et al. 2008; and Coppin et al. 2004). Because classification accuracy generally decreases with an increasing number of classes (Foody 2002), we use the land-cover classification hierarchy of Anderson et al. (1976) when referring to the accuracy of different classifications. In this hierarchy, a Level I classification distinguishes basic classes (forest, nonforest vegetation, agricultural, urban) and a Level II classification distinguishes more land-cover classes, including forest types. As mentioned above, Level I accuracy in excess of 85 percent is usually observed with moderate-resolution imagery, with higher accuracy at higher resolution (Salajanu and Olson 2001; Peterson et al. 2009). Generally, accuracy decreases with an increasing number of classes. Published Level II classifications have ranged from 65 to 85 percent accuracy (references in Patenaude et al. 2005). In general, extending Level II classification algorithms developed in one region to other regions is a technical challenge that is not always met (Sanchez-Azofeifa et al. 2009; Loveland et al. 2002; Xian et al. 2009; Rogan et al. 2008; Foody et al. 2003).

Distinguishing among forest types, forest ages, degraded and intact forests, and tree-based agroecosystems can also be challenging (Sanchez-Azofeifa et al. 2009; Olander et al. 2008; Patenaude et al. 2005). In temperate forests, Salajanu and Olson (2001) were able to classify a forested area in Michigan to Level 1 with 89–91 percent accuracy, but accuracy decreased to 77–84 percent for distinguishing 10 forest types. In Siberia's Baikal region, Peterson et al. (2009) were able to distinguish four boreal forest classes with 80–98 percent accuracy. In tropical forests, Thenkabail et al. (2004) found that moderate-resolution, multispectral sensors had poor (40–50 percent) accuracy in distinguishing nine forest types and ages. By contrast, Sesnie et al. (2008) were able to discriminate 17 forest classes with 93 percent accuracy using a fusion of spectral, DEM, and climatic GIS layers. Sesnie et al. (2008) had 69 percent accuracy with spectral classes alone, indicating that detailed Level II classification in tropical areas may require GIS fusion or hyperspectral data. We explore this further below (Section 4.1.6).

In both tropical and temperate zones, moderate-resolution imagery cannot distinguish forest regrowth from mature forest after 15–30 years of growth (Steininger 1996, 2000; Nelson et al. 2000; Song et al. 2007; Fiorella and Ripple 1993). Partially logged or cleared forests have long been difficult to distinguish from intact forests (Sader et al. 2003; Wilson and Sader 2002; Achard et al. 2007), but recently, promising spectral analysis techniques have been developed to map subpixel forest degradation in the Brazilian Amazon using moderate-resolution imagery (Asner et al. 2005; Souza et al. 2005b).

In the tropics, distinguishing forests from tree-based agriculture (i.e., agroforestry, tree plantations) is difficult using moderate-resolution imagery; the plantations often appear similar to secondary forests (Sanchez-Azofeifa et al. 2009). In Malaysia, Baban and Yosuf (2001) were able to distinguish rubber plantations with 74 percent accuracy and found that plantations were most often confused with intact forests. Sesnie et al. (2008) were able to distinguish tree plantations with approximately 90 percent accuracy in Costa Rica, but accuracy decreased to 55 percent when the

entire image was examined across diverse plantation types. Kuplich et al. (2000) were able to distinguish planted Eucalyptus and Pinus forests with 89 percent accuracy in a fragmented Brazilian agricultural landscape. In eastern Ecuador, Santos and Messina (2008) used Landsat 7 to do a Level II classification of an oil palm-secondary forest landscape with 77 percent accuracy.

Despite these challenges in Level II classification of forests, classification of moderate-resolution imagery has progressed significantly in recent years (Coppin et al. 2004). One promising approach is the classification of land-cover trajectories over time (rather than static images) made possible by the recent opening of the Landsat image archive (Kennedy et al. 2007; Masek et al. 2008; Coppin et al. 2004; Song et al. 2007). For example, Helmer et al. (2009) mapped age classes of tropical forest regrowth with very high accuracy by using the entire, 37-year Landsat archive to age regrowth on previously cleared pixels. This new trajectory classification method, in addition to the compositing methods mentioned above (Hansen et al. 2008a), underscores the importance of long, continuous time-series of moderate-resolution imagery to land-cover analysis (and the critical nature of the success of the LDCM).

4.1.6 Hyperspectral Sensors: Forest Area and Beyond

Hyperspectral images, although they have limited global coverage, are markedly better (e.g., 40–70 percent better) than multispectral moderate-resolution images in distinguishing and mapping diverse forest types and other land covers (Thenkabail et al. 2004; Ustin and Xiao 2001; Goodenough et al. 2003). Even though the potential is still being explored, hyperspectral images already have a wide diversity of applications due to the ability to measure the absorption of light by chemicals. This ability in turn allows direct measurement of leaf chemistry and the quantification of photosynthetic and non-photosynthetic (woody) cover (Asner and Martin 2009; Chambers et al. 2007; Ustin et al. 2004). Hyperspectral imagery improves measurement of LAI (Lee et al. 2004; Schlerf et al. 2005), forest productivity (via canopy nitrogen; Smith et al. 2002; Ollinger and Smith 2005), canopy structure (Arroyo-Mora et al. 2009), and drought stress (Asner et al. 2004). The imagery also makes new measurements of forest diversity possible, including canopy leaf ecophysiology (Asner et al. 2009) and the discrimination of individual species and species groups (Goodwin et al. 2005; Asner et al. 2008; Clark et al. 2005). Moderate-resolution hyperspectral imagery, which will become widespread in the next few years as the EnMap, HyspIRI, and several other satellites are launched, has the potential to revolutionize forest biodiversity measurements in a new science of "remote spectranomics" (Asner and Martin 2009). Although many new hyperspectral sensors will have relatively narrow swaths and may be unsuited for global forest measurement, the HyspIRI sensor will have a 90 km swath (Appendix) and is likely to markedly improve the accuracy of land-cover mapping.

4.1.7 High-Resolution Passive Sensors: Forest Area in Focus

Because high-resolution passive sensors have a narrow swath and pointable, interrupted coverage, there are currently no continuous global land-cover maps or cloud-free image mosaics at high resolution (Loarie et al. 2007). GeoEye's constellation will be mapping the entire globe in the next few years (Mark Brender, pers. comm.), but cloud-free imagery is unlikely to result (Asner 2001; Olander et al. 2008). SPOT-5 has continuous global coverage at 10 m resolution, but the imagery has not been analyzed. RapidEye, a high-resolution constellation with daily repeat capacity

(launched in 2008–2009), has the potential to develop cloud-free, continuous global maps (RapidEye 2009).

Currently, Google Earth has the largest collection of global high-resolution imagery, but the imagery is from a variety of satellite and airborne sources with differing resolutions and undisclosed dates (Potere 2008). Google Earth may not yet be useful for strict change detection on a global scale, but the approach is very useful for land-cover validation and visualization (e.g., IIASA 2009; Bicheron et al. 2008; Helmer et al. 2009; Olander et al. 2006). The same result is true for high-resolution imagery in general: the imagery is an inefficient way to map global forests due to irregular spatial sampling (Loarie et al. 2007; Andersson et al. 2009), relatively high cost (Olander et al. 2008; Andersson et al. 2009), data-sharing restrictions, and radiometric correction challenges (e.g., variable canopy shadowing) (Goetz et al. 2003; Andersson et al. 2009). Current policies about access to data restrict the sharing of original data but allow sharing of data products, such as basic maps, for almost all high-resolution imagery. However, the imagery is useful for identifying local land covers (Wulder et al. 2004) and forest disturbance (Thompson et al. 2008; Wulder et al. 2008; Souza and Roberts 2005a), and even following the population dynamics of individual tree species (Clark et al. 2004a). High-resolution imagery has immense utility for ground-truthing lower resolution imagery, both as a fine-scale validation tool and as training data for algorithms (e.g., Hansen et al. 2003; Wang et al. 2005).

Although high-resolution imagery does not have the spectral resolution of other sensors (most notably missing the short-wave infrared [SWIR] bands), the imagery contains additional information on the shape and texture of objects in the landscape that lower-resolution imagery lacks (Goetz et al. 2003). The accuracy of high-resolution imagery in distinguishing Level I land-cover classes in forested landscapes is very high—in the range 95 percent and greater (Townsend et al. 2009). As such, the imagery is often used as a tree-cover validation for lower resolution imagery either visually (e.g., Kozak et al. 2008; Neigh et al. 2008) or quantitatively (Knorn et al. 2009; Hansen et al. 2003; Wang et al. 2005). Because spectral information is limited (often four bands) and spatial algorithms are still under development, high-resolution imagery is less accurate at Level II classifications (~70–90 percent; Ouma et al. 2008; Mallinis et al. 2008; Gergel et al. 2007; and Morales et al. 2008). The high-resolution sensors are capable of distinguishing small-scale land covers and disturbances that do not appear in moderate-resolution imagery, such as riparian strips (Gergel et al. 2007), pest outbreaks (Wulder et al. 2008), and logging (Souza and Roberts 2005a), and the visual interpretation of the high-resolution imagery is straightforward (Wulder et al. 2004). Automated crown-delineation techniques have been developed recently (Broadbent et al. 2008; Palace et al. 2008), and high-resolution imagery shows potential for using crown size to classify secondary forests that are older than 20 years (Clark et al. 2004a; Kayitakire et al. 2006).

4.1.8 SAR Sensors and Passive-SAR Fusions for Forest Area

SAR has potential for global forest mapping, and SAR capabilities have been extensively reviewed elsewhere (Patenaude et al. 2005; Rosenqvist et al. 2003; Lu 2006; Balzter 2001; and Kasischke et al. 1997). Here, we simply summarize the main conclusions of prior research and focus on recent developments in SAR research. SAR distinguishes land cover based on the strength of backscatter, the variation in backscatter over space (texture), and, depending on the analysis, temporal variation in backscatter signatures. Regional maps of forest cover have been derived from SAR sensors including the Global Rainforest Map (JERS sensor; Rosenqvist et al. 2000) and the

Central Africa Mosaic project maps (ERS sensors; De Grandi et al. 1999). The ALOS Pathfinder mission has created the first global L-band SAR forest map at 50 m resolution, and the mission will continue to do so annually (J. Kellndorfer, pers. comm.).

Scientists fully appreciate the potential of satellite SAR sensors to distinguish land cover; their capabilities are well known from analysis of data from advanced airborne SAR sensors and the multi-polar, multiband SAR sensor (C-, X-, and L-band) aboard the 1994 SIR-C/X shuttle mission (Kasischke et al. 1997; van der Sanden and Hoekman 1999). In general, single-band SAR sensors with one polarization (e.g., ERS-1, JERS-1) have variable accuracy (low to very high) in Level I classifications depending on topography, surface moisture, and the structural complexity of the landscape (Patenaude et al. 2005; Kellndorfer et al. 1998; Podest and Saatchi 2002). As the number of polarizations or SAR bands increases, Level I accuracy can be very high (>90 percent), rivaling or exceeding passive sensors (Dobson et al. 1995a; Kellndorfer et al. 1998; Patenaude et al. 2005). Level II accuracy is also very dependent on the number of polarizations and bands employed, achieving accuracies between 70–90 percent (Kasischke et al. 1997; Kellndorfer et al. 1998). Dobson et al. (1995a), notably, have very high Level I and II regional accuracy with polarized, multiband data in Michigan forests. Saatchi et al. (1997), with multipolar SIR-C/X data, are able to measure Amazon forests with very high (92 percent) Level I accuracy and acceptable (72 percent) Level II accuracy. The L-band JERS-1 and ALOS Phased Array type L-band Synthetic Aperture Radar (PALSAR) sensors have been shown to have very high Level I accuracy when classifying several different forested regions (Thiel et al. 2006; Saatchi et al. 2000; Kellndorfer et al. 2008). Because of the high SAR reflection from water, longer wavelength sensors have created highly accurate maps of mangroves and floodplain forests (Costa 2004).

The accuracy of SAR sensors is affected by ecosystem structure (Almeida et al. 2007; Kellndorfer et al. 1998, 2004), variability in soil and vegetation moisture (Kasischke et al. 1997), and topography (Kellndorfer et al. 1998). High-resolution digital elevation maps are necessary to correct for topographical distortions; accuracy decreases markedly without effective correction (Kellndorfer et al. 1998; Ticehurst et al. 2004). Because of its high moisture sensitivity, the C-band is the least useful for land-cover classifications, although its utility for Level I classification increases when multiple polarizations are used (Saatchi et al. 1997; van der Sanden and Hoekman 1999; Kasischke et al. 1997).

Recent research in SAR land-cover mapping has investigated the potential of optical-SAR fusions (Saatchi et al. 2007; Santos et al. 2008) and InSAR for improved landscape classification (Balzter 2001; Engdahl and Hyyppa 2003; Park and Chi 2008). Interferometric SAR can improve classifications by adding vegetation height information to other SAR measures like texture and backscatter (Balzter 2001). Optical-SAR fusions shows promise for synergistic landscape classification (Kasischke et al. 1997; Kuplich et al. 2000). In Indian dry forests, fusion of moderate-resolution passive and Envisat ASAR C-band data improved Level II classification (>90 percent) (Chand and Badarinath 2007). In Amazonia, Kuplich et al. (2000, 2006) found Landsat–SAR fusions improved Level 2 classifications over Landsat or SAR alone, and Saatchi et al. (2007) used a SAR-optical fusion to derive vegetation and biomass classes for the entire basin. Santos et al. (2008) found that a Level II classification of oil palm plantations and forests was improved by a passive–SAR fusion, to 90 percent from 76 percent (SAR) and 77 percent (Landsat). In central Africa,

Mayaux et al. (2000) used AVHRR and ERS data fusion to classify forests, savannas, mangroves, swamp forests, and tree plantations with 75 percent accuracy.

Given the large number of SAR constellations planned for launch in the 2009–2015 period, it is likely that InSAR, multiband SAR fusions, and optical–SAR fusions will become increasingly important techniques in land-cover classification.

4.2 Forest Structure: Current Measurement Methods

We next review the use and relative accuracy of different remote sensing methods to measure vertical and horizontal forest structure, with an emphasis on forest height. Remote sensors are sensitive to forest structure, which, in conjunction with area (Table 4), is used to estimate forest volume (Section 4.3), biomass (Section 4.4), and carbon (Section 4.5).

Forests are highly complex three-dimensional structures. Forest height can vary markedly over a defined area (i.e., a tree, plot, pixel, or stand). In this report, we define the horizontal and vertical complexity of forest surfaces as forest structure; both active and passive sensors can measure variation in forest structure. Vertical forest structure can be characterized by forest height, canopy depth, leaf density profiles, and other measurements. Horizontal forest structure can be characterized by canopy width, tree density, and tree architecture.

Because of generalities in tree structure from hydraulic constraints (West et al. 2009), forest height allows for accurate estimation of volume, biomass, and other forest properties (Lefsky et al. 2002b), all discussed further below. Forest height can either be measured directly by remote sensing or estimated indirectly from allometric relationships with other remotely sensed measurements (e.g., canopy width; Song 2007). Exact measurements of forest height must derive two key parameters for a given area: ground elevation and canopy-top height. There are multiple approaches to measuring canopy-top height and ground elevation. These approaches include passive stereo, LIDAR, InSAR–ground differencing, and polarimetric InSAR (Sexton et al. 2009; Balzter 2001; St-Onge et al. 2008).

4.2.1 Stereo Measurements of Forest Structure

Multi-angle (stereo) passive sensors are used to estimate the three-dimensional structure of objects from two or more offset observations, much like SAR interferometry (Jensen 2007). Multi-angle sensors include Multi-angle Imaging SpectroRadiometer (MISR); ASTER; PROBA-CHRIS; any of the pointable, high-resolution satellites (e.g., GeoEye, SPOT-5); and aerially mounted stereo digital cameras. High-resolution stereo photography has a long history of measuring object height from aerial images (Jensen 2007). High-resolution stereo images have been effectively used to measure canopy-top height in forests with high accuracy (Brown et al. 2005; St-Onge et al. 2008) and to develop a new global, canopy-top DEM from moderate-resolution ASTER images (ERSDAC 2009). Although the accuracy of stereo imagery in estimating canopy-top height is exceeded by LIDAR and some InSAR measurements, the approach has been proposed as a means to extend LIDAR results to landscapes (St. Onge et al. 2008; Diner et al. 2005). High-resolution stereo imagery is likely to be cheaper than small-footprint LIDAR on a global scale yet it has severe limitations in terms of costs, data usage rights, and cloud-free coverage (see Section 4.1.6), and could only provide validation data for monitoring the global forest.

Coarser resolution multi-angle sensors (e.g., MISR, PROBA-CHRIS, Polarization and Directionality of the Earth's Reflectances [POLDER], repeat-pass MODIS) require locally fitted algorithms to model how reflection and absorption from multiple angles relate to subpixel canopy height and structure (Diner et al. 2005). Simple metrics of variance in reflection have been used to successfully estimate tree density and height in open forests (Sedano et al. 2008; Heiskanen 2006), and MISR estimates of height and roughness have been used to improve Level II classification accuracies in forests (Galvao et al. 2009; Liu and Kafatos 2007). Chopping et al. (2008) recently used a complex canopy model to estimate tree height and biomass in Arizona with acceptable to high accuracy (r^2 values of 0.69 and 0.81, respectively) from MISR data, and Kimes et al. (2006) found that large-footprint LIDAR estimates of forest height were closely related (r^2 =0.89) to Airborne MISR (AirMISR) height predictions in New Hampshire. Although coarse-resolution, multi-angle image analysis is in the experimental stage, the analysis has potential for relatively low cost, global estimates of forest structure (Chopping et al. 2008; Diner et al. 2005; Kimes et al. 2006). Possible inaccuracies in closed-canopy forests as well as the need for localized model creation and extensive validation make it unclear whether coarse-resolution, multi-angle sensors will yield global forest structure measurements in the next decade (Kimes et al. 2006; Chopping et al. 2008; Schull et al. 2007).

4.2.2 LIDAR Measurements of Forest Structure

Both small-footprint and large-footprint LIDAR provide excellent measurements of vertical forest structure that exceed the accuracy of other remote sensing measurements (Sexton et al. 2009; Hyde et al. 2006; Nelson et al. 2006; St-Onge et al. 2008; Balzter et al. 2007; Wolter et al. 2009; Hyyppa et al. 2008). LIDAR measurements meet standards of accuracy for ground-based measurements for forest canopy-top height (Dean et al. 2009; Naesset et al. 2004), and LIDAR measurements are distinctive because they also measure ground-elevation at the same time, allowing accurate calculations of forest height. Large-footprint LIDARs have measured forest canopy height with greater than 75 percent accuracy across a wide variety of forest types (Lefsky et al. 2002a, b; Harding 2002; Means et al. 1999; Hyde et al. 2005; Lefsky et al. 2007). Airplane-mounted, small footprint LIDARs have high accuracy (>80 percent) in measuring canopy height (Balzter et al. 2007; Clark et al. 2004b) and can measure horizontal canopy structure and other characteristics due to their high sampling density (Lefsky et al. 2002; Hyyppa et al. 2008). Small footprint LIDARs make excellent ground-truthing datasets but their small swath makes global measurement challenging (Dubayah et al. 2000; Balzter et al. 2007). Although large areas could be surveyed via aerial, small-footprint LIDAR, it would take a fleet of five planes 1,063 cloud-free days to survey Brazil's 8.5 million square kilometers (Swanson et al. 2009). Given the cloudiness of the tropics, real flight time might be six years for complete coverage.

Global, wall-to-wall coverage by LIDAR sensors is probably unlikely in the near future; even with long-range, UAS, wall-to-wall global LIDAR coverage would be logistically difficult. Obstacles include the requirement of obtaining permission to fly over countries, the amount of flying needed for global coverage, and high costs of purchasing and running multiple UAS sensors (roughly $460 million for four sensors over five years [Swanson et al. 2009]). However, three methods of global sampling by LIDAR are possible. The first is coarse-resolution sampling by LIDAR satellites described above (Section 2.2.2, Figure 10). The second, which would cost approximately $80 million, could be accomplished by using a single UAS with LIDAR sensors to conduct targeted

sampling of a diversity of forest types in selected countries. The third is mounting a LIDAR sensor on a satellite.

The large-footprint ICESat GLAS is the only LIDAR sensor in orbit, and the global, wide-interval coverage is being used for forest measurement (Figure 19). The wide spacing between LIDAR shots makes orbital LIDARs like GLAS unsuited for DEM creation or wall-to-wall sampling of forest height, but GLAS LIDAR footprints are well correlated globally with forest height (r^2= 0.83, Lefsky et al. 2007). These approaches provide an important source of data for validation and fusion with other imagery (Lefsky et al. 2002; Baccini et al. 2008; Nelson et al. 2009). For example, GLAS data have been combined with MODIS (Nelson et al. 2009; Boudreau et al. 2008) and Landsat (Helmer et al. 2009) data to create accurate regional biomass and height estimates.

Figure 19. GLAS Footprint Spacing in Africa

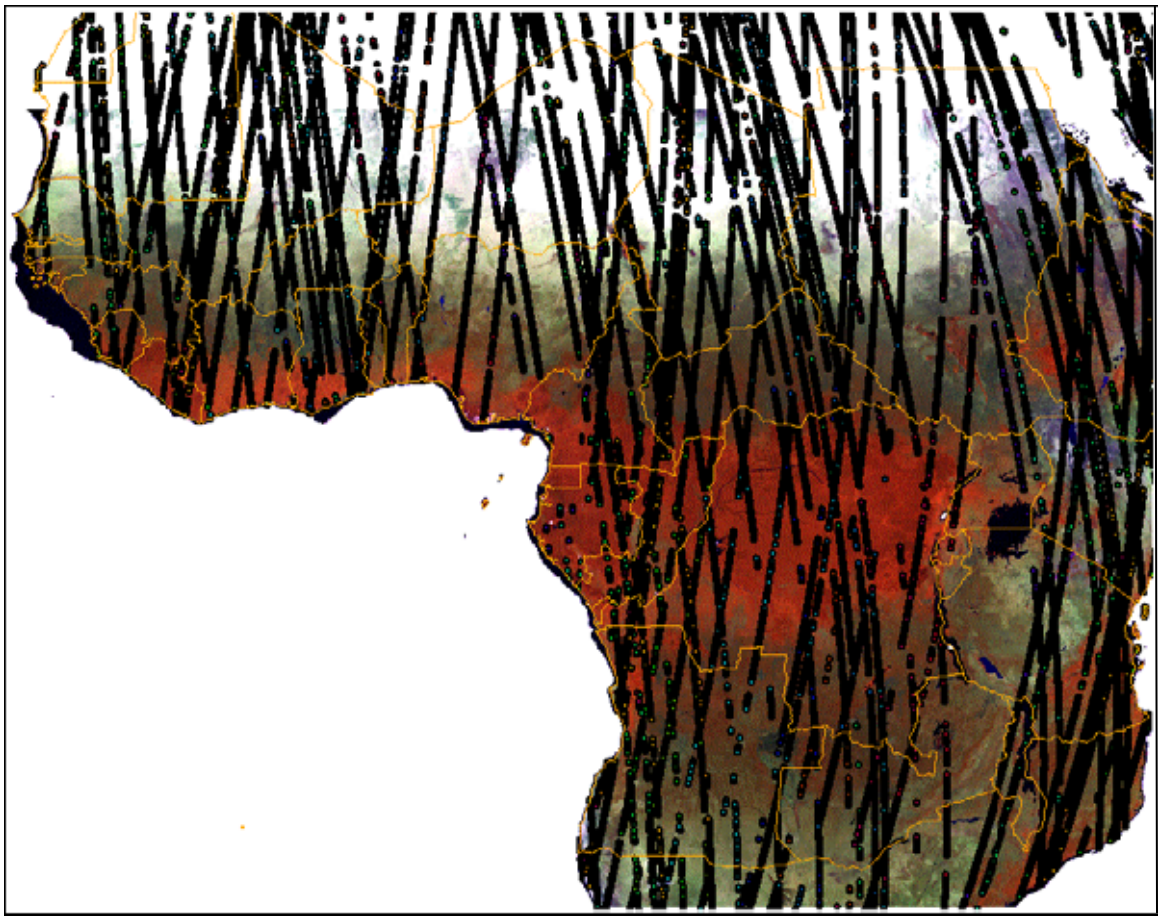

Notes: Each black dot represents a 65 m-wide LIDAR footprint; only 30 percent of all footprints are represented here.
Source: Baccini et al. 2008.

In the 2009–2015 timeframe, ICESat will reach the end of its operating lifetime and is expected to be followed by the ICESat-II and DESDynI LIDAR satellites. DESDynI is a satellite mission planned for launch in 2014 and carrying a large-footprint LIDAR as well as two L-band InSAR systems with multiple polarimetry. The LIDAR capability will be used in conjunction with InSAR to achieve

accurate, moderate-resolution forest height measurements on a global scale (Donnellan et al. 2008). Accurate measurements of ground elevation may also result depending on advances in processing InSAR data (ESA 2009).

4.2.3 InSAR Measurements of Forest Height

Several different methods using SAR interferometry can derive forest height. (Balzter 2001; Sexton et al. 2009). Canopy-top height from short-wavelength InSAR (e.g., the SRTM mission) can be subtracted from independent measures of the ground elevation (Kellndorfer et al. 2004; Walker et al. 2007). Short-wavelength InSAR estimates of canopy-top height can be subtracted from long-wavelength InSAR estimates of ground elevation (Neeff et al. 2005). Polarimetric interferometric SAR (POLinSAR) uses interferometric, polarized SAR and multiple measurements to model the vertical structure and height of forests from SAR scattering models (Treuhaft et al. 2000; Le Toan et al. 2008). POLinSAR is still under development, although the technique has shown promise for height estimation across a diversity of forest types (Le Toan et al. 2008; ESA 2009).

Sexton (2009) compares the accuracy of different InSAR measurement techniques. In general, all InSAR measurements underestimate forest height because they measure to the phase scattering center, which is usually below crown level. This bias can be corrected (Saatchi et al., in review). In a forest in North Carolina, Sexton (2009) found that short-long wavelength differencing (X and P) was more accurate than SRTM-ground differencing but both InSAR methods were less accurate than LIDAR. He also found that SAR differencing was least accurate in shorter stands (due to ground return of canopy-top wavelengths) especially for the SRTM-ground method. Regional calibration would be necessary to correct for this bias in height estimation (Sexton et al. 2009).

Given the number of SAR satellites to be launched in the next six years, InSAR measurement of canopy-top height will increase in frequency and global coverage (Zink et al. 2007). Current satellites only have the capacity to do temporal inferometry and several upcoming SAR constellations and follow-on satellites will continue and extend this capacity (Section 2.4.2). Future capacity for spatial interferometry will come from an InSAR satellite (DESDynI) and several formation SAR constellations (e.g., TerraSAR-X; see the Appendix). Ultimately, the utility of interferometric SAR in measuring global forest height will depend on the creation of a high-resolution, ground-level global DEM (Walker et al. 2007) or the development of multi-band, multi-polarized image datasets that allow the estimation of forest height through POLinSAR or short-long wavelength subtraction algorithms (Neeff et al. 2005; Sexton et al. 2009; ESA 2009). The GLAS and DESDynI LIDARs will improve global DEMs (but not at a high spatial resolution) and the large number of SAR satellites to be launched will allow for InSAR synergies between C-, X-, L-, and possibly P-band sensors (NASA 2009a; ESA 2009; Saatchi et al. in review; Patenaude et al. 2005).

Development of an accurate, high-resolution global DEM would allow for the creation of references maps of forest height using C-band InSAR from the ERS, RADARSAT, or SRTM missions (Kellndorfer et al. 2004). A ground-level DEM could be achieved by a long-band (VHF) SAR sensor, LIDAR saturation of Earth's surface from satellite and airborne sensors (via the proposed LIST satellite, or using high-elevation, unmanned drones called UAVs), or a formation InSAR constellation with a special variable-baseline orbit (Le Toan 2008; ESA 2009; NRC 2007). Each of these options is in the experimental stages. The Tandem Digital Elevation Mapping satellite (TanDEM-X) and TerraSAR-X will create a variable baseline InSAR for DEM mapping, but accuracy

in forested areas is still to be determined (Zink et al. 2007). In addition, a tomography mode for the proposed P-band BIOMASS sensor and a variable-baseline Tandem-L companion satellite for DESDynI may be launched in the 2009–2015 period (Le Toan 2008; Oberto et al. 2008; ESA 2009).

4.2.4 Fusions of Remotely Sensed Data on Forest Structure

In any imagery fusion, LIDAR provides outstanding interpolated information on ground elevation and can be used to increase the accuracy of forest height estimates from stereo optical or interferometric SAR (Balzter et al. 2007; Hyde et al. 2006). This approach is the main concept behind DESDynI, the InSAR-LIDAR satellite mission described above. To provide more accurate, spatially extensive estimates of forest height and structure, LIDAR can be fused with InSAR (Balzter et al. 2007; Slatton et al. 2001), passive forest-structure estimates (Wolter et al. 2009, Dubayah et al. 2000; Hyde et al. 2006; Hudak et al. 2002), stereo measurements of height (Hyde et al. 2006), or forest classifications from passive or active sources (Dubayah et al. 2000; Helmer et al. 2009; McCombs et al. 2003).

4.2.5 Estimating Forest Structure from Allometric Relationships

Horizontal and vertical forest structure can be derived from three-dimensional stereo imaging as well as from the texture of high-resolution satellite and aerial passive imagery (Song 2007; Wolter et al. 2009). Analysis of canopy texture from optical imagery takes advantage of tree illumination geometries in heterogeneous canopies to estimate canopy width and other structural variables (Wolter et al. 2009; Kayitakire et al. 2006; Hyyppa et al. 2000; Song 2007). Canopy structure (e.g., width) can then be used to estimate tree height, basal area, and stem volume via allometric equations (Song 2007; Lefsky et al. 2002b). Canopy structure has long been derived from remotely sensed imagery (this is reviewed in more depth by Song [2007]; Wolter et al. [2009]; and Palace et al. [2008]). In general, high-resolution imagery is more accurate than moderate-resolution imagery at deriving canopy structure (Hyyppa et al. 2000; Song 2007; but see McRoberts 2008). Recent efforts have focused on automated delineation of canopy structures using a variety of different algorithms. Success has been mixed and studies have largely been restricted to small areas (Song 2007; Wolter et al. 2009; Palace et al. 2008).

Song (2007) achieved acceptable accuracy in canopy-delimitation in conifer forests (72 percent variation in canopy width), but, like several others, had poor accuracy in deciduous forests with overlapping canopies. In northern forests with nonoverlapping canopies, Wolter et al. (2009) found that estimates of canopy width and height rivaled LIDAR accuracies (acceptable to high). Automated canopy delimitation efforts in the Amazon basin, using extensive ground data, observed clumping of overlapping trees, underestimation of understory tree crown area, and overestimation of total forest biomass (Palace et al. 2008; Broadbent et al. 2008). While these efforts have not been extensively validated, biomass estimates were quite comparable to ground estimates.

In general, texture-derived canopy width and height measurements are less accurate than LIDAR measurements, but they can be calculated from existing high-resolution imagery over larger areas (Wolter et al. 2009; Broadbent et al. 2008). Although this technique may be unsuitable for global forest height measurement because of cost and data volumes (DeFries 2008), the approach

may be suitable for extending LIDAR estimates and validating coarser-resolution imagery (DeFries 2008; Wolter et al. 2009).

4.3 Estimating Forest Volume and Biomass Using Remote Sensing

Both the volume and the aboveground biomass (AGB) of forests can be estimated from allometric relationships with canopy width, structure, and/or height, the intensity of SAR backscatter, correlations with passive spectra, and various fusions of the above (Lu et al. 2006; Balzter et al. 2007; Rosenqvist et al. 2003). We review this large body of literature briefly, with a focus on global measurement of forest biomass. A more thorough review of this topic is in Lu (2006), Pateneude et al. (2005), Rosenqvist et al. (2003), and Lefsky et al. 2002b).

4.3.1 Forest Volume and Remote Sensing

Forest volume and geometry directly influence the returns to satellite sensors (Dobson et al. 1995b, Dubayah et al. 2000), but with the exception of several studies in plantations and conifer-dominated forests that estimate bole volume, many remote sensing studies focus on estimating forest biomass (g/m^2) rather than volume (m^3/m^2) (e.g., Drake et al. 2002a; Saatchi et al. 2007). The same allometric equations that are used to estimate ground-truth biomass could be used to estimate bole volume (P. Waggoner, pers. comm.), but bole volume is often not reported. As a result, we will focus in the following sections on estimating biomass, rather than volume, from remote sensing.

Forest volume estimates from remote sensing have often been made in species-poor systems with regular, distinct canopies in support of forest inventories. Active sensor systems have been frequently employed to estimate forest volume. Patenaude et al. (2005) review several studies in temperate conifer-dominated and boreal forests that estimated stem volume using SAR (53–83 percent accuracy) and LIDAR (46–97 percent accuracy). Hyyppa et al. (2008) review the ability of small-footprint LIDAR to estimate stem volume from canopy height measurements. Wolter et al. (2009) review several LIDAR studies that achieved 85–91 percent accuracy for basal area. Means et al. (1999), in the western United States, predict 96 percent of the variance in basal area using large-footprint LIDAR. Notably, Anderson et al. (2008) only predict 25 percent of the variance in basal area with LIDAR in a deciduous forest in the northeastern United States. Maltamo et al. (2006), on the other hand, predict stem volume from LIDAR with less than 14 percent error in a boreal forest. Askne and Santoro (2009) are able to estimate boreal forest stem volume with less than 20 percent error using C-band InSAR.

It is unclear how much the variation in accurately predicting volume is due to differences in LIDAR or SAR sensor types, processing choices, or variability among regions. Experts have hypothesized that LIDAR has more difficulty in predicting forest variables in deciduous areas due to irregular canopy structure (Nelson et al. 2007) but this hypothesis has not been thoroughly tested.

Passive optical sensors, alone and fused with active sensors, have been used to estimate forest volume with mixed results. For example, nearest-neighbor algorithms (k-NN) have processed moderate-resolution imagery, often integrated with forest inventory data, to produce estimates of forest volume and basal area (McRoberts et al. 2008). Franco-Lopez et al. (2001) used nearest-

neighbor techniques, Landsat imagery, and data from the US Forest Service's Forest Inventory and Analysis National Program (FIA) to estimate basal area and volume with approximately 50 percent accuracy, while McRoberts et al. (2008) estimates basal area with 66 percent accuracy using similar techniques. Hall et al. (2006) uses moderate-resolution imagery, forest inventory data, and an allometric forest structure model to predict volume with 69 percent accuracy. These moderate-resolution data algorithms may be too computer intensive for large-area estimation.

High-resolution imagery has also been used to estimate forest volume, often with greater success. Hyyppa et al. (2000) find that high-resolution optical sensors outperformed some, but not all, types of SAR sensors, as well as moderate-resolution passive sensors in predicting basal area and stem volume, with maximum accuracy of 55–58 percent. Wolter et al. (2009) use high-resolution SPOT imagery in an open temperate forest to estimate basal area with 71 percent accuracy. Kayitakire et al. (2006) use texture analysis of 1 m-resolution IKONOS-2 imagery to estimate basal area of a mixed conifer-deciduous forest with 35 percent accuracy. In an open poplar plantation, Wang et al. (2007) use allometric relationships between canopy height and diameter to estimate stem volume with 87–92 percent accuracy. In a boreal forest, Wallerman and Holmgren (2007) estimate stand volume with less than 20 percent error by fusing small-footprint LIDAR with texture analysis of SPOT high-resolution geometric (HRG) images. Popescu et al. (2004) fuse small-footprint LIDAR with high-resolution optical imagery to estimate forest volume with high accuracy (83 percent of variation) in coniferous forests and poor accuracy in deciduous forests (39 percent). As with active sensors, the variation in methods and forest types makes it difficult to draw definitive conclusions, but it is clear that fusions improve estimates (e.g., Popescu et al. 2004) and that readily distinguishable tree canopies improve allometric estimates of stand volume from canopy width (Song 2007).

Because of the similarity of allometric equations that calculate biomass and stem volume, the methods detailed in the following sections could easily be applied to estimation of stem volume. Popescu et al. (2004) and Means et al. (1999), for example, found very close agreement between their estimates of stem volume and biomass from remote sensing. Because variation in wood density is important in global estimation of biomass across regions and forest types (Baker et al. 2004), estimation of volume may be more accurate than biomass in some ecosystems or at regional scales. More studies are needed on the relative accuracy of volume and biomass estimates across diverse forest ecosystems to evaluate this possibility.

4.3.2 Forest Height and Biomass: A Strong Positive Correlation

Tree height and/or diameter, because of the unique constraints of plant structure, is positively correlated with tree biomass within a species (Chave et al. 2005; West et al. 2009; Dubayah et al. 2000). Using well-established allometric relationships, biomass can be calculated from tree diameter, height, and/or wood density (Chave et al. 2005; Schroeder et al. 1997). Remote sensing cannot directly measure wood density, but correlative forest inventory data can use species-specific or region-specific allometric equations to provide accurate estimates of biomass (see Section 3.1.3). Forest height can be measured from a variety of remotely sensed data (see above) and used to estimate biomass (Kellndorfer et al. 2004; Palace et al. 2008, Pflugmacher et al. 2008). Although diameter, height, and wood density are central variables, biomass estimates can be improved by using additional forest structure variables (e.g., canopy width, canopy volume) (Dubayah et al. 2000; Palace et al. 2008; Popescu et al. 2003).

4.3.3 Estimating Biomass Using SAR Backscatter

The magnitude and polarity of SAR backscatter is sensitive to forest structure, with shorter wavelengths (C-, X-bands) interacting primarily with canopy elements, and longer wavelengths interacting primarily with branch, trunk, and ground elements (L-, P-, VHF-bands). Backscatter responds to the density of biomass at different heights, and it can be used to estimate biomass. However, backscatter intensity from C- and X-band SAR tends to saturate at relatively low levels of forest biomass (25–50 megagrams [Mg] per ha]), Rosenqvist et al. 2003). L-band SAR saturates at varying levels (60–150 Mg/ha; Patenaude et al. 2005), depending on species composition and forest structure. P-band SAR saturates at a higher range (100–200 Mg/ha), again dependent on forest biota and structure (Patenaude et al. 2005), and VHF-band SAR is quite sensitive to forest biomass and does not have appreciable saturation as biomass increases (Fransson et al. 2000; Patenaude et al. 2005). P-band SAR and experimental VHF-SAR sensors are mounted in aerial systems now, but neither band will be represented in orbit in the 2009–2015 window unless the P-band BIOMASS satellite proposal is approved by the European Space Agency (Le Toan 2008).

Pateneude et al. (2005) reviews 11 studies and finds that accuracy of biomass predictions from SAR varies between 50 and 96 percent of observed variation, across a variety of forests and bands. SAR backscatter returns are sensitive to topography, variation in soil and canopy moisture, and changes in forest structure (Kellndorfer et al. 1998; Kasischke et al. 1997). In hilly areas, backscatter must be corrected by a high-resolution DEM because of shadowing, layover, and other angular effects. If a high-resolution DEM is not available, the accuracy of biomass estimates from SAR decreases (Kellndorfer et al. 1998; Ticehurst et al. 2004).

Polarized SAR and multiband SAR provide more detail about forest structure, and improve biomass estimates (Dobson et al. 1995b; Rosenqvist et al. 2003). Askne et al. (2003) use short and long wavelength InSAR to estimate biomass in a boreal forest within 15 percent of ground estimates, while Balzter et al. (2007), using a similar method, is able to estimate biomass in a deciduous forest within 36 percent of estimates. Recent research has measured tropical forest biomass with +/-15 percent accuracy using L-band polarized SAR (up to 150 Mg/ha) and with P-band polarized SAR (up to 300+ mg/ha) (Saatchi et al. in review).

Polarized backscatter estimates of biomass may be combined with height-based estimates of biomass from InSAR to increase the range of forest biomass that can be accurately measured from SAR (Saatchi et al. in review). These estimates are complementary: estimates of biomass from tree height are more accurate as tree height increases, while backscatter is less accurate with increasing height (Sexton et al. 2009, Saatchi et al. in review; Le Toan 2008). In Central America, a SAR–InSAR combination method has been found to increase the saturation point of L-band (to 200 t/ha) and increase the accuracy of L- and P-band (Saatchi et al. in review). The BIOMASS and DESDynI missions (P-band and L-band, respectively) will use this combination approach to global biomass estimation, which may lead to frequent, 100 m resolution estimates of a broad range of forest biomass (Le Toan 2008; Donnellan et al. 2008).

4.3.4 Indirectly Estimating Biomass from Forest Spectra

A number of studies have correlated passive remote sensing measurements to net primary productivity and biomass (Lu 2006; DeFries 2008; Goetz et al. 2005; Baccini et al. 2008). Several

vegetation indices derived from passive remote sensing are well correlated with LAI, fraction of absorbed photosynthetically active radiation (fAPAR), and other measurements of productivity (Gao et al. 2000). Net primary productivity is modeled from either LAI or fAPAR estimates; both approaches have been shown to be relatively accurate (Luus and Kelly 2008) even though LAI estimates saturate at 2–4 leaves per unit area (Gao et al. 2000). Most passive sensors (MODIS, Landsat, GeoEye) can estimate fAPAR and LAI, and productivity is linearly correlated with biomass at low levels of biomass (<200 Mg/ha, Keeling and Phillips 2007; Luus and Kelly 2008). In low-biomass systems, including many temperate, boreal, and dry tropical forests, passive sensors are capable of estimating biomass directly from vegetation indices (Lu 2006; Muukkonen and Heiskanen 2007).

Houghton et al. (2001) compare two biomass maps of the Amazon basin from remote sensing (MODIS and AVHRR) and find little spatial agreement between them but overall agreement on total biomass (~10 percent difference). Piao et al. (2009) model productivity and biomass across China and find good agreement between remotely sensed biomass and productivity estimates and two other independent estimation methods. Baccini et al. (2008) use a combination of MODIS and ground data to model Africa's biomass with 80–90 percent accuracy. Houghton et al. (2007) use MODIS to map biomass across Russia and are able to predict 60 percent of the variation, although within-site error was highly variable. Zheng et al. (2004) employs Landsat 7 and data on forest age and composition to predict AGB with 67 percent accuracy. Blackard et al. (2008) use a combination of ground data, coarse- and moderate-resolution imagery, and GIS layers to generate a biomass map of the United States with variable predictability (0.31–0.73 across regions). Foody et al. (2003) use Landsat spectral data and a neural network algorithm to predict biomass at three tropical forest sites with 71–84 percent of the variance explained. However, in the study by Foody et al. (2003), vegetation indices optimized to predict biomass at one site have very poor performance at other sites, underscoring the difficulty of developing general spectral relationships across moderate-resolution imagery taken in different seasons, cloud levels, and lighting conditions (Schroeder et al. 2006, but see Woodcock et al. 2001).

The biomass-productivity relationship saturates in tropical and high-biomass temperate forests (>200 Mg/ha, Keeling and Phillips 2007), so attempts to estimate biomass there often use other metrics besides spectral response, including image texture and forest age (Lu 2006). As reviewed above (Section 4.2.5), high-resolution image texture can be used to derive forest structure metrics (e.g., canopy width, height) (Wolter et al. 2009), which then could be used to estimate biomass through allometric relationships (Palace et al. 2008; Broadbent et al. 2008). However, Song (2007) shows that the accuracy of this canopy-delimitation approach is low in forests with overlapping canopies. In dense tropical forests, Broadbent et al. (2008) also find that biomass estimates had low accuracy (excluding emergent trees), and emergent trees covered smaller tree canopies from view and made detailed ground-data correction necessary for any biomass estimates. In more open, lower-biomass forests, texture metrics can aid spectral estimates of forest structure and biomass (Lu 2006; Wolter et al. 2009). Although texture metrics based on high-resolution imagery are limited in areal coverage and dependent on local ground data and radiometric correction, the metrics could be a valuable adjunct to more accurate, spatially coarse LIDAR measurements of forest structure (Wolter et al. 2009).

Forest biomass can be indirectly estimated by using remote sensing to map forest age classes (Castro et al. 2003; Chambers et al. 2007). If accurate local relationships can be developed between biomass and detectable forest age classes (e.g., Zheng et al. 2004), the distribution of forest age classes across the landscape can be used to estimate biomass and model future productivity (Sanchez-Azofeifa et al. 2009; Castro et al. 2003; Lu 2006; Zheng et al. 2004; Helmer et al. 2009). However, secondary forests over 15–30 years of age are difficult to distinguish from mature forests using forest spectra (Steininger 1996; Nelson et al. 2000; Song et al. 2007). Secondary forest also varies markedly in its growth rate due to a variety of factors, including species composition, climate, land use history, soil fertility, human disturbance, and regional differences (Nelson et al. 2000; Castro et al. 2003; Sanchez-Azofeifa et al. 2009). Both of these facts present severe challenges to using forest age classes as a predictor of forest biomass, in addition to the intensive fieldwork required to establish a relationship between forest age and biomass (Castro et al. 2003; Uhl et al. 1988; Zheng et al. 2004; but see Helmer et al. 2009). Sanchez-Azofeifa et al. (2009) argue that improving the detection of forest age classes is a critical goal for forest carbon measurement. However, continuing human disturbance from logging and fires (e.g., Alencar et al. 2006; Asner et al. 2006; Uhl et al. 1988), as well as the variability in forest regrowth biomass with age (e.g., Helmer et al. 2009) make forest age a metric of questionable utility in measuring global biomass. Direct estimation of forest regrowth biomass and productivity is a more parsimonious goal, and it may be achievable with expected advances in the spectral and spatial resolution of sensors, polarized and InSAR satellites and constellations, increased LIDAR coverage, and improvements in modeling forest reflectance.

4.3.5 LIDAR Estimations of Biomass

LIDAR is considered a promising approach to estimate local forest biomass (Lu 2006) because direct measurement of forest canopy structure and height can be converted to biomass using allometric equations (Dubayah et al. 2000; Broadbent et al. 2008; Chave et al. 2005). Earlier in this report, we reviewed the basic capabilities of LIDAR technology (Section 2.2.2), the high accuracy of LIDAR in measuring forest height (usually with height errors of less than 1 m, Section 4.2.2), and the variable but often high accuracy of LIDAR in estimating forest volume (Section 4.3.1). The accuracy of LIDAR in estimating biomass is also often good, but methods differ among LIDAR technologies.

Small-footprint LIDAR, taken from aerial sensors, excels at measuring forest height and delimiting canopy width and overall structure. With this technology, biomass is usually estimated by its correlation with forest height and/or canopy widths. It is challenging to distinguish ground-returns in dense forests but algorithms exist for efficient processing of small-footprint data even in these challenging conditions (e.g., Clark et al. 2004b). Small footprint LIDAR has achieved poor to very high accuracy in estimating forest biomass with many studies having accuracy in excess of 80 percent (Patenaude et al. 2005). Patenaude et al. (2005) review several temperate forest studies with predictive accuracies between 45–91 percent, and Popescu et al. (2004) observe predictive accuracies between 32–81 percent in deciduous and pine forests, respectively. Asner et al. (2009) are able to use small-footprint LIDAR to predict biomass in tropical Hawaiian forests with 78 percent accuracy, Nelson et al. (2007) estimate biomass in temperate North Carolina pine forests with 93 percent accuracy, and Naesset and Gobakken (2008) estimate biomass in boreal forests

with 88 percent accuracy. Zhao et al. (2009) use LIDAR height distributions to estimate forest biomass in east Texas with up to 95 percent accuracy. Similarly, van Aardt et al. (2008) use small-footprint LIDAR to both distinguish temperate forest types and estimate their biomass with greater than 95 percent accuracy. As with estimation of forest volume, it is difficult to assess whether the observed variability in accuracy arises from the methods used, from regional variability among forests in growth form, or from regional variability in species wood density.

Large-footprint LIDAR, with its full waveform describing three-dimensional canopy structure, is well correlated with biomass. In temperate and boreal forests, predictive accuracies of biomass from aerial, large-footprint LIDAR have ranged between a low of 61 percent (northeast United States, deciduous; Andersen et al. 2006) and a high of 95 percent (Pacific Northwest conifers, Means et al. 1999). In studying three U.S. biomes, Lefsky et al. (2002a) achieve 84 percent accuracy. Nilsson (1996) predicts biomass for Scots pine with 78 percent accuracy, and Hyde et al. (2005) predict 86 percent of mountain conifer biomass in a U.S. study. In northern China, Sun et al. (2007) predict biomass with 73 percent accuracy and Boudreau et al. (2008) achieve 81 percent accuracy in boreal Russia. In tropical forests, predictive accuracies of biomass from large-footprint LIDAR have been between 66 and 93 percent (Drake et al. 2003; Drake et al. 2002a, b). Drake et al. (2002b) find that one parameter (HOME) from the LIDAR waveform was highly predictive of forest biomass across sites. Baccini et al. (2008) use that relationship to validate a regional map of African biomass with ICESat GLAS sampling.

Because of the close correlation with global forest height and biomass (Lefsky et al. 2007; Helmer et al. 2009), LIDAR pulses from the orbiting ICESat GLAS satellite have provided a wealth of data for forest biomass mapping and validation (Baccini et al. 2008; Helmer et al. 2009; Boudreau et al. 2008; Nelson et al. 2008; Pflugmacher et al. 2008). The launch of DESDynI promises to increase this new source of global biomass data, but both ICESat and DESDynI will collect data at coarse spatial resolution: measurement sites will be separated by several kilometers (Oberto et al. 2008; NASA 2009a). For the near future, all LIDAR satellites are expected to sample only at coarse resolution.

Overall, LIDAR has the potential for good to high accuracy and can measure both forest canopy height and ground elevation, thus overcoming a key limitation of current SAR and InSAR approaches to estimating biomass. The greatest limitation of LIDAR mapping of biomass is the coarse spatial resolution of satellite LIDAR sensors and the narrow swath of aerial LIDAR sensors. These limits can potentially be overcome by integrating LIDAR data with other remote datasets that have greater resolution or swaths (e.g., InSAR, passive; see below for more detail). Fusion of LIDAR data with other types of imagery will allow accurate estimates of biomass on a global scale (Baccini et al. 2008; Anderson et al. 2008; Donnellan et al. 2008).

4.3.6 Fusion Approaches to Estimating Forest Biomass

Three main data sources play a role in estimating biomass: GIS data layers, geo-referenced ground data, and satellite imagery (Gibbs et al. 2007; DeFries et al. 2007). It is possible to fuse all three. Biomass estimates from remote imagery can be improved by using any number of geo-referenced data layers: bioclimatic surfaces, roads, general habitat classifications, population layers, and/or ground data (Baccini et al. 2004; GOFC-GOLD 2008; Saatchi et al. 2007; Herold and Johns

2007; Blackard et al. 2008). The volume of global GIS data is growing; coarse-resolution, global analyses of human impact on forests are now possible (Sanderson et al. 2002). It is possible to discount forest carbon estimates by measures of human impact, including road density and population (GOFC-GOLD 2008; Gibbs et al. 2007). Saatchi et al. (2007) use elevation data and a variety of remote sensing data to estimate biomass across the Amazon basin; comparison with bioclimatic layers indicates that dry season rainfall might be a good additional predictor of biomass. Baccini et al. (2004) use a combination of land-cover classification from MODIS data, ground inventory data, and climate and topographic GIS layers to predict biomass in California with 73 percent accuracy. Baccini et al. (2008) use a similar approach with ground data in Africa to accurately predict biomass but find that GIS layers do not improve the analysis. Walker et al. (2007) use ground data, national GIS layers, and both passive and active remote sensing data to create an accurate (r=0.88) map of forest basal area for central Utah.

Fusion with ground data can provide additional attributes and accuracy to mapped forest classes (Baccini et al. 2004). This approach can also provide continuous data that can be integrated across regions—tree diameter data, for example, has improved allometric estimates of biomass from LIDAR (Means et al. 1999). Boudreau et al. (2008) use a combination of ground data, aerial LIDAR data, satellite LIDAR data, elevation data, and moderate-resolution land-cover classification to estimate biomass for the boreal forests of Quebec. Similarly, Nelson et al. (2008) use ground data to parameterize biomass estimates from GLAS, and then extend the GLAS estimates regionally using MODIS land-cover classifications. Andersen et al. (2006) and Anderson et al. (2008) find that by including ground data on forest composition, GLAS LIDAR estimates of forest biomass are significantly improved. The authors also show that this forest composition data could be estimated accurately by high-resolution hyperspectral data.

The fusion of remote sensing data to predict ground validation datasets is an increasingly common practice with great potential (Rosenqvist et al. 2003). Saatchi et al. (2007) integrate a variety of SAR and passive sensors to estimate Amazon biomass in 16 forest classes with 81–91 percent accuracy. Moghaddam et al. (2002) find that a SAR-Landsat fusion is twice as accurate as Landsat alone in estimating conifer foliage biomass. Treuhaft et al. (2003) use hyperspectral and InSAR data to estimate forest biomass in Oregon with +/- 16 percent error. Hyde et al. (2006) fuse a variety of data sources (SAR, InSAR, LIDAR, high- and moderate-resolution passive) and find that a LIDAR-Landsat fusion predicts biomass the most accurately (80 percent of the variance); an all-sensor fusion is only slightly more accurate (83 percent). Helmer et al. (2009) use global relationships between GLAS data and forest biomass to estimate biomass directly in Brazil, then extend those results to Landsat-derived regional forest age classes. Combining the global GLAS datasets with existing land-cover maps is one promising new fusion method, out of many, for improving global forest biomass estimates in the 2009–2015 time period.

4.4 Estimating Forest Carbon Stocks from Remotely Sensed Data

Satellite imaging can tell us much about global carbon stocks, but there are limits to its accuracy. Dry biomass is approximately 47–55 percent carbon by weight (IPCC 2006), so aboveground biomass estimates from remote sensing can be simply converted into aboveground carbon (AGC) stock estimates (Gibbs et al. 2007). Depending on the method used (e.g., SAR versus spectra), however, remote sensing may not include dead trees in its estimate of AGC stocks. In addition, satellite and aerial estimates of forest carbon are fundamentally limited to aboveground

carbon. Remote sensing cannot measure litter, root, and soil carbon stocks, which can be considerable (GOFC-GOLD 2008; Malhi et al. 1999; Page et al. 2002; but see Foster et al. 2002). Belowground (root) carbon averages around 20–30 percent of AGC globally (Cairns et al. 1997) but varies from 9 to 26 percent in forests across the Amazon basin (Houghton et al. 2001). National estimates of carbon stocks often simply adjust AGC stock estimates by uniform percentages (e.g., 30 percent) to estimate total nonsoil forest carbon stocks (Gibbs et al. 2007; Houghton et al. 2001). Differing methods of estimating dead and belowground carbon lead to much of the observed variation in forest carbon stock estimates (Houghton et al. 2001).

Modeling soil carbon emissions is important in forests: the amount of carbon in litter, nontree vegetation, and soil stocks vary markedly with latitude, forest type, and soil type, but soils alone make up, on average, 49–84 percent of total forest carbon stocks (Table 1; Malhi et al. 1999; GOFC-GOLD 2008). Not all of the soil carbon is emitted with deforestation, but emissions from soil carbon stocks can account for a significant percentage (10 percent or greater) of emissions from deforestation and degradation, especially in northern forests and peat swamps (Houghton 1999; Page et al. 2002). For example, one study estimates that that the 1997 burning and deforestation of Indonesian peat swamps released 253 tons of carbon per ha, which constituted between 13 and 40 percent of total global carbon emissions that year (Page et al. 2002). Although global maps of soil carbon do exist, the accuracy of the maps is difficult to assess with available data (GOFC-GOLD 2008). In the paragraphs below, we review the different methods of estimating forest AGC stocks on a global scale.

4.4.1 Aboveground Carbon Stocks Estimates: Inventory and Remote Sensing

Forest inventories are a starting point for estimating forest AGC stocks by providing measures of tree diameter, tree height, species composition, and density. Applying general allometric equations then allows estimation of tree volume, biomass, and carbon (Chave et al. 2005; see Table 4). Allometric equations are derived from harvesting, drying, and weighing trees in forest plots and can be site and species specific if enough sampling is done (Gibbs et al. 2007). General allometric equations developed across forest types are highly accurate at predicting AGC stocks in local forest plots (Chave et al. 2005; Schroeder et al. 1997) in combination with species-specific wood-density data (Baker et al. 2004). In the tropics, cross-species, stand-level estimates of wood density lead to decreased accuracy in biomass estimation (Baker et al. 2004).

Once aboveground tree carbon is accounted for, carbon in other vegetation, litter and soils can be inventoried as well to improve estimation accuracy and carbon in tree roots is usually estimated as a function of tree size (20–30 percent; Gibbs et al. 2007; Cairns et al. 1997; GOFC-GOLD 2008). If soil information is not included in the forest inventory, the decrease in total carbon estimation accuracy can be marked (GOFC-GOLD 2008; Malhi et al. 1999), but accurate AGC estimates can be combined with global soil carbon maps to get estimates from existing forest inventory data (GOFC-GOLD 2008).

In comparison to remote sensing estimates, forest inventory estimates of total AGC are considered more accurate, although they, too, have estimation inaccuracies (Gibbs et al. 2007; Saatchi et al. 2007; Chave et al. 2005; Baker et al. 2004). On the global scale, however, plot-level measurements of AGC are essentially point measurements. Simple interpolation between plots fails to capture the full range of spatial variation in biomass across landscapes (Houghton et al. 2001;

Gibbs et al. 2007). As a result, there is a wide range of methods to estimate AGC stocks; Goetz et al. (2009) review (and name) several common methods for estimating regional AGC stocks, including:

- "Stratify and Multiply": assigning inventory-derived biomass values to land-cover classes;
- "Combine and Assign": using GIS data layers and land-cover classes to modify biomass estimates within classes (a version of the above); and
- "Direct Remote Sensing" (DRS): using field data to train a rule-based algorithm until it has an optimal prediction of biomass from remotely sensed data.

All these methods involve both remote sensing and ground inventory data. Inventory data are necessary to estimate forest carbon stocks, but these data alone are not sufficient. Goetz et al. (2009) discuss the advantages and disadvantages of each approach and we summarize that analysis here. Use of discrete land-cover classes and discrete biomass values (one per land-cover class) is a Stratify and Multiply approach. Combine and Assign generates discrete land-cover classes and continuous biomass values (varying with GIS layers). The Direct Remote Sensing approach generates continuous land-cover values and continuous biomass estimates (which starts, in the training data, from continuous spectral data and discrete local biomass values).

Each approach can be useful (Goetz et al. 2009). For example, existing land-cover maps (e.g., GLOBCOVER) could be used in a Stratify and Multiply approach as a Tier I approximation of global AGC stocks (GOFC-GOLD 2008). To detect forest degradation near roads, road GIS data could be used to lower biomass estimates in a Combine and Assign approach (GOFC-GOLD 2008). Although it was not originally conceived as such, the DRS approach in Goetz et al. (2009) could utilize GIS data and also perform rule-based classification of land covers into biomass categories at the pixel scale. Where sufficient data are available, DRS is arguably the right approach for two reasons: the approach uses the original data and yields continuous estimates of biomass.

As Goetz et al. (2009) illustrate, the use of broad land-cover classes to detect change in biomass over time ignores within-class heterogeneity and compounds classification error between land-cover maps. Using raw remote sensing data and continuous estimates eliminates errors from the previous classification and homogenization of complex landscapes. As a result the DRS approach will have higher resolution and likely higher accuracy when estimating carbon stocks.

Even with the advantages of DRS, discrete land-cover mapping will remain essential. Continuous maps of biomass and productivity from DRS would be most useful if they were integrated with detailed land-cover maps for two reasons. First, research into distinguishing land covers (e.g., Sesnie et al. 2008) identifies techniques and remote sensing data that would improve the rule-based classification algorithms that produce continuous maps. Second, land-cover classification is important for land-use planning and global modeling. Current carbon and climate models require land-cover information to make accurate projections (DeFries 2008). Human land-use introduces discrete boundaries, distinct land-uses, and legacy effects to forests that vary continuously in biomass (Asner et al. 2009; Uhl et al. 1988; Uriarte et al. 2004). Discrete land-cover classification allows evaluation of human land-cover decisions (e.g., determining if biomass is decreasing due to oil palm plantations replacing intact forest, or due to logging following road construction). Land-cover information also can alter future projections for biomass recovery; in Brazil, forest regrowth has similar biomass to intact primary forest on sandy soil, but regrowth has a very different range of expected growth rates (Castro et al. 2003; Uhl et al. 1988).

4.4.2 From Stocks to Fluxes: Integrating Carbon Pools and Flows

Models are required to integrate carbon fluxes and stocks on a global scale and to calculate carbon emissions from forests (van der Werf et al. 2006). As noted in Section 4.4, AGC stocks represent less than half of total carbon in forests on average (although this varies greatly between forests; see Table 1). In this report, we have not dealt with dynamic carbon gas fluxes from land-use change, which can be fast or slow (e.g., tree stump decay in deforested pasture; Crutzen and Andreae 1990), or with changes in non-AGC stocks (e.g., loss of litter in burned forests). Dynamic carbon fluxes, especially in belowground carbon, are difficult to measure directly and are usually modeled (e.g., van der Werf et al. 2006). We have focused instead on how remote sensing can directly measure two important data inputs to carbon models: AGC stocks (area x biomass), and changes in those stocks over time (deforestation, reforestation, net growth) (DeFries et al. 2007). Model estimates of forest carbon fluxes can be also be improved, however, by satellite measurements of carbon gas uptake and release, vegetation productivity, and the extent and frequency of forest fires (Palmer 2008; Ramankutty et al. 2007; Rosenqvist et al. 2003; Roy et al. 2005; Alencar et al. 2006; Gibbs et al. 2007; Chuvieco 2008; Heinsch et al. 2006; Liu et al. 2002).

The topic of carbon gas fluxes is reviewed extensively elsewhere (Chuvieco 2008; Palmer 2008) and is dealt with only briefly here. The worldwide network of eddy covariance towers, supplemented by bottle data and orbiting carbon-gas measuring satellites, sample carbon gas fluxes over time from vegetation (Palmer 2008; Baldocchi 2008). For example, the IBUKI satellite measures carbon dioxide and methane at 10.5 km resolution globally every three days and is improving our understanding of global carbon sources and sinks (Palmer 2008). This data-collection network, by measuring carbon gas fluxes, is able to capture carbon stock changes from forest degradation (as exposed litter and wood decompose to carbon gases) and vegetation productivity (as vegetation uptakes carbon dioxide to grow). Although the measurements depend on modeling to separate aboveground fluxes from belowground fluxes, carbon gas flux measurements provide an independent, ultracoarse-resolution metric by which to evaluate the higher-resolution estimates of aboveground, net primary productivity derived from passive sensors like MODIS and AVHRR (Heinsch et al. 2006; Xaio et al. 2008).

Biomass burning, in addition to depleting carbon stocks (Chuvieco 2008), has a number of effects on regional air quality, hydrological cycles, and even soil fertility (Crutzen and Andreae 1990). Fires are detectable by a number of high-revisit, coarse-resolution passive sensors with thermal bands (e.g., MODIS, AVHRR, Along Track Scanning Radiometer [ATSR]), by GOES several other ultracoarse resolution sensors, and by several moderate-resolution sensors (e.g., ASTER, Landsat) (Chuvieco 2008; Schroeder et al. 2008b). Real-time, global fire mapping is ongoing at 1 km resolution using MODIS and future satellites will continue this effort (e.g., NPOESS) (Davies et al. 2009). Global fire monitoring has been invaluable in aiding fire detection in wilderness areas and in contributing to carbon and air quality models (Davies et al. 2009; Chuvieco 2008). Although modeling can overcome some of the problems in current global fire detection, shortcomings include lower chances of fire detection in cloudy areas, difficulty in detecting understory fires in dense forests, and the inability of coarser-resolution sensors to detect the majority of smaller fires (Schroeder et al. 2008a, b). Even when fires cannot be detected using direct means, both passive

and SAR sensors are able to map burn scars (Giglio et al. 2005; Siegert and Ruecker 2000). Modeling carbon emissions from fires for carbon emission requires detailed information on vegetation biomass in either active fire locations or burn scars (Chuvieco 2008). Accurate estimates of fire radiative power (FRP) are also a good proxy for biomass lost, but they require frequent measurements by a passive thermal sensor with a large dynamic range to prevent saturation (Giglio et al. 2006). Giglio et al. (2006) map global patterns in FRP using MODIS, and Roberts et al. (2005) are able to predict 90 percent of variation in fire biomass emissions in southern Africa with the geostationary Spinning Enhanced Visible and Infrared Imager (SEVIRI) sensor. Currently, only MODIS and some geostationary satellites meet the revisit and sensitivity requirements for calculating FRP (Giglio et al. 2006), but several fire-detecting coarse- and moderate-resolution fire sensors are planned for launch in the next six years, including the NPOESS series, the higher-resolution GOES Advanced Baseline Imager (ABI) sensors, and the SAC-D fire satellite (Appendix). As global biomass maps and satellite measurements of FRP improve, modeled estimates of biomass emissions from fire will also continue to improve.

Carbon modeling is critical to any global forest monitoring effort as a method of integrating aboveground carbon stock measurements with belowground carbon estimates and important carbon fluxes (e.g., the effect of fires, or soil uptake of carbon) (e.g., van der Werf et al. 2006). Such modeling can also make possible independent tests of biomass and productivity estimates using ground data (e.g., eddy covariance measurements of carbon dioxide). Future advances in remote sensing will help to decrease uncertainty in carbon models by improving the accuracy of measurements of land cover, standing biomass, vegetation productivity and decomposition, and emissions from biomass burning.

Chapter 5. Forests from Space: Unparalleled Measurements, Timely Moment

With developments in satellite technology and the globalization of GIS layers, we can view the whole Earth with more detail than ever before. These developments lead to a timely moment for global forest monitoring, an effort further enhanced by technological innovation and an accumulation of forest inventory data (Herold 2009). With the tools now at hand, a global forest monitoring effort can be guided by principles of repeatability, longevity, and accuracy. To be successful, monitoring will have to reduce the greatest sources of error in measuring forest characteristics. Currently forest area can be measured quite accurately but only at a coarse, two-class resolution. Forest biomass and carbon stocks cannot be estimated at high resolution but conservative estimates are possible by combining forest inventory and LIDAR data with more spatially extensive satellite imagery. This concluding chapter examines how current satellite data and expected sensor launches between 2009 and 2015 could be used in a global forest monitoring effort.

5.1 Improving Forest Biomass and Carbon Estimates

In global forest measurement, estimates of forest biomass and carbon are the most variable because it is difficult to estimate existing stocks reliably and detect when those stocks have decreased (Houghton 2005). In general, remote sensing is much better at detecting large, canopy-level changes in biomass than small (subpixel), below-canopy changes in biomass (Peres et al. 2006; DeFries et al. 2007; Broadbent et al. 2008). Variable conditions of illumination, elevation, and moisture make detection of temporal change more challenging (Sanchez-Azofeifa et al. 2009; Asner 2001; Kellndorfer et al. 1998; Schroeder et al. 2006). From the standpoint of cost, image availability, and repeat time, global efforts to map forests will not be able to use large amounts of high-resolution imagery to detect small-scale forest changes (e.g., logging; Achard et al. 2007; DeFries et al. 2007; Rosenqvist et al. 2003). As stated in Chapter 4, it is more desirable to use other types of sensors to detect changes in aboveground forest biomass and structure. Several steps can be taken to reduce uncertainty in area, biomass, and carbon estimates from satellite sensors.

5.1.1 First-Order Uncertainties: Forest Area

Because even degraded forests contain a large amount of biomass relative to agricultural ecosystems, measuring intact and degraded forest area is the first step in forest biomass estimation (DeFries et al. 2007; Ramankutty et al. 2007; Houghton 2007). Forest/nonforest area (a Level I classification) can be mapped with very high accuracy, but the only global forest maps are at a coarse-scale and miss the majority of deforestation. Global, moderate-resolution estimates have been made by subsampling (Achard et al. 2008). Further, it is not possible to distinguish tree plantations, agroforestry, and forest regrowth from mature forest using current coarse-resolution forest maps (Sanchez-Azofeifa et al. 2009; Hansen et al. 2008b). Given the increase in tropical forest regrowth in deforested areas (Asner et al. in press) and the rapid expansion of tree plantations globally (FAO 2006), these shortcomings have large and growing importance for global biomass estimates.

Moderate-resolution optical time series have been used in several national mapping efforts and have enabled mapping of forest types and deforestation with medium to good accuracy (Section 4.1.5). This approach could be used to map global forest area to Level II forest types, although achieving good global accuracy would be challenging. As an added benefit, these series extend back to before1980.

5.1.2 Forest Area and the Promise of New Technology

Between 2009 and 2015, global high-resolution coverage will likely be achieved by the GeoEye and RapidEye constellations. This global dataset will be invaluable in validation and algorithm training for forest monitoring efforts. The geostationary GOES satellite constellation, among others, should improve to 1 km resolution at nadir and make real-time, coarse-resolution deforestation detection possible. The launch of several moderate-resolution satellites would continue these imagery series, increase the number of bands available for multispectral land-cover mapping, and make possible highly accurate, hyperspectral global land-cover maps. The dramatic increase in the number of SAR satellites, available bands, and constellations should make SAR-passive fusion a common technique and allow multi-polar and InSAR mapping of land cover and structure. The creation of annual forest maps from ALOS is a first effort in this direction (Kellndorfer et al. 2008). Opening the Landsat archive has enabled several new efforts, including the reanalysis of past imagery, the use of temporal information in classifying moderate-resolution images (e.g., Helmer et al. 2009), and the creation of global, moderate-resolution land-cover classifications (e.g., Cunningham et al. 2002). All these developments should help to increase the accuracy of land-cover mapping, both past and future.

5.1.3 Second-Order Uncertainties: Forest Biomass, Degradation, and Global Change

Forest biomass and carbon can be estimated using fusions of passive, sensors, active sensors, and field data although the accuracy of remote estimates depends on accurate field data (see Section 3.1.3). The global availability of LIDAR data from ICESat GLAS, when combined with MODIS imagery, SAR sensors, and large ground-truth datasets, has made regional biomass mapping and validation feasible (e.g., Saatchi et al. 2007; Baccini et al. 2008; Boudreau et al. 2008). Unlike forest area however, historical reference maps for global forest biomass do not exist. Conservative estimates of baseline forest biomass will have to be generated from current remote sensing and forest inventory data (Gibbs et al. 2007; GOFC-GOLD 2008; Rosenqvist et al. 2003; Olander et al. 2008). The lack of reference biomass maps before 2005–2009 impedes both international policy and scientific inquiry (Gibbs et al. 2007; Grainger 2008). Temporal change in biomass is important for carbon modeling, monitoring forest degradation, characterizing forest regrowth, and predicting forest carbon stocks. Rosenqvist et al. (2003) argue that it may be possible to use the JERS-1 data to develop reference global biomass maps, but this is may be unlikely given the low biomass saturation of L-band SAR. Given the number and variety of expected active sensors in the next few years, a hindcasting approach that uses modern data to create past biomass estimates might be possible (see below).

Large-scale human and natural disturbances—logging, fires, pest outbreaks, and global warming—also cause uncertainty in forest biomass estimates. This uncertainty exists because these disturbances are either difficult to detect (logging, some pest outbreaks, fires in cloudy areas) or because effects are difficult to predict and pervasive (fires in tropical frontiers, global warming).

Progress is taking place in detecting logging using moderate-resolution imagery (Asner et al. 2005), and the increased number of high-resolution and SAR sensors in orbit (e.g., the RapidEye or Sentinel-1 constellations) are likely to make the global mapping of structural changes in forests possible (although at larger cost than previously). Determining how global forest biomass will respond to the effects of tropical fires, deforestation-climate interactions, and increases in forest respiration rates in a warmer world will require accurate inputs to carbon and climate models from remotely sensed data, including land cover, fire frequency, carbon gas fluxes, phenology data, and carbon stocks. To create these estimates, concerted global forest monitoring using both remote sensing and ground data is required.

5.1.4 Forest Biomass and the Promise of New Technology

With the plethora of SAR bands, polarities, and constellations expected to launch between 2009 and 2015, a number of multi-band fusion possibilities will arise. The accumulation of LIDAR data by new satellites and aerial sensors will refine biomass maps based on optical and SAR sensors. It is likely that big steps forward will be taken in measurement of forest height, structure, biomass, and ground elevation in the next few years because of the ICESat-2 mission, the DESDynI and BIOMASS missions, and the wealth of SAR data. The development of forest biomass maps is very likely in the near term particularly with the expected launch of DESDynI in 2015 and the potential launch of BIOMASS in late 2015 or early 2016. Estimation of biomass from remote sensors faces two key challenges, however. The first challenge is to collect adequate reference, or ground-truth, data—we address this issue below. The second challenge is to create accurate reference biomass maps for 2000 or 1990, like those requested by political agreements and scientists (Gibbs et al. 2007; Rosenqvist et al. 2003). This challenge can only be solved by conservative estimates and/or hindcasting.

Hindcasting past forest biomass from the current relationship of biomass with remote sensing data is possible using, for example, either the Direct Remote Sensing approach or the Stratify and Multiply approach (Section 4.4.1). One possible DRS approach would combine a still-to-be-developed ground-level DEM with reference InSAR data from the 1994 and 2000 shuttle missions, creating global forest height maps (e.g., Walker et al. 2007; Kellndorfer et al. 2004). These historic height maps could be converted into biomass estimates using current relationships between InSAR heights and biomass (LIDAR and ground derived). These biomass estimates could even be improved by fusing them with spectral information from the Landsat archive. Alternatively, an Stratify and Multiply approach could use ground, SAR, and LIDAR data to develop relationships between moderate-resolution, Level II land-cover maps and current, conservative biomass estimates (e.g., Helmer et al. 2009). Historic, moderate-resolution Level II land-cover maps would be used to estimate reference forest biomass.

In the next six years, multi-polar, repeat-pass InSAR and the GLAS and DESDynI footprint archives will markedly improve DEM and BIOMASS measurements (ESA 2009; NASA 2009a, Saatchi et al. in review). The eight-year MODIS record of vegetation productivity and its continuation by the NPOESS, GCOM, and Sentinel-3 series will continue to be useful in monitoring land cover and vegetation response to climate change. The record of MODIS in daily phenology and fire measurement could be improved to real time by coarse-resolution geostationary satellites. Global modeling of carbon stocks and fluxes will be aided by all of these sensors. Global carbon gas

monitors (e.g., IBUKI) and hyperspectral refinement of global leaf area estimates will also be beneficial (DeFries 2008; Palmer 2008).

5.1.5 Improved Estimates Require Improved Ground-Truthing

Despite the promise of new technology, high-quality geo-referenced ground-truth data will continue to be essential in validating and improving estimates from satellite imagery (Gibbs et al. 2007; Goetz et al. 2009). For example, one of the biggest causes of uncertainty in estimating biomass in the Amazon and Congo basins is the lack of ground-truth forest inventory data over large areas to train remote sensing algorithms (Saatchi et al. 2007; Baccini et al. 2008). Larger, higher-quality ground-truth datasets improve estimates from remote sensing imagery (Foody 2002). To achieve accurate estimates, a global forest measurement effort will have to collate a large number of existing ground-truth datasets and coordinate additional data collection in gap areas (e.g., central Africa; Herold 2009) and needed measurements (regional wood density patterns; Baker et al. 2004). Ideally, ground-truthing and high-resolution LIDAR and optical imagery (satellite or airborne) should both be used, but collection of forest inventory data and aerial LIDAR data has lagged behind satellite data collection in many countries (Herold 2009).

The dependence of accurate remote sensing estimates on large amounts of ground-truth data has important implications for any global forest measurement effort. As noted in Section 3.5, ground-truthing is usually the most expensive part of large-scale remote-sensing analysis. Different types of ground-truthing (e.g., forest inventory, LIDAR, high-resolution optical) would need to be coordinated in a sampling hierarchy for efficiency (Table 3; Patenaude et al. 2005; DeFries et al. 2007). In a global forest measurement effort, the logistical difficulties of air and ground access are not trivial, and careful coordination of aerial and ground data with satellite imagery is a practical necessity (Achard et al. 2007; GOFC-GOLD 2008; Rosenqvist et al. 2003; DeFries et al. 2007).

5.2 In Conclusion: Toward Improved Measures and Monitoring

Accurate global estimates of forest area, forest structure, forest biomass, and carbon are achievable using remote sensing technologies that are available now or that will come on-line by 2015. Forest biomass and forest carbon stocks cannot be measured directly, but conservative estimates are possible using fusions of current forest inventory data and satellite imagery. Global measurement of biomass should be possible with new remote sensing technology especially from 2015 onward.

Any global effort to measure forests using remote sensing technologies will face several technical challenges. Ground-truth data must be acquired across diverse countries and ecosystems and shared globally. Creating global forest maps with high, regionally consistent accuracy is demanding. Choices are necessary in selecting imagery with the appropriate trade-off in cost, resolution, swath, and repeat time. Challenges also remain to process and fuse large amounts of imagery in a globally consistent manner and to use new remote sensing technologies to measure biomass accurately over large areas.

Surmounting these challenges will require planning, global coordination, and understanding of the advantages and limitations of individual remote sensing technologies. Given the number of inaccuracies in current global forest measurement by the FAO, country-level censuses, and other bodies (Waggoner 2009), there is a need for improved monitoring of the world's forests. Remote

sensing has a strong track record in global forest measurement and planned sensor launches in the next few years have even greater potential. Institutional arrangements that implement a systematic approach, integrating satellite and ground-truth data, would allow us, for the first time in history, to conduct accurate, global monitoring of the world's forests.

Satellite, Sensor, and Remote Sensing Acronyms and Abbreviations

AirMISR	Airborne Multi-Angle Imaging SpectroRadiometer
ABI	Advanced Baseline Imager
ALOS	Advanced Land Observing Satellite
ASTER	Advanced Spaceborne Thermal Emission and Reflection Radiometer
ATSR	Along Track Scanning Radiometer
AVHRR	Advanced Very High Resolution Radiometer
Avnir	Advanced Visible and Near Infrared Radiometer
CBERS	China-Brazil Earth Resources Satellite
CHRIS	Compact High Resolution Imaging Spectrometer
COSMO-SkyMed	Constellation of Small Satellites for Mediterranean Basin Observation
DESDynI	Deformation, Ecosystem Structure and Dynamics of Ice satellite
DETEX	Detection and Monitoring of Selective Logging Activities
DMC	Disaster Monitoring Constellation
DMSAR	Disaster Management Synthetic Aperature Radar
EnMAP	Environmental Mapping and Analysis Program
Envisat	Environmental Satellite
EO-1	Earth Observing One
EOS	Earth-observing satellites
ERS-1	European Remote Sensing Satellite
FY	Fengyun
GCOM	Global Change Observation Mission
GLAS	Geoscience Laser Altimeter System
GLC 2000	Global Land Cover 2000
GOES	Geostationary Operational Environmental Satellites
HJ	Huanjing

HRG	High-resolution geometrical
HyspIRI	Hyperspectral Infrared Imager
HySI	Hyper-Spectral Imager
ICESat	Ice, Cloud, and land Elevation Satellite
IMS	Interactive Multisensor Snow and Ice Mapping System
InSAR	Interferometric Synthetic Aperture Radar
IRS	Indian Remote Sensing
JERS-1	Japanese Earth Resources Satellite
LDCM	Landsat Data Continuity Mission
LIDAR	Light Detection and Ranging
MERIS	Medium Resolution Imaging Spectrometer
MetOp	Meteorological Operational Satellite
MISR	Multi-angle Imaging SpectroRadiometer
MODIS	Moderate Resolution Imaging Spectroradiometer
NPOESS	National Polar-orbiting Operational Environmental Satellite System
PALSAR	Phased Array type L-band Synthetic Aperture Radar
POLDER	Polarization and Directionality of the Earth's Reflectances
POLinSAR	Polarimetric and Interferometric Synthetic Aperture Radar
PROBA	Project for On-Board Autonomy
SAC	Satélite de Aplicaciones Científicas
SAOCOM	Satélite Argentino de Observación Con Microondas
SAR	Synthetic Aperture Radar
SEVIRI	Spinning Enhanced Visible and Infrared Imager
SIR	Shuttle Imaging Radar
SPOT	Satellite Pour l'Observation de la Terre
SRTM	Shuttle Radar Topography Mission
SWIR	short-wave infrared

TanDEM-X	Tandem Digital Elevation Mapping Satellite
TerraSAR-X	Terra Synthetic Aperture Radar Satellite
TES-HYS	Technology Experimental Satellite Hyperspectral
UAS	Unmanned Aerial Systems
VENμS	Vegetation and Environment Monitoring New Micro-satellite
VNIR	visible and near-infrared

General Abbreviations and Acronyms

AGB	aboveground biomass
AGC	aboveground carbon
DBH	tree diameter at breast height
DEM	digital elevation model
DRS	direct remote sensing
FAO	Food and Agriculture Organization of the United Nations
fAPAR	fraction of absorbed photosynthetically active radiation
FIA	U.S. Forest Service's Forest Inventory and Analysis Program
FRA	Forest Resource Assessments
FRP	fire radiative power
GI	global imagery
GIS	geographic information systems
ha	hectare
INPE	Brazilian National Institute for Space Research
IPCC	Intergovernmental Panel on Climate Change
kg	kilograms
km	kilometers
LAI	leaf area index

m	meters
m^3	cubic meters
Mg	megagrams
NASA	National Aeronautics and Space Administration
REDD	reducing emissions from deforestation and forest degradation
UAE	United Arab Emirates
µm	micrometers
UNFCCC	United Nations Framework Convention on Climate Change
USGS	United States Geologic Survey

Appendix. Current and Near-Term Earth-Observing Satellite Technology: An Overview

This guide to current and future (2009 to early 2016) Earth-observing satellites is not an exhaustive list. The authors attempted to cover all satellites that are likely to create regional to global coverage but anticipate that some satellites were accidentally missed. Most ultra-coarse (2+ km spatial resolution), military, and non-land imaging satellites were excluded.

The information provided in the section on "Future Satellites" is as current as possible, but improvements in technology, delays in satellite launching, mission cancellations, and outdated information sources are inevitable. The authors welcome corrections and updates from readers.

The satellites' specifications in this appendix come primarily from publicly available governmental and commercial websites. The following are the main sources used to compile the appendix.

Committee on Earth Observation Satellites. 2009. Committee on Earth Observation Satellites. http://www.ceos.org/ (accessed March 28, 2009).

eoPortal (sponsored and run by the European Space Agency). 2009. List of EO and non-EO Satellite Missions. http://directory.eoportal.org/missions_all_list.php?filter=&view_all&order=start_date&dir=ASC (accessed July 23, 2009).

GOFC-GOLD. 2008. *Reducing Greenhouse Gas Emissions from Deforestation and Degradation in Developing Countries: A Sourcebook of Methods and Procedures for Monitoring, Measuring, and Reporting*. GOFC-GOLD Report version COP13-2, edited by GOFC-GOLD Project Office. Alberta, Canada: Natural Resources Canada.

Kramer, H.J. 2002. *Observation of the Earth and Its Environment: Survey of Missions and Sensors*, 4th edition. New York: Springer-Verlag.

Powell, S.L., D. Pflugmacher, A.A. Kirschbaum, Y. Kim, and W.B. Cohen. 2007. Moderate resolution remote sensing alternatives: a review of Landsat-like sensors and their applications. *Journal of Applied Remote Sensing* 1.

Current Moderate-Resolution (200 to 15 m) Optical Sensors Relevant to Forest Mapping

Satellite & sensor	Launch date	Source	Spectrum	Resolution, return interval	Image width	Notes & global imagery (GI) extent	Cost for data acquisition
Landsat 5 TM	1984	USA	VTIR, 7 bands	30 m, 16 days	185 km	Images every 16 days to any satellite receiving station. Operating beyond expected lifetime. Continuous GI to 1985, spotty 1985 to present.	Free. Formerly 600 US$/scene, 0.02 US$/km2.
Landsat 7 ETM+	1999	USA	VTIR, 8 bands	30 m (15 pan), 16 days	185 km	On April 2003, the failure of the scan line corrector resulted in data gaps outside of the central portion of images, seriously compromising data quality. Still operating. Continuous GI.	Free. Formerly 600 US$/scene, 0.02 US$/km²
Terra ASTER	1999	USA/Japan	VTIR, 14 bands	15–30 m, 16 days	60 km	Data is acquired on request and is not routinely collected for all areas. Spotty GI, pointable.	60 US$/scene, 0.02 US$/km²
EO-1 ALI	2000	USA	VSWIR, 10 bands	30 m (10 pan), 16 days	37 km	An experimental sensor, ALI's lifetime was extended at the request of researchers. Spotty GI.	Free
EO-1 Hyperion	2000	USA	VSWIR, 220 bands	30 m, 16 days	7.5 km	As an experimental sensor, Hyperion has had issues with signal-to-noise ratio. Spotty GI.	Free
Resourcesat-1 LISS-III & AWiFS	2003	India	VSWIR, 4 bands	23.5 m, 24 days & 56 m, 5 days	142 km & 730 km	Constellation member, hosts two moderate-resolution sensors. Continuous GI.	860 US$/scene, 0.05 US$/km, & 1790 US$/scene, 0.004 US$/km
IRS-1C/1D LISS-III & WiFS	1995, 1997	India	VSWIR, 4 bands & 2 bands	23.5 m, 24 days, & 188 m, 5 days	142 km & 810 km	Constellation twin satellites, each hosts two moderate-resolution sensors. Continuous GI?	860 US$/scene, 0.05 US$/km, & TBD

Satellite & sensor	Launch date	Source	Spectrum	Resolution, return interval	Image width	Notes & global imagery (GI) extent	Cost for data acquisition
CBERS-2, 2B HRCCD	1999, 2003	China/ Brazil	VNIR, 5 bands	20 m, 26 days	113 km	Experimental; Brazil uses on-demand images to bolster their coverage. Continuous over Brazil, Africa, and China only.	Free in South America, China, and Africa
CBERS/IR-MSS	1999, 2003	China/ Brazil	VTIR, 4 bands	80–160 m, 26 days	120 km	Mounted on the same satellites as the HRCCD sensor, above. Continuous over Brazil, Africa, and China only.	Free in South America, China, and Africa
DMC series	2002–2008	Algeria/ China/ Nigeria/ Turkey/UK	VNIR, 3 bands	22–32 m, daily possible	160–600 km	Commercial; Brazil uses alongside Landsat data. Consists of multiple satellites in the same track. Continuous GI.	585 €/scene, 0.048 €/km²
SPOT-2 HRV	1990	France	VNIR, 4 bands	20 m (10 pan), 2–3 days	60–117 km	Two sensors can expand width of image. Pointable, continuous GI.	2000 €/scene, 0.5 €/km²
SPOT-4 HRVIR	1998	France	VSWIR, 5 bands	20 m (10 Pan), 2–3 days	60 km	Two sensors can expand width of image. Pointable, continuous GI.	2000 €/scene, 0.5 €/km²
Proba CHRIS	2001	Europe	VNIR, 63 bands (18 full)	34 m (17 m full), TBD	17 km	Experimental hyperspectral sensor with extended lifespan. It has two modes: full-resolution has fewer bands. Spotty GI.	Free to researchers, TBD
SAC-C HRTC	2000	Argentina	VNIR, 1 band	35 m, TBD	90 km	This panchromatic camera has spotty GI, with a concentration over South America.	Free
Monitor-E RDSA	2005	Russia	VNIR, 3 bands	20 or 40 m, TBD	160 or 890 km	Two sensing modes, higher or lower resolution.	TBD

Satellite & sensor	Launch date	Source	Spectrum	Resolution, return interval	Image width	Notes & global imagery (GI) extent	Cost for data acquisition
THEOS MS	2008	Thailand	VNIR, 4 bands	15 m, 1–5 days	90 km	Pointable, with a pan imager detailed in the high-resolution section.	TBD
IMS-1 MxT	2008	India	VNIR, 4 bands	37 m, TBD	151 km	This mini-satellite's imagery will be provided to developing countries. It is unclear whether this satellite's data is available to the public.	Free
HJ-1A/1B	2008	China	VNIR, 4 bands	30 m, 4 days	360 or 720 km	Pointable, two sensors. Onboard hyperspectral imager detailed in the coarse-resolution section. It is unclear whether this satellite's data is available to the public.	TBD
WFC (Calipso)	2006	USA	visible, 1 band	125 m, TBD	60 km	This cloud imager is combined with a LIDAR instrument for analysis of clouds.	TBD

Current Coarse-Resolution (>200 m pixel) Optical Sensors Relevant to Forest Mapping

Satellite & sensor	Launch date	Source	Spectrum	Resolution, return interval	Image width	Notes & global imagery extent (GI)	Cost for data acquisition
AVHRR	1978–2005	USA	VTIR, 4–6 bands	1.1 km, bi-daily	3,000 km	A long-term satellite constellation, the most recent is AVHRR/3. Continuous GI.	Free
MODIS Terra & Aqua	2000, 2002	USA	VTIR, 36 bands	250–1,000 m, 2 days	2,330 km	Mounted on two satellites. Vegetation bands are 250 m resolution. Thermal bands are used to detect fires. Continuous GI.	Free
GOES 10-13 Imager	1975–2006	USA	VTIR, 5 bands	1 km visible, 5 km IR, real-time	Full Earth disc	GOES is included as an example of geostationary meterological imagers and is ultra-coarse (5 km pixel) outside the single visible band. India, Russia, China, and Europe all have geostationary meteorological constellations as well. It is not included in Figure 13.	Free
SPOT-4/5-Vegetation	1998	France	VNIR, 4 bands	1.1 km, bi-daily	2,200 km	Continuous GI.	TBD
MISR	1999	USA	VNIR, 4 bands	275 m OR 550–1,100 m (global), 9 days	360 km (local)	Stereo imaging from nine angles. It takes 6 images on Local setting (275 m) each day, and the rest on Global.	Free
Orbview-2 SeaWiFS	1997	Comm. (USA)	VNIR, 8 bands	1.13 km, daily	1500 km	This coarse-resolution sensor is optimized for ocean remote sensing. Continuous GI.	TBD
ERS-2 ATSR-2	1995	ESA	VTIR, microwave, 10 bands	1 km, TBD	500 km	This coarse-resolution sensor can monitor sea-surface temperature and fires. Continuous GI.	TBD
Envisat MERIS	2002	ESA	VNIR, 15 bands	260 x 300 m, 3 days	1150 km	Band-programmable, can be selected across VNIR range. Continuous GI.	TBD
Envisat AATSR	2002	ESA	V-TIR, 7 bands	1 km, TBD	500 km	Thermal bands are used to dectect fires. Continuous GI.	TBD

Satellite & sensor	Launch date	Source	Spectrum	Resolution, return interval	Image width	Notes & global imagery extent (GI)	Cost for data acquisition
ADEOS-II GLI	2002–2003	Japan	VTIR, 36 bands	250–1,000 m, 4 days	1,600 km	This short-lived satellite was very similar to MODIS, but with 29 bands in the VNIR.	TBD
Insat 2E, 3A	1999	India	VTIR, 6 bands	1 km, TBD	6,000 km	This satellite has a programmable orientation within its wide field of view.	TBD
HY-1B, 1C, 1D	2007	China	VTIR, 10 bands	1 km, TBD	3,083 km	These satellites are optimized for ocean observation, with 6 bands in the visible.	TBD
COMS-1 GOCI	2009	Korea	VNIR, 8 bands	236–360 m, daily	1,440 km	This geostationary ocean color observation satellite will observe a limited area.	TBD
SAC-C MMRS, HTSC	2000	Argentina	VSWIR, 5 bands	175 m (300 pan), TBD	360 km (700 pan)	This satellite mounts a panchromatic fire and lightning imager and a land imaging sensor.	TBD
HJ-1A/1B	2008	China	VNIR, 110 bands	100 m, TBD	50 km	This hyperspectral satellite's imagery may not be available for public purchase.	TBD
IMS-1 HySI	2008	India	VNIR, 64 bands	505.6 m	125.5 km	This experimental hyperspectral satellite will be operated over India only.	TBD
FY-3 series: MERSI, VIRR	2008	China	VSWIR, 20 bands, & VTIR, 10 bands	250 m–1 km & 1.1 km, TBD	2,800 km	The FY-3 constellation will host the MERSI and VIRR instruments for coarse-resolution Earth observation.	TBD
MSU-MR (Meteor-M N1) [[not listed]]	2008	Russia	VTIR, 6 bands	1 km, TBD	2,800 km	This temperature and cloud-mapping instrument can also take land-cover data.	TBD
MVISR (FY-1D) [[not listed]]	2002	China	VTIR, 10 bands	1.1 km, TBD	2,800 km	It is unclear if this land- and ocean-observing satellite's imagery is available for purchase.	TBD
OCM (Oceansat-1/2)	1999, 2008	India	VNIR, 8 bands	236–360 m, 2 days	1,440 km	These satellites are primarily ocean color monitors and take data primarily around India.	TBD
OLS (DMSP series)	1997–2009	USA	VTIR, 3 bands	560 m, TBD	3,000 km	This cloud- and cloud-temperature monitoring sensor can also detect fires.	TBD

WFI (CBERS-2/2B)	2003, 2007	Brazil/ China	VNIR, 2 bands	258 m, TBD	890 km	This sensor is designed to detect vegetation.	TBD

Current High-Resolution Optical Sensors Relevant to Forest Mapping

Satellite & sensor	Launch date	Source	Spectrum	Resolution, return interval	Image width	Notes & global imagery (GI) extent	Cost for data acquisition
SPOT-5 HRG	2002	Comm. (France)	VSWIR, 5 bands	10 m (2.5–5 pan), 2–3 days	60–120 km	Commercial; Indonesia & Thailand use alongside Landsat data. Pointable.	2700 €/scene, 0.5 €/km²
Formosat-2	2004	Comm. (Taiwan)	VNIR, 5 bands	8 m (2 pan), 1 day	24 km	Commercial. Unique orbit: early arrival at equator, GI is selected areas in strips	TBD
IKONOS	2000	Comm. (USA)	VNIR, 5 bands	4 m (1 pan), 3 days	11–14 km	Pointable, stereo capability. Spotty GI, developing continuous GI.	TBD
Geoeye-1	2008	Comm. (USA)	VNIR, 5 bands	1.65 m (0.41 pan), 3 days	15.2 km	Pointable, pan imagery released at 0.5 m. Spotty GI, developing continuous GI.	380 US$/scene, 25 US$/km²
Quickbird	2001	Comm. (USA)	VNIR, 5 bands	2.4 m (0.61 pan, 3 days	16.5 km	Pointable. Spotty GI, developing continuous GI.	TBD
RapidEye 1-5	2008	Comm. (Germany)	VNIR, 5 bands	5 m, daily	78 km	Constellation, allows frequent imaging. Designed for global crop monitoring.	TBD
ALOS Avnir-2	2006	Japan	VNIR, 4 bands	10 m	70 km	This high-resolution sensor operates with the ALOS PALSAR sensor, allowing imagery fusion.	TBD
Resourcesat-1 LISS-4	2003	India	VNIR, 4 bands	5.8 m, 5 days	70 km	Pointable and mounted with two moderate-resolution sensors. Two launched?	1070 US$/scene, 0.3 US$/km²
Sumbandila Sat Imager	2009	South Africa	V-NIR, 6 bands	6.25 m, TBD	45 km	South Africa's first satellite, this small satellite is not likely to develop continuous GI.	TBD

Satellite & sensor	Launch date	Source	Spectrum	Resolution, return interval	Image width	Notes & global imagery (GI) extent	Cost for data acquisition
Resurs DK-1 Geoton-L1	2006	Russia	VNIR, 5 bands (pan)	2.5–3.5 m (1 m pan), TBD	30 km	This commercial satellite has a variable orbital distance, affecting its swath and resolution.	TBD
Kompsat-2	2006	Korea	VNIR, 5 bands	4 m (1 pan), 28 days (max)	15 km	Pointable sensor, commercially available.	TBD
TopSAT Telescope	2005	UK	visible, 4 bands	5.6 m (2.8 m pan), TBD	17 km (pan), 12 km	Experimental, low-cost microsatellite.	TBD
Cartosat 1, 2	2005, 2007	India	VNIR, 1 band (pan)	2.5 m, TBD	30 km	Panchromatic camera.	TBD
IRS-1C/1D PAN	1995, 1997	India	VNIR, 1 band (pan)	6.5 m, 24 days (max)	70 km	Pointable, panchromatic camera.	TBD
ALOS PRISM	2006	Japan	VNIR, 1 band (pan)	2.5 m, TBD	70 km (35 km stereo)	Panchromatic camera with triple-stereo option.	TBD
EROS-A	2000	Comm. (Israel)	VNIR, 1 band (pan)	1.9 m	14 km	Highly pointable, panchromatic camera.	TBD
EROS-B	2000, 2006	Comm. (Israel)	VNIR, 1 band (pan)	0.7 m	7 km	Pointable, panchromatic camera.	TBD
Worldview-1	Comm. (USA), 2004	Comm. (USA), 2004	VNIR, 1 band (pan)	0.5 m pan, 2 days	17.5 km (110 x 60 poss.)	Pointable, pan imagery released at 0.5 m. Spotty GI, developing continuous GI.	TBD
BJ-1 PAN	2005	China	VNIR, 1 band (pan)	4 m pan, TBD	24 km	Panchromatic camera, unclear if available for public purchase.	TBD
Monitor-E PSA	2005	Russia	VNIR, 1 band (pan)	8 m, TBD	90 km	Panchromatic commercial camera.	TBD
TES PAN	2001	India	visible, 1 band (pan)	1 m, TBD	Not available	This military panchromatic camera is not included in Figure 13.	Not available

Current Coarse- to Moderate-Resolution Active Sensors Relevant to Forest Mapping

Satellite & sensor	Launch date	Source	Spectrum	Resolution, return interval	Image width	Notes & global imagery (GI) extent	Cost for data acquisition
SRTM	2000 (one-time)	USA	InSAR, C- and X-band, quad-polar (C-band only)	30 x 30 m, N/A	50–225 km	Result of a 10-day shuttle mission. Used to create a 30 m DEM (90 m outside US). Continuous GI between 60° N and 56° S.	Free DEM and data.
SIR-C/X mision	1994 (one time)	USA	InSAR, X, C, L-band, quad-polar	30 x 10–30 m, N/A	15–90 km	Result of a shuttle mission. Continuous GI.	Free
JERS-1	1992 (launch), 1997 (end)	Japan	SAR, L-band, HH-polarity	18 x 18 m, 44 days	75 km	Continuous GI, with temporal inferometry in select areas.	Free
ERS-1, 2	1991, 1995	ESA	SAR, C-band, VV polar	30 x 26 m, TBD	100 km x 100 km	Continuous GI, with temporal inferometry in select areas.	Free
RADARSAT	1995	Canada	SAR, C-band, HH polar	8–100 m x 8–100 m, TBD	50–500 km x 50–500 km	Pointable. Continuous GI, with temporal inferometry in select areas.	Free
RADARSAT-2	2006	Canada	SAR, C-band, quad-polar	3–100 m x 2.4–100 m, TBD	20–500 km x 20–500 km	Pointable. Continuous GI, with temporal inferometry in select areas.	TBD
Envisat ASAR	2002	EU	SAR, C-band, quad-polar	30–1,000 m x 30–1,000 m, TBD	5–150 km x 5–150 km	Pointable. Continuous GI, with temporal inferometry in select areas.	TBD

Satellite & sensor	Launch date	Source	Spectrum	Resolution, return interval	Image width	Notes & global imagery (GI) extent	Cost for data acquisition
TerraSAR-X	2007	Comm. (Germany)	SAR, X-band, quad-polar	1–18 m x 1–18 m, 2.5–11 days	10–100 km x 5–150 km	Commercial, variable resolution, and first in a satellite constellation.	TBD
ALOS PALSAR	2006	Japan	SAR, L-band, quad-polar	7–100 m, TBD	40–350 km	Resolution and swath vary depending on mode. Continuous GI.	210.04 US$/scene, 0.017 US$/km²
COSMO-SkyMed	2007–2009	Italy	SAR, X-band, quad-polar	3–30 m, 26 days	10–200 km	Variety of scanning modes. First three members of SAR constellation, tandem orbit for DEM.	TBD
ICESAT GLAS	2004	USA	LIDAR	70 m footprint, 183 days	Footprint centers 170 m apart	Tracks are currently spaced at 15 km (equator) and 2.5 km (80 degrees lat.).	Free
IBUKI (GOSAT)	2009	Japan	Gas-sampling, NIR-TIR	10.5 km, TBD	N/A	10.5 km footprint, operates in cloud-free areas globally. Takes instantaneous measurements of CO_2 and CH_4.	TBD

Expected Sensors Relevant to Forest Mapping (2009–2016)

Satellite & sensor	Launch date	Source	Spectrum	Resolution, return interval	Image width	Notes
WorldView-2	2009	Comm. (USA)	VNIR, 9 bands	1.8 m (0.5 m pan),1–4 days	16.4 km	Eight bands (+ pan) in the VNIR, pointable.
ARGO (RapidEye-6)	2009	Taiwan/ Germany	VNIR, 5 bands	5 m, daily	78 km	Commercial, part of the RapidEye constellation.
RazakSat	2009	Malaysia	VNIR, 5 bands	5 m (2.5 pan), TBD	20 km	Pointable high-resolution. May not develop continuous GI.
DubaiSat	2009	UAE	VNIR, 5 bands	5 m (2.5 pan), TBD	20 km	Pointable high-resolution. May not develop continuous GI.
ALSAT-2A, 2B	2009	Algeria	VNIR, 5 bands	10 m (2.5 m), TBD	17 km	Pointable high-resolution, not likely to develop continuous GI.
EROS-C	2009	Israel	VNIR, bands TBD (5?)	2.8 m (0.7 m pan)	11 km	Pointable, high-resolution. May not develop continuous GI.
TanDEM-X	2009	Comm. (Germany)	SAR, X-band, quad-polar	1–18 m x 1–18 m, 2.5–11 days	10–100 km x 5–150 km	Commercial, variable resolution. A twin satellite orbiting in formation with TerraSAR-X to create a global DEM.
Resourcesat-2 (ISRO)	2009	India	VSWIR, 4 bands	23.5 m, 24 days	141 x 141 km²	This satellite will be very similar to Resourcesat-1, with its moderate and high-resolution imagery capability.
RASAT (Tubitak)	2009	Turkey	visible, 4 bands	15 m (7.5 m pan), TBD	30 x 30 km	Still under development.
NigeriaSat-2 (NASRDA)	2009	Nigeria	VNIR, 5 & 4 bands	5 m (2.5 pan) & 32 m, TBD	20 km & 300 km	This satellite will mount two sensors. The high-resolution sensor has a smaller image size but more bands.
COSMO-SkyMed 4 (ASI/MiD)	2009	Italy	SAR, X-band, quad-polar	3–30 m, TBD	10–200 km x 10–200 km	Variety of scanning modes, last satellite addition to COSMO SAR constellation.

Satellite & sensor	Launch date	Source	Spectrum	Resolution, return interval	Image width	Notes
Meteor-M N1 (Roshydromet/ Roscosmos)	2009	Russia	1) SAR, X-band, VV polarized. 2) VTIR, 6 bands. 3) VNIR, 3–6 bands.	1) 400–1,000 m. 2) 1,000 m. 3) 60–120 m.	1) 450–600 km. 2) 2800 km. 3) 960 km.	This innovative satellite will host three distinct sensors, numbered here. The last moderate-resolution will combine three camera images for 60 m resolution in three bands. The satellite will produce regional imagery over Russia. First in a series.
Meteor-M N2 (Roshydromet/ Roscosmos)	2009	Russia	1) SAR, X-band, VV polarized. 2) VTIR, 6 bands. 3) VNIR, 3–6 bands.	1) 400–1000 m, 2) 1,000 m, 3) 60120 m.	1) 450–600 km. 2) 2,800 km. 3) 960 km.	This innovative satellite will host three distinct sensors, numbered here. The last moderate-resolution will combine three camera images for 60 m resolution in three bands. The satellite will develop a regional GI only, over Russia.
Kanopus-V N1 (Roshydromet/ Roscosmos)	2009	Russia	VNIR, TBD	10.5–26 m (2.1 pan) TBD	250 km	Sources conflict on the exact resolution or bands of this small Russian satellite.
Sich-2	2009	Ukraine	VNIR, 4 bands	7.8 m (pan higher?)	46.6 km	Pointable high-resolution sensor.
RISAT-1	2009	India	SAR, C-band, quad-polar	3–40 m	30-240 km	High-resolution SAR satellite.
HJ-1C (S-band SAR)	2009	China	SAR, S-band	20 m	100 km	Unusual S-band SAR.
Svea	2010	Sweden	TBD, passive high-resolution	1.2–1.5 m	8–12 km	Under development.
Pleiades 1 (CNES)	2010	France	VNIR, 5 bands	0.7 m, TBD	20 km x 20 km	Extremely pointable satellite gives +/- 50 degrees off track.

Satellite & sensor	Launch date	Source	Spectrum	Resolution, return interval	Image width	Notes
TES-HYS (ISRO)	2010	India	VSWIR, 200 bands	15 m, TBD	30 km x 30 km	Moderate-resolution hyperspectral imager, under development/experimental.
GISAT (ISRO)	2010	India	VTIR, 3, 4, & 150 bands	1.5 km, 50 m, & 192–320 m, TBD	TBD	Proposed geostationary satellite with two coarse imagers (one hyperspectral) and one moderate imager.
SARE-1 (CONAE)	2010	Argentina	SAR	TBD	TBD	Proposed satellite with a SAR component and high-resolution optical cameras.
SAC-D (CONAE/ NASA)	2010	Argentina/USA	TIR, 3 bands	350 m, TBD	182–1,000 km	A multi-sensor satellite, but the fire sensor is summarized here. It will measure temperature and released energy of fires and other hot events.
HY-1C (NSOAS/ CAST)	2010	China	VTIR, 4 & 10 bands	250 m & 1.1 km	500 km & 3,083 km	Two instruments: Coast Region Imager and coarser Ocean Color and Temperature scanner. Constellation.
NPP (NASA/NOAA/ DoD)	2010	USA	VTIR, 22 bands	400 m–1.6 km, TBD	3,000 km	The first in a new NASA series of coarse-resolution satellites intended to follow up the MODIS and AVHRR missions.
VENµS (CNES/ISA)	2010	Israel/France	VNIR, 12 bands	5.3 m, TBD	27 km	A superspectral camera intended to take high-resolution, multiple-band images for land-cover applications.
CBERS-3 (CRESDA/ INPE)	2010	Brazil/China	1) NIR, 4 bands. 2) NIR, 4 bands. 3) VTIR, 4 bands. 4) VSWIR, 4 bands.	1) 20 m. 2) 10 m (5 pan), 3–26 days. 3) 40–80 m, 26 days. 4) 73 m, 5 days.	1) 120 m. 2) 60 km. 3) 120 km. 4) 866 km.	This satellite, the first of two, hosts four sensors with regional coverage. The high- and moderate-resolution sensors are pointable (3–5 day return time). It also has a moderate-resolution fire imager and a coarse-resolution sensor.

Satellite & sensor	Launch date	Source	Spectrum	Resolution, return interval	Image width	Notes
HY-1D (NSOAS/ CAST)	2010	China	visible, 4 bands	250 m	500 km	Coastal region imager. Constellation.
FY-3D (NRSCC/CMA)	2010	China	VSWIR, 20 bands; VTIR, 10 bands	250 m–1 km & 1.1 km, TBD	2,800 km	As an addition to the FY-3 constellation, it will host the MERSI and VIRR instruments for coarse-resolution Earth observation.
Elektro-L N2 (Roshydromet/ Roscosmos)	2010	Russia	VTIR, 10 bands	1 km visible 4 km IR, daily	Full Earth disc imaged	Geostationary satellite, second in a series.
Meteor-M N3 (Roshydromet/ Roscosmos)	2010	Russia	1) SAR, X-band. 2) Visible, 1 band.	1) 400–1,000 m. 2) 700–1,400 m.	1) 450–600 km. 2) 2,600 km.	This coarse-resolution satellite is mainly designed for cloud and ice measurement.
SSOT	2010	Chile	VNIR, 5 bands	5.8 m (1.45 pan), TBD	TBD	This high-resolution satellite will have regional coverage.
Kompsat-3	2010	South Korea	VNIR, 5 bands	2.8 m (0.7 m pan)	TBD	Commercial high-resolution satellite.
Kompsat-5	2011	South Korea	SAR, X-band	TBD	TBD	This satellite is under development.
GeoEye-2	2011	Comm. (USA)	VNIR, TBD	1.65 m, (0.25 pan)	TBD	The highest-resolution satellite to date. It is still under development.
SAOCOM 1A (CONAE/ASI)	2011	Argentina/Italy	SAR, L-band	10–100 m, TBD	40–320 km	First in a SAR constellation. Variable resolution, still under development. With COSMO-SkyMed, this joint-constellation will provide twice daily coverage in two SAR bands.
ASNARO	2011	Japan	passive high resolution	1 m, TBD	TBD	High-resolution passive satellite, under development.
CARTOSAT-3 (ISRO)	2011	India	visible, 1 band (pan)	0.3 m, TBD	6 km	High-resolution panchromatic imager.

Satellite & sensor	Launch date	Source	Spectrum	Resolution, return interval	Image width	Notes
MetOp-B (EUMETSAT)	2011	EU	VTIR, 6 bands	1.1 km, twice daily	3,000 km	This is the second in the MetOp constellation, carrying an AVHRR/3 instrument. It will cover the entire globe twice daily.
Pleiades 2 (CNES)	2011	France	VNIR, 5 bands	0.7 m, TBD	20 km	The second in a constellation. Pointable satellite gives +/- 50 degrees off track.
DMSAR (ISRO)	2011	India	SAR, C/X-band	TBD	TBD	This proposed satellite is currently an airborne system with high resolution and variable modes.
Resourcesat-3 (ISRO)	2011	India	VSWIR, 4 bands	23 m, 26 days	700 km	This will carry a more advanced sensor than previous Resourcesats, with an atmospheric correction instrument.
Prisma (ASI)	2011	Italy	VSWIR, 200 bands	30 m (2.5 pan), TBD	30 km	This hyperspectral imager will have a narrow image swath but high spectral and spatial resolution.
LDCM	2011	USA	VSWIR, 9 bands	30 m (15 pan), 16 days	185 km	Landsat Data Continuity Mission, free imagery, global coverage.
Sentinel-1 A (ESA/EC)	2011	EU	SAR, C-band, quad-polar	5–100 m, TBD	8–400 km	Variable resolution and swath-width SAR, first in a constellation.
AMAZÔNIA-1 (INPE)	2011	Brazil	VNIR, 4 bands	40 m & 12 m, 5 days & TBD	800 km & 110 km	This satellite will host the moderate-resolution AWFI sensor and the higher-resolution RALCam-3 sensor.

Satellite & sensor	Launch date	Source	Spectrum	Resolution, return interval	Image width	Notes
SAOCOM 1B (CONAE/ASI)	2012	Argentina/Italy	SAR, L-band	10–100 m, TBD	40–320 km	Second in a SAR constellation. Variable resolution, still under development.
Astroterra (SPOT-6)	2012	Comm. (France)	V-NIR, 5 bands	8 m (2 pan), 1-5 days	60	The next in SPOT series has stereo capability and highly pointable.
SAC-E/SABIA/mar (CONAE/INPE)	2012	Argentina/Brazil	VTIR, 15 bands	TBD	TBD	Under development.
Ingenio (SEOSAT) (CDTI/ESA)	2012	2012, Spain/EU	VNIR, 5 bands	10 m (2.5 pan), TBD	60 km	High-resolution satellite, may not develop GI.
EnMAP (DLR)	2012	Germany	VNIR, TBD	30 m	30 km	Moderate-resolution hyperspectral imager.
HY-3A (NSOAS/CAST)	2012	2012	SAR, X-band, TBD	1–10 m, TBD	40–150 km	High-resolution SAR imager.
SABRINA (ASI)	2012	Italy	SAR, X-band, Quad-polar	TBD	TBD	Under development.
Sentinel-2 A (ESA/EC)	2012	EU	VSWIR, 13 bands	10 m (VNIR) and 20–60 m (higher), TBD	290 km	First in a constellation, this high-quality moderate-resolution sensor will have dedicated atmospheric correction bands and a wide swath.
Sentinel-1 B (ESA/EC)	2012	EU	SAR, C-band, Quad-polar	5–20 m (extra wide 25 x 100 m), TBD	80–400 km	Second in a constellation, this SAR sensor has an interferometric mode, a wide-field mode, and an extra-wide mode.
Sentinel-3 A (ESA/EC)	2012	EU	VSWIR, 21 bands	300 m, TBD	750–1,675 km	This dual swath instrument will be a MODIS, AATSR, and MERIS follow-up. The first in a series.
ALOS-2	2012	Japan	SAR, L-band, Quad-polar	TBD	TBD	ALOS follow-on, under development, likely to be higher resolution.

Satellite & sensor	Launch date	Source	Spectrum	Resolution, return interval	Image width	Notes
FY-3E (NRSCC/CMA)	2012	China	VSWIR, 20 bands, & VTIR, 10 bands	250 m–1 km & 1.1 km, TBD	2,800 km	As an addition to the FY-3 constellation, it will host the MERSI and VIRR instruments for coarse-resolution Earth observation.
FY-4 O/A (NRSCC/CMA)	2012	China	VTIR, 12 bands	1 km visible, 2 km IR, 4 km TIR, daily.	Full Earth disc imaged	The first in a new geostationary series, this sensor will have higher VNIR resolution than previous geostationary imagers, and thus be more suitable for real-time vegetation monitoring.
TerraSAR-X2 (DLR)	2013	Comm. (Germany)	SAR, X-band, Quad-polar	1–18 m, 2.5–11 days	10–100 km x 5–150 km	The last of a three-satellite SAR constellation for deriving a high-quality DEM, this satellite may be joined or replaced by another satellite, Tandem-L.
NPOESS-1 (NOAA)	2013	USA	VTIR, 22 bands	400 m–1.6 km, TBD	3,000 km	The second in a new NASA series of coarse-resolution satellites intended to follow up the MODIS and AVHRR missions.
CBERS-4 (CRESDA/INPE)	2013	Brazil/China	1) NIR, 4 bands. 2) NIR, 4 bands. 3) VTIR, 4 bands. 4) VSWIR, 4 bands.	1) 20 m. 2) 10 m (5 pan), 3–26 days. 3) 40–80 m, 26 days. 4) 73 m, 5 days.	1) 120 m. 2) 60 km. 3) 120 km. 4) 866 km.	This satellite, the second of two, hosts four sensors with regional coverage. The high- and moderate-resolution sensors are pointable (3–5 day return time). It also has a moderate-resolution fire imager and a coarse-resolution sensor.
MAPSAR (INPE/DLR)	2013	Brazil/Germany	SAR, L-band, quad-polar	3–20 m, weekly revisit.	30–55 km	This high-resolution L-band SAR satellite may potentially acquire continuous GI.
RADARSAT CONSTELLATION-1 (CSA)	2013	Canada	SAR, C-band, quad-polar	3–100 m, TBD	20–500 km	First in a SAR constellation, this satellite has a wide range of resolution modes.
SAC-F (CONAE)	2014	Argentina	VSWIR, 5 bands	10 m (5 pan)	60–117 km	High-resolution, pointable sensors; still under development. It may be joined by a hyperspectral sensor and a thermal sensor.

Satellite & sensor	Launch date	Source	Spectrum	Resolution, return interval	Image width	Notes
SAOCOM-2A (CONAE)	2014	Argentina	SAR, L-band	10–100 m, TBD	40–320 km	Third in a SAR constellation. Variable resolution, still under development.
COMS-2	2014	Japan	VNIR, 8 bands	236 x 360 m	1,440 km	Geostationary Ocean Color Imager.
GCOM-C1 (JAXA)	2014	Japan/USA	VTIR, 35 bands	250–1,000 m, TBD	1,150–1,400 km	This MODIS-like sensor will have 11 bands at 250 m resolution in the VNIR.
Sentinel-2 B (ESA/EC)	2014	EU	VSWIR, 13 bands	10 (VNIR) and 20–60 m (higher), TBD	290 km	Second in a constellation, this high-quality moderate-resolution sensor will have dedicated atmospheric correction bands and a wide swath.
RISAT-L (ISRO)	2014	India	SAR, L-band	TBD	TBD	Under development.
RADARSAT CONSTELLATION-3 (CSA)	2014	Canada	SAR, C-band, quad-polar	3–100 m, TBD	20–500 km	Second in a SAR constellation, this satellite has a wide range of resolution modes.
GOES-S (NOAA)	2014	USA	VTIR, 26 bands	0.5 km in the visible, 1 km NIR-SWIR, 2 km TIR	Full Earth disc imaged.	The latest in the geostationary GOES constellation, this improved ABI sensor has a 0.5–1 km resolution for real-time vegetation monitoring.
FY-3F (NRSCC/CMA)	2014	China	VSWIR, 20 bands, & VTIR, 10 bands	250–1,000 m & 1.1 km, TBD	2,800 km	As an addition to the FY-3 constellation, it will host the MERSI and VIRR instruments for coarse-resolution Earth observation.
Elektro-L N3 (Roshydromet/ Roscosmos)	2014	Russia	VTIR, 10 bands	1 km visible, 4 km IR, daily	Full Earth disc imaged	Geostationary satellite; third in a series.
SAOCOM-2B (CONAE)	2015	Argentina	SAR, L-band	10–100 m, TBD	40–320 km	Fourth in a SAR constellation. Variable resolution, still under development.
ICESat-II (NASA)	2015	USA	LIDAR	70 m footprint, 183 days	Footprint centers 170 m apart	A mission follow-on. Racks are currently spaced at 15 km (equator) and 2.5 km (80 degrees lat.).

Satellite & sensor	Launch date	Source	Spectrum	Resolution, return interval	Image width	Notes
RADARSAT CONSTELLATION-2 (CSA)	2015	Canada	SAR, C-band, quad-polar	3–100 m, TBD	20–500 km	Second in a SAR constellation, this satellite has a wide range of resolution modes.
GOES-R (NOAA)	2015	USA	VTIR, 26 bands	0.5 km in the visible, 1 km NIR-SWIR, 2 km TIR	Full Earth disc imaged	The latest in the geostationary GOES constellation, this improved ABI sensor has a 0.5–1 km resolution for real-time vegetation monitoring.
Sentinel-3 B (ESA/EC)	2015	EU	VSWIR, 21 bands	300 m, TBD	750–1,675 km	This dual swath instrument will be a MODIS, AATSR, and MERIS follow-up. The second in a series.
MetOp-C (EUMETSAT)	2015	EU	VTIR, 4–6 bands	1.1 km, bi-daily	3,000km	This satellite will carry the AVHRR/3 sensor.
FY-4 O/B (NRSCC/ CMA)	2015	China	VTIR, 12 bands	1 km visible, 2 km IR, 4 km TIR, daily	Full Earth disc imaged	The second in a new geostationary series, this sensor will have higher VNIR resolution than previous geostationary imagers and thus be more suitable for real-time vegetation monitoring.
FY-4 O/C (NRSCC/ CMA)	2015	China	VTIR, 12 bands	1 km visible, 2 km IR, 4 km TIR, daily	Full Earth disc imaged	The third in a new geostationary series, this sensor will have higher VNIR resolution than previous geostationary imagers and thus be more suitable for real-time vegetation monitoring.

Satellite & sensor	Launch date	Source	Spectrum	Resolution, return interval	Image width	Notes
HypsIRI (NASA)	2015	USA	VTIR, 210 bands & 5 bands (TIR)	19 m (VSWIR), 90 m (TIR), 9–30 days	90 km (SWIR) & 400 km (TIR)	A high quality, moderate-resolution hyperspectral sensor.
DESDynI (NASA)	2015	USA	LIDAR & InSAR, L-Band, quad-polar	25 m LIDAR footprint, SAR resolution variable, 8 days	>340 km	Still under development. This combined InSAR (2 SAR sensors) and LIDAR sensor will provide an unparalleled global DEM and accurate measurement of ecosystem 3D structure.
NPOESS-2 (NOAA)	2016	USA	VTIR, 22 bands	400 m–1.6 km, TBD	3,000 km	The third in a series, this MODIS/AVHRR follow-on will provide important continuity for the AVHRR time series.
FY-3G (NRSCC/CMA)	2016	China	VSWIR, 20 bands, & VTIR, 10 bands	250–1,000 m & 1.1 km, TBD	2,800 km	As an addition to the FY-3 constellation, it will host the MERSI and VIRR instruments for coarse-resolution Earth observation.
BIOMASS (ESA)	2016?	EU	InSAR, P-band, quad-polar	50 m, 27 days (4 days exptal)	102 km	Still in concept competition and under development, this mission would be focused on mapping forest biomass. It would have InSAR capability and have an experimental, 50-day tomographic mode.

Bibliography

Achard, F., R. DeFries, H. Eva, M. Hansen, P. Mayaux, and H.J. Stibig. 2007. Pan-tropical monitoring of deforestation. *Environmental Research Letters* 2(4): 045022.

Alencar, A., D. Nepstad, and M.D.V. Diaz. 2006. Forest understory fire in the Brazilian Amazon in ENSO and non-ENSO years: Area burned and committed carbon emissions. *Earth Interactions* 10: Paper 6.

Allan, J.D. 2004. Landscapes and riverscapes: The influence of land use on stream ecosystems. *Annual Review of Ecology Evolution and Systematics* 35: 257–284.

Almeida, R., A. Rosenqvist, Y.E. Shimabukuro, and R. Silva-Gomez. 2007. Detecting deforestation with multitemporal L-band SAR imagery: A case study in western Brazilian Amazonia. *International Journal of Remote Sensing* 28(6): 1383–1390.

Andersen, H.E., S.E. Reutebuch, and R.J. McGaughey. 2006. A rigorous assessment of tree height measurements obtained using airborne lidar and conventional field methods. *Canadian Journal of Remote Sensing* 32(5): 355–366.

Anderson, J.E., L.C. Plourde, M.E. Martin, B.H. Braswell, M.L. Smith, R.O. Dubayah, M.A. Hofton, and J.B. Blair. 2008. Integrating waveform lidar with hyperspectral imagery for inventory of a northern temperate forest. *Remote Sensing of the Environment* 112(4): 1856–1870.

Anderson, J. R., E. E. Hardy, et al. 1976. A land use and land cover classification system for use with remote sensor data. Geological survey paper 964. Washington, DC: United States Geological Survey.

Andersson, K., T.P. Evans, and K.R. Richards. 2009. National forest carbon inventories: Policy needs and assessment capacity. *Climatic Change* 93(1–2): 69–101.

Arroyo-Mora, J. P., M. Kalacska, et al. 2009. Spectral unmixing of forest canopy recovery in selectively logged units in a tropical lowland forest, Costa Rica. Anais XIV Simpósio Brasileiro de Sensoriamento Remoto, April 25-30. Natal, Brasil, INPE.

Askne, J.I.H., and M. Santoro. 2009. Automatic model-based estimation of boreal forest stem volume from repeat pass C-band InSAR coherence. *IEEE Transactions on Geoscience and Remote Sensing* 47(2): 513–516.

Askne, J., M. Santoro, G. Smith, and J.E.S. Fransson. 2003. Multitemporal repeat-pass SAR interferometry of boreal forests. *IEEE Transactions on Geoscience and Remote Sensing* 41(7): 1540–1550.

Asner, G.P. 2001. Cloud cover in Landsat observations of the Brazilian Amazon. *International Journal of Remote Sensing* 22(18): 3855–3862.

Asner, G. P., T. K. Rudel, et al. (*in press.*). A Contemporary Assessment of Global Humid Tropical Forest Change. *Conservation Biology*.

Asner, G.P., E.N. Broadbent, P.J.C. Oliveira, M. Keller, D.E. Knapp, and J.N.M. Silva. 2006. Condition and fate of logged forests in the Brazilian Amazon. *Proceedings of the National Academy of Sciences of the United States of America* 103(34): 12947–12950.

Asner, G.P., R.F. Hughes, T.A. Varga, D.E. Knapp, and T. Kennedy-Bowdoin. 2009. Environmental and biotic controls over aboveground biomass throughout a tropical rain forest. *Ecosystems* 12(2): 261–278.

Asner, G.P., M.O. Jones, R.E. Martin, D.E. Knapp, and R.F. Hughes. 2008. Remote sensing of native and invasive species in Hawaiian forests. *Remote Sensing of the Environment* 112(5): 1912–1926.

Asner, G.P., D.E. Knapp, E.N. Broadbent, P.J.C. Oliveira, M. Keller, and J.N. Silva. 2005. Selective logging in the Brazilian Amazon. *Science* 310(5747): 480–482.

Asner, G.P., and R.E. Martin. 2009. Airborne spectranomics: Mapping canopy chemical and taxonomic diversity in tropical forests. *Frontiers in Ecology and the Environment* 7(5): 269–276.

Asner, G.P., D. Nepstad, G. Cardinot, and D. Ray. 2004. Drought stress and carbon uptake in an Amazon forest measured with spaceborne imaging spectroscopy. *Proceedings of the National Academy of Sciences of the United States of America* 101(16): 6039–6044.

Asner, G.P., T.K. Rudel, T.M. Aide, R. DeFries, and R. Emerson. 2009. A contemporary assessment of global humid tropical forest change. *Conservation Biology* 23(6): 1386–1395.

Baban, S.M.J., and K.W. Yusof. 2001. Mapping land use/cover distribution on a mountainous tropical island using remote sensing and GIS. *International Journal of Remote Sensing* 22(10): 1909–1918.

Baccini, A., M.A. Friedl, C.E. Woodcock, and R. Warbington. 2004. Forest biomass estimation over regional scales using multisource data. *Geophysical Research Letters* 31(10): L10501.

Baccini, A., N. Laporte, S.J. Goetz, M. Sun, and H. Dong. 2008. A first map of tropical Africa's above-ground biomass derived from satellite imagery. *Environmental Research Letters* 3: 1–9.

Baker, T.R., O.L. Phillips, Y. Malhi, S. Almeida, L. Arroyo, A. Di Fiore, T. Erwin, et al. 2004. Variation in wood density determines spatial patterns in Amazonian forest biomass. *Global Change Biology* 10(5): 545–562.

Bala, G., K. Caldeira, M. Wickett, T. Phillips, D. Lobell, C. Delire, and A. Mirin. 2007. Combined climate and carbon-cycle effects of large-scale deforestation. *Proceedings of the National Academy of Sciences of the United States of America* 104(16): 6550.

Baldocchi, D.D. 2003. Assessing the eddy covariance technique for evaluating carbon dioxide exchange rates of ecosystems: past, present and future. *Global Change Biology* 9(4): 479–492.

Balzter, H. 2001. Forest mapping and monitoring with interferometric synthetic aperture radar (InSAR). *Progress in Physical Geography* 25(2): 159–177.

Balzter, H., C.S. Rowland, and P. Saich. 2007. Forest canopy height and carbon estimation at Monks Wood National Nature Reserve, UK, using dual-wavelength SAR interferometry. *Remote Sensing of Environment* 108(3): 224–239.

Bicheron, P., P. Defourny, C. Brockmann, L. Schouten, C. Vancutsem, M. Huc, S. Bontemps, M. Leroy, F. Achard, M. Herold, F. Ranera, and O. Arino. 2008. *GLOBCOVER Products Description and Validation Report*. MEDIAS-France, ftp://uranus.esrin.esa.int/pub/globcover_v2/global/.

Blackard, J.A., M.V. Finco, E.H. Helmer, G.R. Holden, M.L. Hoppus, D.M. Jacobs, A.J. Lister, et al. 2008. Mapping US forest biomass using nationwide forest inventory data and moderate resolution information. *Remote Sensing of Environment* 112(4): 1658–1677.

Boudreau, J., R.F. Nelson, H.A. Margolis, A. Beaudoin, L. Guindon, and D.S. Kimes. 2008. Regional aboveground forest biomass using airborne and spaceborne LiDAR in Quebec. *Remote Sensing of Environment* 112(10): 3876–3890.

Bourgine, B., and N. Baghdadi. 2005. Assessment of C-band SRTM DEM in a dense equatorial forest zone. *Comptes Rendus Geoscience* 337(14): 1225–1234.

Broadbent, E.N., G.P. Asner, M. Pena-Claros, M. Palace, and M. Soriano. 2008. Spatial partitioning of biomass and diversity in a lowland Bolivian forest: Linking field and remote sensing measurements. *Forest Ecology and Management* 255(7): 2602–2616.

Brown, S., T. Pearson, D. Slaymaker, S. Ambagis, N. Moore, D. Novelo, and W. Sabido. 2005. Creating a virtual tropical forest from three-dimensional aerial imagery to estimate carbon stocks. *Ecological Applications* 15(3): 1083–1095.

Cairns, M.A., S. Brown, E.H. Helmer, and G.A. Baumgardner. 1997. Root biomass allocation in the world's upland forests. *Oecologia* 111(1): 1–11.

Canadell, J.G., C. Le Quere, M.R. Raupach, C.B. Field, E.T. Buitenhuis, P. Ciais, T.J. Conway, N.P. Gillett, R.A. Houghton, and G. Marland. 2007. Contributions to accelerating atmospheric CO_2 growth from economic activity, carbon intensity, and efficiency of natural sinks. *Proceedings of the National Academy of Sciences of the United States of America* 104(47): 18866-18870.

Castro, K.L., G.A. Sanchez-Azofeifa, and B. Rivard. 2003. Monitoring secondary tropical forests using space-borne data: Implications for Central America. *International Journal of Remote Sensing* 24(9): 1853–1894.

CEOS (Committee on Earth Observation Satellites). 2009. Committee on Earth Observation Satellites. http://www.ceos.org/ (accessed March 28, 2009).

Chambers, J.Q., G.P. Asner, D.C. Morton, L.O. Anderson, S.S. Saatch, F.D.B. Espirito-Santo, M. Palace, and C. Souza. 2007. Regional ecosystem structure and function: Ecological insights from remote sensing of tropical forests. *Trends in Ecology & Evolution* 22(8): 414–423.

Chand, T.R.K., and K.V.S. Badarinath. 2007. Analysis of ENVISAT ASAR data for forest parameter retrieval and forest type classification—A case study over deciduous forests of central India. *International Journal of Remote Sensing* 28(22): 4985–4999.

Chave, J., C. Andalo, S. Brown, M.A. Cairns, J.Q. Chambers, D. Eamus, H. Folster, et al. 2005. Tree allometry and improved estimation of carbon stocks and balance in tropical forests. *Oecologia* 145(1): 87–99.

Chazdon, R.L., C.A. Harvey, O. Komar, D.M. Griffith, B.G. Ferguson, M. Martinez-Ramos, H. Morales, et al. 2009. Beyond reserves: A research agenda for conserving biodiversity in human-modified tropical landscapes. *Biotropica* 41(2): 142–153.

Chopping, M., G.G. Moisen, L.H. Su, A. Laliberte, A. Rango, J.V. Martonchik, and D.P.C. Peters. 2008. Large area mapping of southwestern forest crown cover, canopy height, and biomass using the NASA Multiangle Imaging Spectro-Radiometer. *Remote Sensing of Environment* 112(5): 2051–2063.

Chuvieco, E. 2008. *Satellite Observation of Biomass Burning: Implications in Global Change Research*. Dordrecht: Springer Netherlands.

Clark, D.B., J.M. Read, M.L. Clark, A.M. Cruz, M.F. Dotti, and D.A. Clark. 2004a. Application of 1-M and 4-M resolution satellite data to ecological studies of tropical rain forests. *Ecological Applications* 14(1): 61–74.

Clark, M.L., D.B. Clark, and D.A. Roberts. 2004b. Small-footprint lidar estimation of sub-canopy elevation and tree height in a tropical rain forest landscape. *Remote Sensing of Environment* 91(1): 68–89.

Clark, M.L., D.A. Roberts, and D.B. Clark. 2005. Hyperspectral discrimination of tropical rain forest tree species at leaf to crown scales. *Remote Sensing of Environment* 96(3–4): 375–398.

Cohen, W.B., and S.N. Goward. 2004. Landsat's role in ecological applications of remote sensing. *Bioscience* 54(6): 535–545.

Coppin, P., I. Jonckheere, K. Nackaerts, B. Muys, and E. Lambin. 2004. Digital change detection methods in ecosystem monitoring: A review. *International Journal of Remote Sensing* 25(9): 1565–1596.

Costa, M.P.F. 2004. Use of SAR satellites for mapping zonation of vegetation communities in the Amazon floodplain. *International Journal of Remote Sensing* 25(10): 1817–1835.

Crutzen, P.J., and M.O. Andreae. 1990. Biomass burning in the tropics—impact on atmospheric chemistry and biogeochemical cycles. *Science* 250(4988): 1669–1678.

Cunningham, D., J. Melican, E. Wemmelmann, and T. Jones. 2002. GeoCover LC-A moderate resolution global land cover database. Paper presented at the ESRI International User Conference. July 2002, San Diego, CA.

Dalponte, M., L. Bruzzone, and D. Gianelle. 2008. Fusion of hyperspectral and LIDAR remote sensing data for classification of complex forest areas. IEEE *Transactions on Geoscience and Remote Sensing* 46(5): 1416–1427.

Davies, D.K., S. Ilavajhala, M.M. Wong, and C.O. Justice. 2009. Fire information for resource management system: Archiving and distributing MODIS active fire data. *IEEE Transactions on Geoscience and Remote Sensing* 47(1): 72–79.

De Grandi, G., J.P. Malingreau, and M. Leysen. 1999. The ERS-1 Central Africa mosaic: A new perspective in radar remote sensing for the global monitoring of vegetation. *IEEE Transactions on Geoscience and Remote Sensing* 37(3): 1730–1746.

Dean, T.J., Q.V. Cao, S.D. Roberts, and D.L. Evans. 2009. Measuring heights to crown base and crown median with LiDAR in a mature, even-aged loblolly pine stand. *Forest Ecology and Management* 257(1): 126–133.

DeFries, R. 2008. Terrestrial vegetation in the coupled human-earth system: Contributions of remote sensing. *Annual Review of Environment and Resources* 33: 369–390.

DeFries, R., F. Achard, S. Brown, M. Herold, D. Murdiyarso, B. Schlamadinger, and C. de Souza. 2007. Earth observations for estimating greenhouse gas emissions from deforestation in developing countries. *Environmental Science and Policy* 10(4): 385–394.

DeFries, R.S., R.A. Houghton, M.C. Hansen, C.B. Field, D. Skole, and J. Townshend. 2002. Carbon emissions from tropical deforestation and regrowth based on satellite observations for the 1980s and 1990s. *Proceedings of the National Academy of Sciences of the United States of America* 99(22): 14256–14261.

DeFries, R.S., and J.R. Townshend. 1994. NDVI-derived land cover classification at global scales. *International Journal of Remote Sensing* 15(17): 3567–3586.

Diner, D.J., B.H. Braswell, R. Davies, N. Gobron, J.N. Hu, Y.F. Jin, R.A. Kahn, et al. 2005. The value of multiangle measurements for retrieving structurally and radiatively consistent properties of clouds, aerosols, and surfaces. *Remote Sensing of Environment* 97(4): 495–518.

Dixon, R.K., S. Brown, R.A. Houghton, A.M. Solomon, M.C. Trexler, and J. Wisniewski. 1994. Carbon pools and flux of global forest ecosystems. *Science* 263: 185–190.

Dobson, M.C., F.T. Ulaby, and L.E. Pierce. 1995a. Land cover classification and estimation of terrain attributes using synthetic-aperture radar. *Remote Sensing of Environment* 51(1): 199–214.

Dobson, M.C., F.T. Ulaby, L.E. Pierce, T.L. Sharik, K.M. Bergen, J. Kellndorfer, J.R. Kendra, et al. 1995b. Estimation of forest biophysical characteristics in northern Michigan with SIR-C/X-SAR. *IEEE Transactions on Geoscience and Remote Sensing* 33(4): 877–895.

Donnellan, A., P. Rosen, J. Graf, A. Loverro, A. Freeman, R. Treuhaft, R. Oberto, et al. 2008. Deformation, ecosystem structure, and dynamics of ice (DESDynI). Paper presented at the ESRI International User Conference. April 2008, Washington, DC.

Drake, J.B., R.O. Dubayah, D.B. Clark, R.G. Knox, J.B. Blair, M.A. Hofton, R.L. Chazdon, et al. 2002. Estimation of tropical forest structural characteristics using large-footprint lidar. *Remote Sensing of Environment* 79(2–3): 305–319.

Drake, J.B., R.O. Dubayah, R.G. Knox, D.B. Clark, and J.B. Blair. 2002. Sensitivity of large-footprint lidar to canopy structure and biomass in a neotropical rainforest. *Remote Sensing of Environment* 81(2–3): 378–392.

Drake, J.B., R.G. Knox, R.O. Dubayah, D.B. Clark, R. Condit, J.B. Blair, and M. Hofton. 2003. Above-ground biomass estimation in closed canopy neotropical forests using lidar remote sensing: factors affecting the generality of relationships. *Global Ecology and Biogeography* 12(2): 147–159.

Dubayah, R., R. Knox, M. Hofton, J. Blair, and J. Drake (eds.). 2000. *Land Surface Characterization using LIDAR Remote Sensing.* London: CRC Press.

Engdahl, M.E., and J.M. Hyyppa. 2003. Land-cover classification using multitemporal ERS-1/2 InSAR data. *IEEE Transactions on Geoscience and Remote Sensing* 41(7): 1620–1628.

eoPortal. 2009. List of EO and non-EO Satellite Missions. European Space Agency. http://directory.eoportal.org/missions_all_list.php?filter=&view_all&order=start_date&dir=ASC (accessed July 23, 2009).

ERSDAC (Earth Remote Sensing Data Analysis Center). 2009. ASTER Global Digital Elevation Model. http://www.ersdac.or.jp/GDEM/E/4.html (accessed June 22, 2009).

ESA. 2009. Summaries and recommendations of the POLinSAR 2009 Workshop. January 2009, Frascati, Italy.

Fan, S., M. Gloor, J. Mahlman, S. Pacala, J. Sarmiento, T. Takahashi, and P. Tans. 1998. A large terrestrial carbon sink in North America implied by atmospheric and oceanic carbon dioxide data and models. *Science* 282(5388): 442–446.

FAO (Food and Agriculture Organization). 2006. Global forest resources assessment 2005. FAO Forestry Paper 147. Rome: Food and Agriculture Organization of the United Nations.

Field, C.B., D.B. Lobell, H.A. Peters, and N.R. Chiariello. 2007. Feedbacks of terrestrial ecosystems to climate change. *Annual Review of Environment and Resources* 32: 1–29.

Fiorella, M., and W.J. Ripple. 1993. Determining successional stage of temperate coniferous forests with LANDSAT satellite data. *Photogrammetric Engineering and Remote Sensing* 59(2): 239–246.

Foody, G.M. 2002. Status of land cover classification accuracy assessment. *Remote Sensing of Environment* 80(1): 185–201.

Foody, G.M., D.S. Boyd, and M.E.J. Cutler. 2003. Predictive relations of tropical forest biomass from Landsat TM data and their transferability between regions. *Remote Sensing of Environment* 85(4): 463–474.

Foster, J., C. Kingdon, and P. Townsend. 2002. Predicting tropical forest carbon from EO-1 hyperspectral imagery in Noel Kempff Mercado National Park, Bolivia. Paper

presented at IEEE International Geoscience and Remote Sensing Symposium. July 2008, Boston, MA.

Franco-Lopez, H., A. Ek, and M. Bauer. 2001. Estimation and mapping of forest stand density, volume, and cover type using the k-nearest neighbors method. *Remote Sensing of Environment* 77(3): 251–274.

Fransson, J.E.S., F. Walter, and L.M.H. Ulander. 2000. Estimation of forest parameters using CARABAS-II VHFSAR data. *IEEE Transactions on Geoscience and Remote Sensing* 38(2): 720–727.

Galvao, L.S., F.J. Ponzoni, V. Liesenberg, and J.R. dos Santos. 2009. Possibilities of discriminating tropical secondary succession in Amazonia using hyperspectral and multiangular CHRIS/PROBA data. *International Journal of Applied Earth Observation and Geoinformation* 11: 8–14.

Gao, X., A.R. Huete, W.G. Ni, and T. Miura. 2000. Optical-biophysical relationships of vegetation spectra without background contamination. *Remote Sensing of Environment* 74(3): 609–620.

Gardner, T. A., J. Barlow, et al. 2007. Predicting the uncertain future of tropical forest species in a data vacuum. *BIOTROPICA* 39(1): 25–30.

Gardner, T.A., J. Barlow, L.W. Parry, and C.A. Peres. 2007. Predicting the uncertain future of tropical forest species in a data vacuum. *Biotropica* 39(1): 25–30.

Gergel, S.E., Y. Stange, N.C. Coops, K. Johansen, and K.R. Kirby. 2007. What is the value of a good map? An example using high spatial resolution imagery to aid riparian restoration. *Ecosystems* 10(5): 688–702.

Gibbs, H.K., S. Brown, J.O. Niles, and J.A. Foley. 2007. Monitoring and estimating tropical forest carbon stocks: Making REDD a reality. *Environmental Research Letters* 2(4): 045023.

Giglio, L., I. Csiszar, and C.O. Justice. 2006. Global distribution and seasonality of active fires as observed with the Terra and Aqua Moderate Resolution Imaging Spectroradiometer (MODIS) sensors. *Journal of Geophysical Research-Biogeosciences* 111:G02016.

Giglio, L., G.R. van der Werf, J.T. Randerson, G.J. Collatz, and P. Kasibhatla. 2005. Global estimation of burned area using MODIS active fire observations. *Atmospheric Chemistry and Physics* 5: 11091–11141.

Giri, C., Z.L. Zhu, and B. Reed. 2005. A comparative analysis of the Global Land Cover 2000 and MODIS land cover data sets. *Remote Sensing of Environment* 94(1): 123–132.

Goetz, S.J., A. Baccini, N.T. Laporte, T. Johns, W. Walker, J. Kellndorfer, R.A. Houghton, and M. Sun. 2009. Mapping and monitoring carbon stocks with satellite observations: A comparison of methods. *Carbon Balance and Management* 4(2).

Goetz, S.J., A.G. Bunn, G.J. Fiske, and R.A. Houghton. 2005. Satellite-observed photosynthetic trends across boreal North America associated with climate and fire disturbance.

Proceedings of the National Academy of Sciences of the United States of America 102(38): 13521–13525.

Goetz, S.J., R.K. Wright, A.J. Smith, E. Zinecker, and E. Schaub. 2003. IKONOS imagery for resource management: Tree cover, impervious surfaces, and riparian buffer analyses in the mid-Atlantic region. *Remote Sensing and Environment* 88(1–2): 195–208.

GOFC-GOLD (Global Observation of Forest and Land Cover Dynamics). 2008. *Reducing Greenhouse Gas Emissions from Deforestation and Degradation in Developing Countries: A Sourcebook of Methods and Procedures for Monitoring, Measuring, and Reporting.* GOFC-GOLD Report version COP13-2. Alberta, Canada: Natural Resources Canada.

Goodenough, D.G., A. Dyk, O. Niemann, J.S. Pearlman, H. Chen, T. Han, M. Murdoch, and C. West. 2003. Processing Hyperion and ALI for forest classification. *IEEE Transactions on Geoscience and Remote Sensing* 41(6): 1321–1331.

Goodwin, N., R. Turner, and R. Merton. 2005. Classifying Eucalyptus forests with high spatial and spectral resolution imagery: An investigation of individual species and vegetation communities. *Australian Journal of Botany* 53(4): 337–345.

Grainger, A. 2008. Difficulties in tracking the long-term global trend in tropical forest area *Proceedings of the National Academy of Sciences of the United States of America* 105(2): 818–823.

Grassi, G., S. Monni, S. Federici, F. Achard, and D. Mollicone. 2008. Applying the conservativeness principle to REDD to deal with the uncertainties of the estimates. *Environmental Research Letters* 3(3): 035005.

Hall, R.J., R.S. Skakun, E.J. Arsenault, and B.S. Case. 2006. Modeling forest stand structure attributes using Landsat ETM+ data: Application to mapping of aboveground biomass and stand volume. *Forest Ecology and Management* 225(1–3): 378–390.

Hansen, M.C., R.S. DeFries, J.R.G. Townshend, M. Carroll, C. Dimiceli, and R.A. Sohlberg. 2003. Global percent tree cover at a spatial resolution of 500 meters: First results of the MODIS vegetation continuous fields algorithm. *Earth Interactions* 7(10): 1–15.

Hansen, M.C., D.P. Roy, E. Lindquist, B. Adusei, C.O. Justice, and A. Altstatt. 2008a. A method for integrating MODIS and Landsat data for systematic monitoring of forest cover and change in the Congo Basin. *Remote Sensing of Environment* 112(5): 2495–2513.

Hansen, M.C., S.V. Stehman, P.V. Potapov, T.R. Loveland, J.R.G. Townshend, R.S. DeFries, K.W. Pittman, et al. 2008b. Humid tropical forest clearing from 2000 to 2005 quantified by using multitemporal and multiresolution remotely sensed data. *Proceedings of the National Academy of Sciences of the United States of America* 105(27): 9439–9444.

Heinsch, F.A., M.S. Zhao, S.W. Running, J.S. Kimball, R.R. Nemani, K.J. Davis, P.V. Bolstad, et al. 2006. Evaluation of remote sensing based terrestrial productivity from MODIS

using regional tower eddy flux network observations. *IEEE Transactions on Geoscience and Remote Sensing* 44(7): 1908–1925.

Heiskanen, J. 2006. Tree cover and height estimation in the Fennoscandian tundra-taiga transition zone using multiangular MISR data. *Remote Sensing of Environment* 103(1): 97–114.

Helmer, E. H., M. A. Lefsky, et al. 2009. Biomass accumulation rates of Amazonian secondary forest and biomass of old-growth forests from Landsat time series and the Geoscience Laser Altimeter System. *Journal of Applied Remote Sensing* 3(1): 033505

Herold, M. 2009. *An Assessment of National Forest Monitoring Capabilities in Tropical Non-Annex I Countries: Recommendations for Capacity Building*. Report prepared for The Prince's Rainforests Project and The Government of Norway. Thuringia, Germany: Friedrich Schiller University Jena and GOFC-GOLD. http://unfccc.int/files/methods_science/redd/country_specific_information/application/pdf/redd_nat_capacity_report_herold_july09_publ.pdf.

Herold, M., and T. Johns. 2007. Linking requirements with capabilities for deforestation monitoring in the context of the UNFCCC-REDD process. *Environmental Research Letters* 2(4): 045025.

Herold, M., P. Mayaux, et al. 2008. Some challenges in global land cover mapping: An assessment of agreement and accuracy in existing 1 km datasets. *Remote Sensing of Environment* 112(5): 2538–2556.

Hoekman, D.H., and M.J. Quinones. 2000. Land cover type and biomass classification using AirSAR data for evaluation of monitoring scenarios in the Colombian Amazon. *IEEE Transactions on Geoscience and Remote Sensing* 38(2): 685–696.

Houghton, R.A. 1999. The annual net flux of carbon to the atmosphere from changes in land use 1850–1990. *Tellus Series B-Chemical and Physical Meteorology* 51(2): 298–313.

Houghton, R.A. 2005. Aboveground forest biomass and the global carbon balance. *Global Change Biology* 11(6): 945–958.

Houghton, R.A. 2007. Balancing the global carbon budget. *Annual Review of Earth and Planetary Sciences* 35: 313–347.

Houghton, R.A., D. Butman, A.G. Bunn, O.N. Krankina, P. Schlesinger, and T.A. Stone. 2007. Mapping Russian forest biomass with data from satellites and forest inventories. *Environmental Research Letters* 2(4): 045032.

Houghton, R.A., K.T. Lawrence, J.L. Hackler, and S. Brown. 2001. The spatial distribution of forest biomass in the Brazilian Amazon: A comparison of estimates. *Global Change Biology* 7(7): 731–746.

House, J.I., I.C. Prentice, N. Ramankutty, R.A. Houghton, and M. Heimann. 2003. Reconciling apparent inconsistencies in estimates of terrestrial CO_2 sources and sinks. *Tellus Series B-Chemical and Physical Meteorology* 55(2): 345–363.

Hudak, A.T., M.A. Lefsky, W.B. Cohen, and M. Berterretche. 2002. Integration of lidar and Landsat ETM plus data for estimating and mapping forest canopy height. *Remote Sensing of Environment* 82(2-3): 397–416.

Hyde, P., R. Dubayah, B. Peterson, J.B. Blair, M. Hofton, C. Hunsaker, R. Knox, and W. Walker. 2005. Mapping forest structure for wildlife habitat analysis using waveform lidar: Validation of montane ecosystems. *Remote Sensing of Environment* 96(3–4): 427–437.

Hyde, P., R. Dubayah, W. Walker, J.B. Blair, M. Hofton, and C. Hunsaker. 2006. Mapping forest structure for wildlife habitat analysis using multi-sensor (LiDAR, SAR/InSAR, ETM plus, Quickbird) synergy. *Remote Sensing of Environment* 102(1–2): 63–73.

Hyyppa, J., H. Hyyppa, M. Inkinen, M. Engdahl, S. Linko, and Y.H. Zhu. 2000. Accuracy comparison of various remote sensing data sources in the retrieval of forest stand attributes. *Forest Ecology and Management* 128(1–2): 109–120.

Hyyppa, J., H. Hyyppa, D. Leckie, F. Gougeon, X. Yu, and M. Maltamo. 2008. Review of methods of small-footprint airborne laser scanning for extracting forest inventory data in boreal forests. *International Journal of Remote Sensing* 29(5): 1339–1366.

IIASA (International Institute for Applied Systems Analysis). 2009. GeoWiki Project: Help Improve Global Land Cover. International Institute for Applied Systems Analysis. http://geo-wiki.org/ (accessed July 23, 2009).

IPCC (Intergovernmental Panel on Climate Change). 2006. *IPCC Guidelines for National Greenhouse Gas Inventories*, ed. by Intergovernmental Panel on Climate Change, Japan, Hayama. http://www.ipcc-nggip.iges.or.jp/public/2006gl/index.html.

——— 2007. *Climate Change 2007: The Physical Basis. Working Group I Contribution to the Fourth Assessment Report of the Intergovernmental Panel on Climate Change*. New York, NY: Cambridge University Press.

Jensen, J.R. 2007. *Remote Sensing of the Environment: An Earth Resource Perspective*, 2nd Edition. Upper Saddle River, NJ: Prentice Hall.

Kasischke, E. S. and N. H. F. French. 1997. Constraints on using AVHRR composite index imagery to study patterns of vegetation cover in boreal forests. *International Journal of Remote Sensing* 18(11): 2403–2426.

Kasischke, E.S., J.M. Melack, and M.C. Dobson. 1997. The use of imaging radars for ecological applications—A review. *Remote Sensing of Environment* 59(2): 141–156.

Kauppi, P.E., J.H. Ausubel, J.Y. Fang, A.S. Mather, R.A. Sedjo, and P.E. Waggoner. 2006. Returning forests analyzed with the forest identity. *Proceedings of the National Academy of Sciences of the United States* 103(46): 17574–17579.

Kayitakire, F., C. Hamel, and P. Defourny. 2006. Retrieving forest structure variables based on image texture analysis and IKONOS-2 imagery. *Remote Sensing of Environment* 102(3–4): 390–401.

Keeling, H.C., and O.L. Phillips. 2007. The global relationship between forest productivity and biomass. *Global Ecology and Biogeography* 16(5): 618–631.

Kellndorfer, J.M., L.E. Pierce, M.C. Dobson, and F.T. Ulaby. 1998. Toward consistent regional-to-global-scale vegetation characterization using orbital SAR systems. *IEEE Transactions on Geoscience and Remote Sensing* 36(5): 1396–1411.

Kellndorfer, J., W. Walker, D. Nepstad, C. Stickler, P. Brando, P. Lefebvre, A. Rosenqvist, and M. Shimada. 2008. Implementing REDD: The potential of ALOS/PALSAR for forest mapping and monitoring. Paper presented at the Second GEOSS Asia-Pacific Symposium. April 2008, Tokyo, Japan.

Kellndorfer, J., W. Walker, L. Pierce, C. Dobson, J.A. Fites, C. Hunsaker, J. Vona, and M. Clutter. 2004. Vegetation height estimation from shuttle radar topography mission and national elevation datasets. Remote Sensing of *Environment* 93(3): 339–358.

Kennedy, R.E., W.B. Cohen, and T.A. Schroeder. 2007. Trajectory-based change detection for automated characterization of forest disturbance dynamics. *Remote Sensing of Environment* 110(3): 370–386.

Kimes, D.S., R.F. Nelson, W.A. Salas, and D.L. Skole. 1999. Mapping secondary tropical forest and forest age from SPOT HRV data. *International Journal of Remote Sensing* 20(18): 3625–3640.

Kimes, D.S., K.J. Ranson, G. Sun, and J.B. Blair. 2006. Predicting lidar measured forest vertical structure from multi-angle spectral data. *Remote Sensing of Environment* 100(4): 503–511.

Knorn, J., A. Rabe, V.C. Radeloff, T. Kuemmerle, J. Kozak, and P. Hostert. 2009. Land cover mapping of large areas using chain classification of neighboring Landsat satellite images. *Remote Sensing of Environment* 113(5): 957–964.

Kozak, J., C. Estreguil, and K. Ostapowicz. 2008. European forest cover mapping with high resolution satellite data: The Carpathians case study. *International Journal of Applied Earth Observation and Geoinformation* 10(1): 44–55.

Kramer, H.J., and A.P. Cracknell. 2008. An overview of small satellites in remote sensing. *International Journal of Remote Sensing* 29(15): 4285–4337.

Kuplich, T.M. 2006. Classifying regenerating forest stages in Amazonia using remotely sensed images and a neural network. *Forest Ecology and Management* 234(1–3): 1–9.

Kuplich, T.M., C.C. Freitas, and J.V. Soares. 2000. The study of ERS-1 SAR and Landsat TM synergism for land use classification. *International Journal of Remote Sensing* 21(10): 2101–2111.

Latifovic, R., and I. Olthof. 2004. Accuracy assessment using sub-pixel fractional error matrices of global land cover products derived from satellite data. *Remote Sensing of Environment* 90(2): 153–165.

Laurance, W.F. 2007. Environmental science: Forests and floods. *Nature* 449(7161): 409–410.

Le Toan, T., H. Baltzer, P. Paillou, K.P. Papathanassiou, S. Plummer, S. Quegan, F. Rocca, and L. Ulander. 2008. *BIOMASS: To Observe Global Forest Biomass for a Better Understanding of the Carbon Cycle. Report for Asssessment 2*. Noordwijk, The Netherlands: European Space Agency. http://esamultimedia.esa.int/docs/SP1313-2_BIOMASS.pdf.

Le Toan, T., S. Quegan, I. Woodward, M. Lomas, N. Delbart, and G. Picard. 2004. Relating radar remote sensing of biomass to modelling of forest carbon budgets. *Climatic Change* 67(2–3): 379–402.

Lee, K.S., W.B. Cohen, R.E. Kennedy, T.K. Maiersperger, and S.T. Gower. 2004. Hyperspectral versus multispectral data for estimating leaf area index in four different biomes. *Remote Sensing of Environment* 91(3–4): 508–520.

Lefsky, M.A., W.B. Cohen, D.J. Harding, G.G. Parker, S.A. Acker, and S.T. Gower. 2002a. Lidar remote sensing of above-ground biomass in three biomes. *Global Ecology and Biogeography* 11(5): 393–399.

Lefsky, M.A., W.B. Cohen, G.G. Parker, and D.J. Harding. 2002b. Lidar remote sensing for ecosystem studies. *Bioscience* 52(1): 19–30.

Lefsky, M.A., M. Keller, Y. Pang, P.B. de Camargo, and M.O. Hunter. 2007. Revised method for forest canopy height estimation from Geoscience Laser Altimeter System waveforms. *Journal of Applied Remote Sensing* 1: 013537.

Lindquist, E.J., M.C. Hansen, D.P. Roy, and C.O. Justice. 2008. The suitability of decadal image data sets for mapping tropical forest cover change in the Democratic Republic of Congo: Implications for the global land survey. *International Journal of Remote Sensing* 29(24): 7269–7275.

Liu, J., J.M. Chen, J. Cihlar, and W. Chen. 2002. Net primary productivity mapped for Canada at 1-km resolution. *Global Ecology and Biogeography* 11(2): 115–129.

Liu, X., and M. Kafatos. 2007. MISR multi-angular spectral remote sensing for temperate forest mapping at 1.1-km resolution. *International Journal of Remote Sensing* 28(1–2): 459–464.

Loarie, S.R., L.N. Joppa, and S.L. Pimm. 2007. Satellites miss environmental priorities. *Trends in Ecology and Evolution* 22(12): 630–632.

Loehle, C. 2000. Forest ecotone response to climate change: Sensitivity to temperature response functional forms. *Canadian Journal of Forest Research-Revue Canadienne De Recherche Forestiere* 30(10): 1632–1645.

Loveland, T.R., M.A. Cochrane, and G.M. Henebry. 2008. Landsat still contributing to environmental research—Response. *Trends in Ecology and Evolution* 23(4): 182–183.

Loveland, T.R., T.L. Sohl, S.V. Stehman, A.L. Gallant, K.L. Sayler, and D.E. Napton. 2002. A strategy for estimating the rates of recent United States land-cover changes. *Photogrammetric Engineering and Remote Sensing* 68(10): 1091–1099.

Loveland, T.R., Z.L. Zhu, D.O. Ohlen, J.F. Brown, B.C. Reed, and L.M. Yang. 1999. An analysis of the IGBP global land-cover characterization process. *Photogrammetric Engineering and Remote Sensing* 65(9): 1021–1032.

Lu, D., P. Mausel, E. Brondizio, and E. Moran. 2004. Change detection techniques. *International Journal of Remote* Sensing 25(12): 2365–2407.

Lu, D.S. 2006. The potential and challenge of remote sensing-based biomass estimation. *International Journal of Remote Sensing* 27(7): 1,297–1,328.

Luus, K.A., and R.E.J. Kelly. 2008. Assessing productivity of vegetation in the Amazon using remote sensing and modeling. *Progress in Physical Geography* 32(4): 363–377.

MacDonald, G.M., K.V. Kremenetski, and D.W. Beilman. 2008. Climate change and the northern Russian treeline zone. *Philosophical Transactions of the Royal Society B-Biological Sciences* 363(1501): 2285–2299.

Malhi, Y., L. Aragão, D. Galbraith, C. Huntingford, R. Fisher, P. Zelazowski, S. Sitch, et al. 2009. Exploring the likelihood and mechanism of a climate-change-induced dieback of the Amazon rainforest. *Proceedings of the National Academy of Sciences of the United States of America*. Early Edition. February 13, 2009 [doi: 10.1073/pnas.0804619106], http://www.pnas.org/content/early/2009/02/12/0804619106.full.pdf+html.

Malhi, Y., D.D. Baldocchi, and P.G. Jarvis. 1999. The carbon balance of tropical, temperate and boreal forests. *Plant Cell and Environment* 22(6): 715–740.

Mallinis, G., N. Koutsias, M. Tsakiri-Strati, and M. Karteris. 2008. Object-based classification using Quickbird imagery for delineating forest vegetation polygons in a Mediterranean test site. *ISPRS Journal of Photogrammetry and Remote Sensing* 63(2): 237–250.

Maltamo, M., K. Eerikainen, P. Packalen, and J. Hyyppa. 2006. Estimation of stem volume using laser scanning-based canopy height metrics. *Forestry* 79(2): 217–229.

Marsh, G.P. 1878. *The Earth as Modified by Human Action: A New Edition of Man and Nature.* Project Gutenberg Release #6019. July 2004.

Masek, J.G., C.Q. Huang, R. Wolfe, W. Cohen, F. Hall, J. Kutler, and P. Nelson. 2008. North American forest disturbance mapped from a decadal Landsat record. *Remote Sensing of Environment* 112(6): 2914–2926.

Mayaux, P., H. Eva, J. Gallego, A.H. Strahler, M. Herold, S. Agrawal, S. Naumov, et al. 2006. Validation of the global land cover 2000 map. *IEEE Transactions on Geoscience and Remote Sensing* 44(7): 1728–1739.

Mayaux, P., G. De Grandi, and J.P. Malingreau. 2000. Central African forest cover revisited: A multisatellite analysis. *Remote Sensing of Environment* 71(2): 183–196.

Mayaux, P., P. Holmgren, F. Achard, H. Eva, H. Stibig and A. Branthomme. 2005. Tropical forest cover change in the 1990s and options for future monitoring. *Philosophical Transactions of the Royal Society B-Biological Sciences* 360(1454): 373–384.

McCombs, J.W., S.D. Roberts, and D.L. Evans. 2003. Influence of fusing lidar and multispectral imagery on remotely sensed estimates of stand density and mean tree height in a managed loblolly pine plantation. *Forest Science* 49(3): 457–466.

McRoberts, R.E. 2008. Using satellite imagery and the k-nearest neighbors technique as a bridge between strategic and management forest inventories. *Remote Sensing of Environment* 112(5): 2212–2221.

Means, J.E., S.A. Acker, D.J. Harding, J.B. Blair, M.A. Lefsky, W.B. Cohen, M.E. Harmon, and W.A. McKee. 1999. Use of large-footprint scanning airborne lidar to estimate forest stand characteristics in the Western Cascades of Oregon. *Remote Sensing of Environment* 67(3): 298–308.

Moghaddam, M., J.L. Dungan, and S. Acker. 2002. Forest variable estimation from fusion of SAR and multispectral optical data. *IEEE Transactions on Geoscience and Remote Sensing* 40(10): 2176–2187.

Morales, R.M., T. Miura, and T. Idol. 2008. An assessment of Hawaiian dry forest condition with fine resolution remote sensing. *Forest Ecology and Management* 255(7): 2524–2532.

Morton, D.C., R.S. DeFries, Y.E. Shimabukuro, L.O. Anderson, F.D.B. Espirito-Santo, M. Hansen, and M. Carroll. 2005. Rapid assessment of annual deforestation in the Brazilian Amazon using MODIS data. *Earth Interactions* 9(8): 1–22.

Muukkonen, P., and J. Heiskanen. 2007. Biomass estimation over a large area based on standwise forest inventory data and ASTER and MODIS satellite data: A possibility to verify carbon inventories. *Remote Sensing of Environment* 107(4): 617–624.

Myneni, R.B., W.Z. Yang, R.R. Nemani, A.R. Huete, R.E. Dickinson, Y. Knyazikhin, K. Didan, et al. 2007. Large seasonal swings in leaf area of Amazon rainforests. *Proceedings of the National Academy of Sciences of the United States of America* 104(12): 4820–4823.

Naesset, E., and T. Gobakken. 2008. Estimation of above- and below-ground biomass across regions of the boreal forest zone using airborne laser. *Remote Sensing of Environment* 112(6): 3079–3090.

Naesset, E., T. Gobakken, J. Holmgren, H. Hyyppa, J. Hyyppa, M. Maltamo, M. Nilsson, et al. 2004. Laser scanning of forest resources: The Nordic experience. *Scandinavian Journal of Forest Research* 19(6): 482–499.

NASA (National Aeronautics and Space Administration). 2009a. IceSat Homepage. http://icesat.gsfc.nasa.gov/index.php (accessed July 21, 2009).

———. 2009b. The Earth Sensing Legacy. Earth Observatory. http://earthobservatory.nasa.gov/Features/EO1/eo1_2.php.

Natural Resources Canada. 2005. Horizontal transmit—Vertical receive polarization. Glossary of remote sensing terms. Canada Centre for Remote Sensing. http://www.cct.nrcan.gc.ca/glossary/index_e.php?id=1560.

Neeff, T., L.V. Dutra, J.R. dos Santos, C.D. Freitas, and L.S. Araujo. 2005. Tropical forest measurement by interferometric height modeling and P-band radar backscatter. *Forest Science* 51(6): 585–594.

Neigh, C.S.R., C.J. Tucker, and J.R.G. Townshend. 2008. North American vegetation dynamics observed with multi-resolution satellite data. *Remote Sensing of Environment* 112(4): 1749–1772.

Nelson, R., K.J. Ranson, G. Sun, D.S. Kimes, V. Kharuk, and P. Montesano. 2009. Estimating Siberian timber volume using MODIS and ICESat/GLAS. *Remote Sensing of Environment* 113(3): 691–701.

Nelson, R.F., P. Hyde, P. Johnson, B. Emessiene, M.L. Imhoff, R. Campbell, and W. Edwards. 2007. Investigating RaDAR-LiDAR synergy in a North Carolina pine forest. *Remote Sensing of Environment* 110(1): 98–108.

Nelson, R.F., D.S. Kimes, W.A. Salas, and M. Routhier. 2000. Secondary forest age and tropical forest biomass estimation using thematic mapper imagery. *Bioscience* 50(5): 419–431.

Nilsson, M. 1996. Estimation of tree weights and stand volume using an airborne lidar system. *Remote Sensing of Environment* 56(1): 1–7.

NRC (National Research Council). 2007. *Earth Science and Applications from Space: National Imperatives for the Next Decade and Beyond*. Washington, DC: National Research Council, The National Academies Press.

Oberto, B., A. Loverro, S. Hu, and B. Blair. 2008. Mission and Spacecraft Configuration Studies (Priority Tasks 1, 2, & 4). DESDynI Science Study Group Meeting. June 2008, Greenbelt, MD.

Olander, L.P., H.K. Gibbs, M. Steininger, J.J. Swenson, and B.C. Murray. 2008. Reference scenarios for deforestation and forest degradation in support of REDD: A review of data and methods. *Environmental Research Letters* 3(2): 025011.

Ollinger, S.V., and M.L. Smith. 2005. Net primary production and canopy nitrogen in a temperate forest landscape: An analysis using imaging spectroscopy, modeling and field data. *Ecosystems* 8(7): 760–778.

Ouma, Y.O., J. Tetuko, and R. Tateishi. 2008. Analysis of co-occurrence and discrete wavelet transform textures for differentiation of forest and non-forest vegetation in very-high-resolution optical-sensor imagery. *International Journal of Remote Sensing* 29(12): 3417–3456.

Page, S.E., F. Siegert, J.O. Rieley, H.D.V. Boehm, A. Jaya, and S. Limin. 2002. The amount of carbon released from peat and forest fires in Indonesia during 1997. *Nature* 420(6911): 61–65.

Palace, M., M. Keller, G.P. Asner, S. Hagen, and B. Braswell. 2008. Amazon forest structure from IKONOS satellite data and the automated characterization of forest canopy properties. *Biotropica* 40(2): 141–150.

Palmer, P.I. 2008. Quantifying sources and sinks of trace gases using space-borne measurements: Current and future science. *Philosophical Transactions of the Royal Society A-Mathematical Physical and Engineering Sciences* 366(1885): 4509–4528.

Park, N.W., and K.H. Chi. 2008. Integration of multitemporal/polarization C-band SAR data sets for land-cover classification. *International Journal of Remote Sensing* 29(16): 4667–4688.

Patenaude, G., R. Milne, and T.P. Dawson. 2005. Synthesis of remote sensing approaches for forest carbon estimation: Reporting to the Kyoto Protocol. *Environmental Science and Policy* 8(2): 161–178.

[[Add Peres et al. 2006, cited on page 71.]]

Peterson, L.K., K.M. Bergen, D.G. Brown, L. Vashchuk, and Y. Blam. 2009. Forested land-cover patterns and trends over changing forest management eras in the Siberian Baikal region. *Forest Ecology and Management* 257(3): 911–922.

Pflugmacher, D., W. Cohen, R. Kennedy, and M. Lefsky. 2008. Regional applicability of forest height and aboveground biomass models for the geoscience laser altimeter system. *Forest Science* 54(6): 647–657.

Phillips, O.L., L. Aragao, S.L. Lewis, J.B. Fisher, J. Lloyd, G. Lopez-Gonzalez, Y. Malhi, et al. 2009. Drought sensitivity of the Amazon rainforest. *Science* 323(5919): 1344–1347.

Piao, S.L., J.Y. Fang, P. Ciais, P. Peylin, Y. Huang, S. Sitch, and T. Wang. 2009. The carbon balance of terrestrial ecosystems in China. *Nature* 458(7241): 1009–1082.

Podest, E., and S. Saatchi. 2002. Application of multiscale texture in classifying JERS-1 radar data over tropical vegetation. *International Journal of Remote Sensing* 23(7): 1487–1506.

Popescu, S.C., R.H. Wynne, and R.F. Nelson. 2003. Measuring individual tree crown diameter with lidar and assessing its influence on estimating forest volume and biomass. *Canadian Journal of Remote Sensing* 29(5): 564–577.

Popescu, S.C., R.H. Wynne, and J.A. Scrivani. 2004. Fusion of small-footprint lidar and multispectral data to estimate plot-level volume and biomass in deciduous and pine forests in Virginia, USA. *Forest Science* 50(4): 551–565.

Potere, D. 2008. Horizontal positional accuracy of Google Earth's high-resolution imagery archive. *Sensors* 8(12): 7973–7981.

Powell, S.L., D. Pflugmacher, A.A. Kirschbaum, Y. Kim, and W.B. Cohen. 2007. Moderate resolution remote sensing alternatives: A review of Landsat-like sensors and their applications. *Journal of Applied Remote Sensing* 1: 012506.

Qian, D., N.H. Younan, R. King, and V.P. Shah. 2007. On the performance evaluation of pan-sharpening techniques. *IEEE Geoscience and Remote Sensing Letters* 4(4): 518–522.

Ramankutty, N., H.K. Gibbs, F. Achard, R. DeFries, J.A. Foley, and R.A. Houghton. 2007. Challenges to estimating carbon emissions from tropical deforestation. *Global Change Biology* 13(1): 51–66.

Ramos Da Silva, R., D. Silva, and R. Avissar. 2008. Regional impacts of future land-cover changes on the Amazon basin wet-season climate. *Journal of Climate* 21: 1153–1170.

RapidEye, A. 2009. RapidEye: Geofacts Turned Into Knowledge. http://www.rapideye.de/ (accessed July 23, 2009).

Read, J.M., D.B. Clark, E.M. Venticinque, and M.P. Moreira. 2003. Application of merged 1-m and 4-m resolution satellite data to research and management in tropical forests. *Journal of Applied Ecology* 40(3): 592–600.

Roberts, G., M.J. Wooster, G.L.W. Perry, N. Drake, L.M. Rebelo, and F. Dipotso. 2005. Retrieval of biomass combustion rates and totals from fire radiative power observations: Application to southern Africa using geostationary SEVIRI imagery. *Journal of Geophysical Research-Atmospheres* 110: D21111.

Rogan, J., J. Franklin, D. Stow, J. Miller, C. Woodcock, and D. Roberts. 2008. Mapping land-cover modifications over large areas: A comparison of machine learning algorithms. *Remote Sensing of Environment* 112(5): 2272–2283.

Rosenqvist, A., A. Milne, R. Lucas, M. Imhoff, and C. Dobson. 2003. A review of remote sensing technology in support of the Kyoto Protocol. *Environmental Science and Policy* 6(5): 441–455.

Rosenqvist, A., M. Shimada, B. Chapman, A. Freeman, G. De Grandi, S. Saatchi, and Y. Rauste. 2000. The Global Rain Forest Mapping project—A review. *International Journal of Remote Sensing* 21(6–7): 1375–1387.

Roy, D.P., Y. Jin, P.E. Lewis, and C.O. Justice. 2005. Prototyping a global algorithm for systematic fire-affected area mapping using MODIS time series data. *Remote Sensing of Environment* 97(2): 137–162.

Roy, D.P., J. Ju, P. Lewis, C. Schaaf, F. Gao, M. Hansen, and E. Lindquist. 2008. Multi-temporal MODIS-Landsat data fusion for relative radiometric normalization, gap filling, and prediction of Landsat data. *Remote Sensing of Environment* 112(6): 3112–3130.

Rudel, T.K., O.T. Coomes, E. Moran, F. Achard, A. Angelsen, J.C. Xu, and E. Lambin. 2005. Forest transitions: Towards a global understanding of land use change. *Global Environmental Change-Human and Policy Dimensions* 15(1): 23–31.

Saatchi, S.S., R.A. Houghton, R. Alvala, J.V. Soares, and Y. Yu. 2007. Distribution of aboveground live biomass in the Amazon basin. *Global Change Biology* 13(4): 816–837.

Saatchi, S.S., M. Marlier, R.L. Chazdon, D.B. Clark, and A.E. Russell, in review. Impact of Spatial Variability of forest structure on Radar Estimation of Aboveground Biomass inTropical Forests. *Remote Sensing of Environment*.

Saatchi, S.S., B. Nelson, E. Podest, and J. Holt. 2000. Mapping land cover types in the Amazon Basin using 1 km JERS-1 mosaic. *International Journal of Remote Sensing* 21(6–7): 1201–1234.

Saatchi, S.S., J.V. Soares, and D.S. Alves. 1997. Mapping deforestation and land use in Amazon rainforest by using SIR-C imagery. *Remote Sensing of Environment* 59(2): 191–202.

Sader, S.A., M. Bertrand, and E.H. Wilson. 2003. Satellite change detection of forest harvest patterns on an industrial forest landscape. *Forest Science* 49(3): 341–353.

Salajanu, D., and C.E. Olson. 2001. The significance of spatial resolution—Identifying forest cover from satellite data. *Journal of Forestry* 99(6): 32–38.

Salati, E., and P.B. Vose. 1984. Amazon basin: A system in equilibrium. *Science* 225(4658): 129.

Sanchez-Azofeifa, G.A., K.L. Castro-Esau, W.A. Kurz, and A. Joyce. 2009. Monitoring carbon stocks in the tropics and the remote sensing operational limitations: From local to regional projects. *Ecological Applications* 19(2): 480–494.

Sanderson, E.W., M. Jaiteh, M.A. Levy, K.H. Redford, A.V. Wannebo, and G. Woolmer. 2002. The human footprint and the last of the wild. *Bioscience* 52(10): 891–904.

Santos, C., and J.P. Messina. 2008. Multi-sensor data fusion for modeling African palm in the Ecuadorian Amazon. *Photogrammetric Engineering and Remote Sensing* 74(6): 711–723.

Schlerf, M., C. Atzberger, and J. Hill. 2005. Remote sensing of forest biophysical variables using HyMap imaging spectrometer data. *Remote Sensing of Environment* 95(2): 177–194.

Schroeder, P., S. Brown, J.M. Mo, R. Birdsey, and C. Cieszewski. 1997. Biomass estimation for temperate broadleaf forests of the United States using inventory data. *Forest Science* 43(3): 424–434.

Schroeder, T.A., W.B. Cohen, C.H. Song, M.J. Canty, and Z.Q. Yang. 2006. Radiometric correction of multi-temporal Landsat data for characterization of early successional forest patterns in western Oregon. *Remote Sensing of Environment* 103(1): 16–26.

Schroeder, W., I. Csiszar, and J. Morisette. 2008. Quantifying the impact of cloud obscuration on remote sensing of active fires in the Brazilian Amazon. *Remote Sensing of Environment* 112(2): 456–470.

Schroeder, W., E. Prins, L. Giglio, I. Csiszar, C. Schmidt, J. Morisette and D. Morton. 2008. Validation of GOES and MODIS active fire detection products using ASTER and ETM plus data. *Remote Sensing of Environment* 112(5): 2711–2726.

Schull, M.A., S. Ganguly, A. Samanta, D. Huang, N.V. Shabanov, J.P. Jenkins, J.C. Chiu, et al. 2007. Physical interpretation of the correlation between multi-angle spectral data and canopy height. *Geophysical Research Letters* 34: L18405.

Sedano, F., D. Gomez, P. Gong, and G.S. Biging. 2008. Tree density estimation in a tropical woodland ecosystem with multiangular MISR and MODIS data. *Remote Sensing of Environment* 112(5): 2523–2537.

Sesnie, S.E., P.E. Gessler, B. Finegan, and S. Thessler. 2008. Integrating Landsat TM and SRTM-DEM derived variables with decision trees for habitat classification and change detection in complex neotropical environments. *Remote Sensing of Environment* 112(5): 2145–2159.

Sexton, J.O., T. Bax, P. Siqueira, J.J. Swenson, and S. Hensley. 2009. A comparison of lidar, radar, and field measurements of canopy height in pine and hardwood forests of southeastern North America. *Forest Ecology and Management* 257(3): 1136–1147.

Siegert, F., and G. Ruecker. 2000. Use of multitemporal ERS-2 SAR images for identification of burned scars in south-east Asian tropical rainforest. *International Journal of Remote Sensing* 21(4): 831–837.

Short, N.M. 2009. The Remote Sensing Tutorial. http://rst.gsfc.nasa.gov. Accessed August 2009.

Slatton, K.C., M.M. Crawford, and B.L. Evans. 2001. Fusing interferometric radar and laser altimeter data to estimate surface topography and vegetation heights. *IEEE Transactions on Geoscience and Remote Sensing* 39(11): 2470–2482.

Smith, M.L., S.V. Ollinger, M.E. Martin, J.D. Aber, R.A. Hallett, and C.L. Goodale. 2002. Direct estimation of aboveground forest productivity through hyperspectral remote sensing of canopy nitrogen. *Ecological Applications* 12(5): 1286–1302.

Song, C. 2007. Estimating tree crown size with spatial information of high resolution optical remotely sensed imagery. *International Journal of Remote Sensing* 28(15): 3305–3322.

Song, C., T.A. Schroeder, and W.B. Cohen. 2007. Predicting temperate conifer forest successional stage distributions with multitemporal Landsat Thematic Mapper imagery. *Remote Sensing of Environment* 106(2): 228–237.

Soudani, K., G. le Maire, E. Dufrene, C. Francois, N. Delpierre, E. Ulrich, and S. Cecchini. 2008. Evaluation of the onset of green-up in temperate deciduous broadleaf forests derived from Moderate Resolution Imaging Spectroradiometer (MODIS) data. *Remote Sensing of Environment* 112(5): 2643–2655.

Souza, C.M., and D. Roberts. 2005a. Mapping forest degradation in the Amazon region with Ikonos images. *International Journal of Remote Sensing* 26(3): 425–429.

Souza, C.M., D.A. Roberts, and M.A. Cochrane. 2005b. Combining spectral and spatial information to map canopy damage from selective logging and forest fires. *Remote Sensing of Environment* 98(2–3): 329–343.

Steininger, M.K. 1996. Tropical secondary forest regrowth in the Amazon: Age, area and change estimation with Thematic Mapper data. *International Journal of Remote Sensing* 17(1): 9–27.

Steininger, M.K. 2000. Satellite estimation of tropical secondary forest above-ground biomass: Data from Brazil and Bolivia. *International Journal of Remote Sensing* 21(6–7): 1139–1157.

St-Onge, B., Y. Hu, and C. Vega. 2008. Mapping the height and above-ground biomass of a mixed forest using lidar and stereo Ikonos images. *International Journal of Remote Sensing* 29(5): 1277–1294.

Sun, G., K. Ranson, J. Masek, A. Fu, and D. Wang. 2007. Predicting tree height and biomass from GLAS data. Paper presented at the 10th International Symposium on Physical Measurements and Signatures in Remote Sensing. March 2007, Davos, Switzerland.

Swanson, A., L. Abelson, T. Manning, and L. Newhart. 2009. *Remote Sensing Assessment of Forest Carbon Content*. Washington, DC: Northrop Grumman Aerospace Systems, Northrop Grummond Corporation.

Ter-Mikaelian, M.T., and M.D. Korzukhin. 1997. Biomass equations for sixty-five North American tree species. *Forest Ecology and Management* 97(1): 1–24.

Thenkabail, P.S., E.A. Enclona, M.S. Ashton, C. Legg, and M.J. De Dieu. 2004. Hyperion, IKONOS, ALI, and ETM plus sensors in the study of African rainforests. *Remote Sensing of Environment* 90(1): 23–43.

Thiel, C., P. Drezet, C. Weise, S. Quegan, and C. Schmullius. 2006. Radar remote sensing for the delineation of forest cover maps and the detection of deforestation. *Forestry* 79(5): 589–597.

Thompson, S.D., S.E. Gergel, and N.C. Coops. 2008. Classification of late seral coastal temperate rainforests with high spatial resolution QuickBird imagery. *Canadian Journal of Remote Sensing* 34: S460–S470.

Tian, H., J.M. Melillo, D.W. Kicklighter, A.D. McGuire, J.V.K. Helfrich, B. Moore, and C.J. Vorosmarty. 1998. Effect of interannual climate variability on carbon storage in Amazonian ecosystems. *Nature* 396(6712): 664–667.

Ticehurst, C., A. Held, and S. Phinn. 2004. Integrating JERS-1 imaging radar and elevation models for mapping tropical vegetation communities in Far North Queensland, Australia. *Photogrammetric Engineering and Remote Sensing* 70(11): 1259–1266.

Townsend, P.A., T.R. Lookingbill, C.C. Kingdon, and R.H. Gardner. 2009. Spatial pattern analysis for monitoring protected areas. *Remote Sensing of Environment* 113(7): 1410–1420.

Townshend, J. R. G. and C. O. Justice. 2002. Towards operational monitoring of terrestrial systems by moderate-resolution remote sensing. *Remote Sensing of Environment* 83(1–2): 351–359.

Townshend, J.R., C.O. Justice, and V.T. Kalb. 1987. Characterization and classification of South American land cover types using satellite data. *International Journal of Remote Sensing* 8: 1189–1207.

Treuhaft, R.N., G.P. Asner, and B.E. Law. 2003. Structure-based forest biomass from fusion of radar and hyperspectral observations. *Geophysical Research Letters* 30(9): 1472–1476.

Treuhaft, R.N., and P.R. Siqueira. 2000. Vertical structure of vegetated land surfaces from interferometric and polarimetric radar. *Radio Science* 35(1): 141–177.

Tucker, C.J., J.R. Townshend, and T.E. Goff. 1985. African land-cover classification using satellite data. *Science* 227: 369–375.

Tucker, C.J., and J.R.G. Townshend. 2000. Strategies for monitoring tropical deforestation using satellite data. *International Journal of Remote Sensing* 21(6–7): 1,461–1,471.

UCS (Union of Concerned Scientists). 2009. UCS Satellite Database. http://www.ucusa.org/nuclear_weapons_and_global_security/space_weapons/technical_issues/ucs-satellite-database.html (accessed July 23, 2009).

Uhl, C., R. Buschbacher, and E.A.S. Serrao. 1988. Abandoned pastures in eastern Amazonia. I. Patterns of plant succession. *Journal of Ecology* 76(3): 663–681.

UNFCCC (United Nations Framework Convention on Climate Change). 2001. *COP-7: The Marrakech Accords*. Bonn, Germany.

UNOOSA (United Nations Office for Outer Space Affairs). 2009. General Assembly Resolution 41/65: Principles Relating to Remote Sensing of the Earth from Outer Space. http://www.oosa.unvienna.org/oosa/en/SpaceLaw/gares/html/gares_41_0065.html (accessed July 23, 2009).

Uriarte, M., L.W. Rivera, J.K. Zimmerman, T.M. Aide, A.G. Power, and A.S. Flecker. 2004. Effects of land use history on hurricane damage and recovery in a neotropical forest. *Plant Ecology* 174(1): 49–58.

Ustin, S.L., D.A. Roberts, J.A. Gamon, G.P. Asner, and R.O. Green. 2004. Using imaging spectroscopy to study ecosystem processes and properties. *Bioscience* 54(6): 523–534.

Ustin, S.L., and Q.F. Xiao. 2001. Mapping successional boreal forests in interior central Alaska. *International Journal of Remote Sensing* 22(9): 1779–1797.

van Aardt, J.A.N., R.H. Wynne, and J.A. Scrivani. 2008. Lidar-based mapping of forest volume and biomass by taxonomic group using structurally homogenous segments. *Photogrammetric Engineering and Remote Sensing* 74(8): 1033–1044.

van der Sanden, J.J., and D.H. Hoekman. 1999. Potential of airborne radar to support the assessment of land cover in a tropical rain forest environment. *Remote Sensing of Environment* 68(1): 26–40.

van der Werf, G.R., J.T. Randerson, L. Giglio, G.J. Collatz, P.S. Kasibhatla, and A.F. Arellano. 2006. Interannual variability in global biomass burning emissions from 1997 to 2004. *Atmospheric Chemistry and Physics* 6: 3423–3441.

Waggoner, P.E. (ed.). 2009. Forest inventories: Discrepancies and uncertainties. Discussion paper 09-29. Washington, DC: Resources for the Future.

Walker, W.S., J.M. Kellndorfer, E. LaPoint, M. Hoppus, and J. Westfall. 2007. An empirical InSAR-optical fusion approach to mapping vegetation canopy height. *Remote Sensing of Environment 109*(4): 482–499.

Wallerman, J., and J. Holmgren. 2007. Estimating field-plot data of forest stands using airborne laser scanning and SPOT HRG data. *Remote Sensing of Environment* 110(4): 501–508.

Wang, C.Z., J.G. Qi, and M. Cochrane. 2005. Assessment of tropical forest degradation with canopy fractional cover from landsat ETM plus and IKONOS imagery. *Earth Interactions* 9: 1–18.

Wang, X.Q., Z.Y. Li, X.E. Liu, G. Deng, and Z.H. Jiang. 2007. Estimating stem volume using QuickBird imagery and allometric relationships for open Populus xiaohei plantations. *Journal of Integrative Plant Biology* 49(9): 1304–1312.

West, G.B., B.J. Enquist, and J.H. Brown. 2009. A general quantitative theory of forest structure and dynamics. *Proceedings of the National Academy of Sciences of the United States of America* 106(17): 7040–7045.

Williams, M. 2008. A new look at global forest histories of land clearing. *Annual Review of Environmental Resources* 33: 345–367.

Wilson, E.H., and S.A. Sader. 2002. Detection of forest harvest type using multiple dates of Landsat TM imagery. *Remote Sensing of Environment* 80(3): 385–396.

Wolter, P., P. Townsend, and B. Sturtevant. 2009. Estimation of forest structural parameters using 5 and 10 meter SPOT-5 satellite data. *Remote Sensing of Environment* 113: 2019–2036.

Woodcock, C.E., S.A. Macomber, M. Pax-Lenney, and W.B. Cohen. 2001. Monitoring large areas for forest change using Landsat: Generalization across space, time and Landsat sensors. *Remote Sensing of Environment* 78(1–2): 194–203.

Wulder, M.A., R.J. Hall, N.C. Coops, and S.E. Franklin. 2004. High spatial resolution remotely sensed data for ecosystem characterization. *Bioscience* 54(6): 511–521.

Wulder, M.A., J.C. White, N.C. Coops, and C.R. Butson. 2008. Multi-temporal analysis of high spatial resolution imagery for disturbance monitoring. *Remote Sensing of Environment* 112(6): 2729–2740.

Xian, G., C. Homer, and J. Fry. 2009. Updating the 2001 National Land Cover Database land cover classification to 2006 by using Landsat imagery change detection methods. *Remote Sensing of Environment* 113(6): 1133–1147.

Xiao, J.F., Q.L. Zhuang, D.D. Baldocchi, B.E. Law, A.D. Richardson, J.Q. Chen, R. Oren, et al. 2008. Estimation of net ecosystem carbon exchange for the conterminous United States by combining MODIS and AmeriFlux data. *Agricultural and Forest Meteorology* 148(11): 1827–1847.

Zhao, K.G., S. Popescu, and R. Nelson. 2009. Lidar remote sensing of forest biomass: A scale-invariant estimation approach using airborne lasers. *Remote Sensing of Environment* 113(1): 182–196.

Zheng, D.L., J. Rademacher, J.Q. Chen, T. Crow, M. Bresee, J. le Moine, and S.R. Ryu. 2004. Estimating aboveground biomass using Landsat 7 ETM+ data across a managed landscape in northern Wisconsin, USA. *Remote Sensing of Environment* 93(3): 402–411.

Zink, M., G. Krieger, H. Fiedler, and A. Moreira. 2007. The TanDEM-X mission: Overview and status. Paper presented at the IEEE International Geoscience and Remote Sensing Symposium. July 2007, Barcelona, Spain.